


Università degli Studi di Cagliari

DOTTORATO DI RICERCA

Scienze e Tecnologie Chimiche

Ciclo XXVI

Host Defence Peptides (HDPs): investigating the structure-to-function relationship through bio-phyisical techniques

Settore/i scientifico disciplinari di afferenza

CHIM/02

Presentata da:	Giorgia Manzo
Coordinatore Dottorato	prof. Mariano Casu
Tutor/Relatore	prof. Mariano Casu

Esame finale anno accademico 2012 – 2013

ABSTRACT

During last decades, more and more microorganisms resistant to conventional antibiotics were isolated while few new antimicrobial drugs were developed. The urgent need for novel efficient antibiotics led a great attention on cationic host defense peptides (HDP) since their discovery in 1980s. The role of these molecules in the defense of organism against pathogens attack, together with their high selectivity for bacterial cells over the eukaryotic ones, made them attractive candidates for the development of a new class of antimicrobial drugs. At present, a vast range of both natural and synthetic HDPs sequences are reported in the literature but they still present remarkable limitations to an effective applicability *in vivo*, such as the high sensitivity to proteases and strong activity reduction in the presence of physiological electrolytes concentration. A lot of effort have been put into improving their pharmacokinetics in order to develop new antimicrobial drugs based on their sequences.

The present Ph.D. work is focused on the elucidation of the structure-to-function relationships of three different peptides, chosen as representative of different HDP categories. Esculentin-1b(1-18) is the 'classic' natural antimicrobial peptide (AMP), Plasticin-L1, is an immunomodulatory peptide devoid of direct bactericidal activity, and a group of four synthetic peptide analogues based on a semi-synthetic dendrimeric and lipidated peptide called SB056. The latter, in particular, represent an innovative class of peptides, whose structural features, three-dimensional folding and mode of action are absolutely peculiar and almost completely unknown before this project started.

The interesting and multidisciplinary field of HDPs is presented in the first chapter. The origins, the structural features and the modes of action proposed for these compounds in the literature are briefly summarized. A brief excursus on the limits of their applicability in the clinical practice and the strategies adopted to overcome this issue is also included. In the second chapter, all the materials, the methods and experimental protocols are described, going from typical biological assays to biophysical methods.. The main technique used to elucidate the three-dimensional structure of the peptides, the nuclear magnetic resonance (NMR), is described in more detail. The computational tools used in concert with the NMR data are also described.

The chapters 3, 4 and 5 are devoted to the results and discussion of the studies performed on the three aforementioned peptides. Esculentin-1b(1-18) is the 18-mer N-terminal fragment of the peptide esculentin-1b, which was isolated from the granular skin secretions of the European frog *Pelophylax lessonae/ridibundus*. It is presented in the Chapter 3. The next chapter is dedicated to the studies performed on Plasticin-L1, a 25 amino acid

residue peptide isolated from the skin secretions of the South-American Santa Fe frog *Leptodactylus laticeps* (Leptodactylidae). In Chapter 5 the extensive and challenging work on the four SB056 analogs is reported. Among various scientific collaborations, it has to be emphasized that part of the study on the SB056 peptides was performed in the prof. A.S. Ulrich's labs at the Karlsruhe Institute of Technology, Germany, where I personally spent a 6 months stage.

Finally, in the last chapter, which is devoted to the main conclusions, a general overview of the results is given, highlighting the advance gained in the field of the HDPs and presenting possible outlooks for further peptides improvement.

List of the relevant publications

M.A. Scorciapino, G. Manzo, A.C. Rinaldi, R. Sanna, M. Casu, J.M. Pantic, M.L. Lukic, J.M. Conlon. "Conformational analysis of the frog skin peptide, Plasticin-L1, and its effects on production of proinflammatory cytokines by macrophages". Biochemistry, 2013, 52, 7231-41.

G. Manzo, M. Carboni, A.C. Rinaldi, M. Casu, M.A. Scorciapino. "Characterization of sodium dodecylsulphate and dodecylphosphocholine mixed micelles through NMR and dynamic light scattering". Magnetic Resonance in Chemistry, 2013, 51, 176-83.

G. Manzo, R. Sanna, M. Casu, G. Mignogna, M.L. Mangoni, A.C. Rinaldi, M.A. Scorciapino. " Toward an improved structural model of the frog-skin antimicrobial peptide esculentin-1b(1-18)". Biopolymers, 2012, 97, 873-81.

G. Manzo et al. "The folded structure and insertion depth of the antimicrobial peptide Esculentin-1b(1-18) depends on the negative charge of the mixed micelles" – in preparation

G. Manzo et al. "Optimization of the amphiphilic profile enhances the antimicrobial activity of a short β-stranded peptide" – in preparation

G. Manzo et al. "From linear to dendrimeric antimicrobial peptides: overcoming some of the drawbacks for the applicability *in vivo*" – in preparation

G. Manzo et al. "A dendrimeric and lipidated antimicrobial peptide that folds as a double-helix on mixed micelles: the curious case of SB056" – in preparation

ACKNOWLEDGEMENT

At the end of my Ph.D. period I have to thank all the people who inspired and helped me during these three years.

Thanks to Sardinia Regional Government for the financial support of my Ph.D. scholarship (P.O.R. Sardegna F.S.E. Operational Programme of the Autonomous Region of Sardinia, European Social Fund 2007-2013- Axis IV Human Resources, Objective l.3, Line of Activity l.3.1.).

Thanks to my supervisor prof. Mariano Casu, who gave me the opportunity of undertake this path and experience the world of science and research. His continuously encouragement of doing better made me overcome my limits and reach a high level of competence.

Thanks to dr. Andrea Scorciapino, who followed me during my project either as a teacher and a friend. Under his supervision I tried to learn as much as possible from his knowledge about NMR spectroscopy, research and science in general. His guidance has been precious for my professional and personal growth.

Thanks to prof. Andrea Rinaldi for his collaboration, support, help and precious advices on my work.

Thanks to prof. Anne Ulrich of the Karlsruhe Institute of Technology and all her research group for hosting me during my stage period, which, beside enlarge my scientific knowledge, contribute to broaden my horizons.

Thanks to dr. Roberta Sanna and dr. Cristina Piras, more friends than colleagues, who supported and helped me any time I needed; thanks to my colleagues dr. Federico Amodeo, dr. Andrea Ardu, dr. Federica Orru, dr. Manuela Pintus and the other Ph.D. students, which make me enjoy every single day of these three years.

Thanks to any people who I met and gave any kind of contribute for the growth of my knowledge.

Lastly, the best thanks go to my parents who, with many efforts, allow me to achieve this aim, and to Francesco who supported me even when I was insupportable! You always trust me and I would never arrived at this point without your encouragement.

Table of contents

1.1 Host defense peptides (HDPs): biologically active peptides with a key role in host's immune system

The ubiquitous presence of pathogenic microbes throughout nature constitutes a potential threat for the health of many organisms. Thus, almost all the forms of life during evolution developed a mechanism of defense against the attack of these microbes. These systems can be more or less complicated on the basis of the organism involved, either based on molecular and/or cellular components.

The innate immune system is a broad-range but non-specific shield; it is the most ancient host defense mechanism and the first activated when the host comes in contact with microbes. Only 'recently' (in evolutionary terms) vertebrates have developed a more evolved adaptive immunity, endowed with a molecular memory [1]. An important component of the innate immune system is represented by host defense peptides (HDPs), a class of gene-encoded molecules, generally cationic, ribosomally synthetized in virtually all forms of life [1–4]. Their key role in the immune defense mechanisms was demonstrated for many organisms, ranging from bacteria to multicellular organisms, including humans [5, 6].

During last decades, more and more microorganisms resistant to conventional antibiotics were isolated while few new antimicrobial drugs were developed. The increasing emergence of drug-resistant pathogens and the consequently lack of novel efficient antibiotics evoked a great attention on HDPs, called originally antimicrobial peptides (AMPs), since their discovery in 1980s. AMPs were originally investigated for their activity in killing pathogens of different species and strains, going from bacteria to virus and fungi. This ability, together with the high selectivity of these molecules for bacterial cells over eukaryotic ones, made them attractive candidates for the development of new antimicrobial drugs [5, 6]. Since the first AMPs were isolated, thousands of sequences from natural sources have been reported in literature as potential antibiotic agents; up to now there are over 2100 AMPs listed and this number is still growing [6]. Furthermore, a variety of synthetic peptides have been designed and produced, optimizing the natural occurring sequences to improve their pharmacokinetic. A list of these sequences can be found in several databases (for a complete account on databases development see [7]).

Today, the term host defense peptides (HDPs) is currently more commonly used than AMP, in order to better describe the overall properties/activity of this class of interesting

molecules. Indeed, beside the direct killing activity, many of them were also found to act as immunoregulatory agents [5, 6].

Direct killing action of cationic peptides has been largely studied. Despite in-depth understanding of their mechanisms needs further investigations, a general mode of action has been put forward. On the other hand, the immunomodulatory properties of these peptides only recently attracted significant attention, thus relatively little is known about the involved mechanism(s) of action in this case.

1.1.1 Natural sources of HDPs

HDPs are part of the ancient innate immune system and represent a defense against pathogenic microorganisms for virtually all forms of life. They are expressed constitutively or induced by inflammatory stimuli [4, 8]. In multicellular organisms they may be expressed systematically and/or localized in specific regions/tissues, usually the more susceptible to infections, e.g. skin and mucosal epithelia [4]. These interesting molecules have been originally isolated from insects and amphibians, but today it is known that they are produced by many different organisms. The study of natural peptides is extremely important in order to achieve the fundamental knowledge about their mechanisms of action and thus use these molecules as templates for the development of semi-synthetic novel drugs with improved activity and pharmacokinetics. In this section, a brief excursus on the main natural sources of HDPs is presented.

Bacteriocins are produced by most bacteria. These are extremely potent antimicrobial peptides and are among the first peptide antibiotics identified and studied. An important example is represented by the lantibiotics (lanthionine-containing peptide antibiotics), characterized by thioether-based intramolecular rings [4, 5]. The most extensively investigated lantibiotic is nisin, which is produced by the *Lactococcus lactis* and has been extensively used as food preservative for many years [4].

Cationic peptides isolated from plants generally show remarkable activity in protecting against both bacterial and fungal infections. Only peptides with a β-sheet structure have been isolated from plants. The most studied are thionins, 5 kDa cysteine-rich peptides ubiquitous in all plants. Thionins are compact, L-shaped molecules, with the long arm formed by two disulphide-linked α-helices and the short arm by two antiparallel β-strands [9].

As plants, invertebrates are devoid of adaptive immune system. Their protection against pathogens totally relies on the innate immune response. Indeed, they are rich in HDPs and many of the sequences investigated up to date were originally isolated from invertebrate

species. Examples are α-helical Cecropins (fly hemolymph, [4, 9, 10]), Mellitin (bee venom, [4]) or the β-hairpin-like peptide Tachyplesin [4, 9] and Polyphemusin (horseshoe crab, [4]).

The granular glands of amphibian skin, in particular, is a rich source of HDPs. Peptides isolated from frogs and toads skin secretions usually show a broad spectrum of antimicrobial activity, against either Gram-positive and Gram-negative bacteria. Some of the first studied peptides derived from amphibian sources, e.g. Magainins and Buforin II [4, 9].

Also mammals produce high amounts of HDPs. Two main classes have been characterized: Defensins and Cathelicidins [4, 11]. Defensins are divided in three classes: α-, β- and θ-Defensins. They are 3.5-6 kDa peptides containing six cysteine residues that form intramolecular disulphide bridges [12]. In humans, only α- and β-defensins are found. The former are mainly stored in cytoplasmic granules of neutrophils and in the Paneth cells of small intestine, while β-Defensins are produced by epithelial cells directly exposed to the infection. Finally, θ-defensins are found in the leukocytes of a small group of non-human primates (rhesus macaques and baboons), but have never been isolated in active form from humans, although θ-defensins genes are present in our genome [13]. In humans, only one cathelicidin was described, namely, hCAP18, from which LL-37 active fragment is produced by cleavage [11, 12]. However, humans several other HDPs, including hepticidins (small, cysteine-rich peptides), dermicidins and histatins (a family of histidine–rich peptides). For detailed reviews on human HDPs see [11, 12, 14]. Almost all of these HDPs are endowed with a broad spectrum antimicrobial activity against different types of pathogens, from bacteria to fungi and viruses, with minimal inhibitory concentration (MIC) values ranging between 1-50 μg/ml [15].

1.1.2 Structural features of HDPs

HDPs were identified in almost all living organisms with very low sequence similarity. Amino acid sequence homology is found only among peptides from closely related species. Indeed, HDPs sequence to a large extent varies even among mammalian species. It has been argued that such a large variability arises from the variance in the species-specific pathogens [5].

Despite the low sequence similarity, some interesting structural features are shared by most of the characterized HDPs so far. HDPs are relatively short peptides ranging in length from 12 to 50 amino-acid residues [4–6, 8, 11] with few exceptions such as the anti-infective activity reported for a 6-mer peptide [16] or for larger proteins like lactoferrin [2, 17]. Most HDPs derive from post-translational modifications of larger precursors, including proteolytic

processing, glycosylation, carboxy-terminal amidation, amino-acid isomerization and halogenation.

AMPs have been more extensively investigated than immunoregulatory peptides. Several modes of action have been put forward for AMPs bactericidal activity, almost all involving the interaction with bacterial plasma-membranes as a key step. On the other hand, information about the mechanisms by which HDPs modulate innate immune system in the host organism is scarce [6], but an interaction with bacterial and/or mammals plasma-membranes was suggested also in this case as an early step, presumably followed by internalization of the peptide inside the cell, similarly to the so-called cell-penetrating peptides [6, 18].

Generally speaking, HDPs are typically rich in hydrophobic residues like leucine, isoleucine, valine, phenylalanine and tryptophan (up to 50%) and carry a net positive charge in the range +2 to +9 due to the presence of basic residues like lysine and arginine [4–6, 8, 11]. The alternation of hydrophobic and hydrophilic residues along the amino acid sequence usually causes a typical amphipathic folding. Some HDP is found to preferentially adopt a helical secondary structure, some other a β-strand/sheet structure, others might also show regions characterized by different secondary structural motives, but all of them have a marked amphipathicity as distinctive feature. This facilitates the interaction between the peptide and the lipid membrane: the hydrophobic side-chains interact with the lipid tails, while the hydrophilic ones are oriented towards the aqueous environment of biological fluids and/or embedded between the polar head groups of membrane phospholipids.

Many studies report that almost all the HDPs are unstructured in aqueous solution and adopt their amphipathic secondary structure upon interaction with membrane models and/or membrane-mimicking solvents [1, 5]. The net positive charge, in addition, is essential to preserve the selectivity of AMPs for bacterial cells over the eukaryotic ones. The former, indeed, are rich in negatively charged molecules in their membrane/cell wall (e.g. phospholipid head groups like phosphatidylglycerol and cardiolipin, lipolysaccharide in Gram-negative bacteria, lipoteichoic acids in Gram-positive bacteria), while the latter are mostly characterized by zwitterionic phospholipids [3, 15, 19–21].

HDPs can be classified into four main groups on the basis of their structure [2, 5, 6, 8, 15] (figure 1.1):

- Linear α-helical peptides, are usually less than 40 amino acids long and present a tridimensional amphipathic structure, with a kink or hinge in the middle. A direct correlation has been observed between helical content and antimicrobial activity [15], while an excess of

hydrophobic residue results in an increased toxicity towards mammalian cells [22]. This is the most studied class of HDPs and most of the modes of action reported in the literature were suggested on the basis of their biophysical characteristics. Examples of well characterized helical peptides are Cecropins, Magainins and Cathelicidins;

- β-Sheet peptides are usually characterized by the presence of cysteine residues implicated in disulphide bridges Examples well characterized β-sheet-peptides are Defensins and Protegrin. These usually adopt a β-hairpin folding. Few details are reported about the mode of action of these β-sheet-peptides and it is generally assumed that they act in the same way as helical peptides;

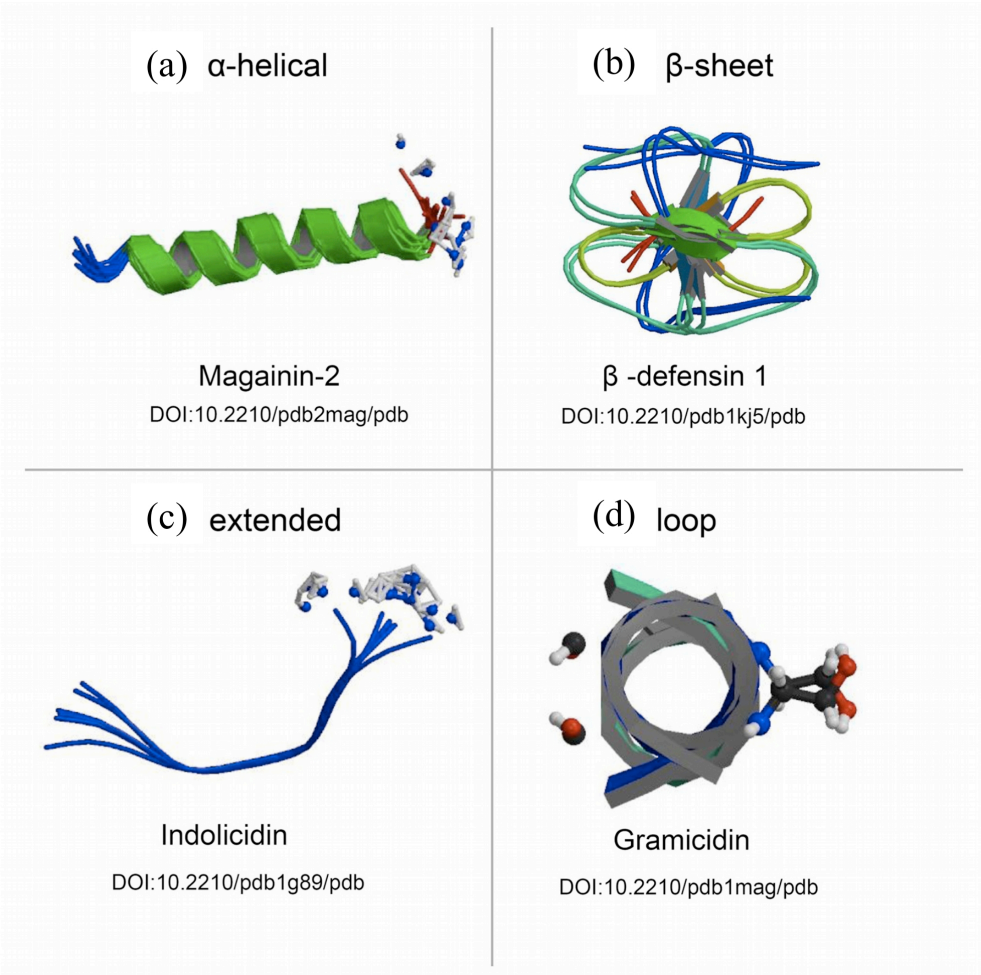

Figure 1.1. Examples of the different structures adopted by HDPs. Peptides can be grouped into four major classes based on their secondary structures, including (a) α-helical peptides, (b) peptides composed of a series of β-sheets, (c) peptides that adopt unconventional structures, such as extended helices, and (d) peptides that assemble into loops. Figure taken from Peters et al. 2010 (figure 1) [22].

- Extended conformation are typically observed for peptides that are rich in specific amino-acids like proline, arginine and tryptophan, lackcysteine residues, resulting in very flexible structures. Examples are Indolicidin and Pig PR39;
- Loop folded peptides are less commonly found, being characterized by peptide cyclization (e.g. cattle bactenecin and Gramicidin).

For a detailed review on the structural features of HDPs see Dathe & Wieprecht 1999 [23].

1.1.3 Biological effects of HDPs: trying to correlate structure to function

Several mechanisms have been proposed to explain HDPs activities. While AMPs, the subclass of HDP peptides endowed with direct antimicrobial activity, were investigated for longer time and much more information are reported in literature about their mode of action, the immunoregulatory properties of cationic HDPs, on the other hand, are still unclear. Much is known about the biological effects produced by these peptides on the host immune system, but very few information are available on the molecular mechanism underlying their activities. This is mostly due to the high number of possible targets peptides could interact with and it is thus hard to correlate structural features of HDPs to the biological function. Moreover, many HDPs resulted to be both immunomodulatory and bactericidal depending on the concentration. For instance, α-defensins are stored in cytoplasmic granules of human neutrophils [2, 12]. They are bactericidal at the high concentration found in neutrophil granules, whereas they act as immunomodulators at the lower concentrations resulting from degranulation at inflammatory sites [4].

Despite the different biological activity, it is likely that each peptide uses a combination of strategies, rather than a unique mechanism, in order to challenge the infections caused by pathogens belonging to different species [4, 5, 19, 22]. It is widely accepted that, regardless of their actual mode of action, almost all HDPs exhibit a remarkable interaction with lipid bilayers as a key step of their activity [4, 22]. The high variability of amino acid sequences and secondary structures is one of the main reasons why it is difficulty to define a unique mode of action. Since AMPs are largely described in the literature, I start this dissertation with the direct microbicidal activity. Actually, a general mechanism involving different steps common to most of the known AMPs was proposed.

First, AMPs are electrostatically attracted by the negatively charged components of the bacterial outer membranes, i.e. lipoteichoic acids and phosphate groups of lipopolysaccharides (LPS) in Gram-positive and -negative bacteria, respectively [4, 5, 15, 24]. Once crossed the outer membrane and approaching the plasma membrane bilayer, AMPs fold

in their native structure and interact with the negatively charged phospholipids, characteristics of prokaryotic membranes. In the case of α-helices, their amphipathic 3D structure is such that the peptide orients parallel to the membrane surface. The amphipathicity of AMPs secondary structure is fundamental for its interaction with the bilayer to be thermodynamically favored. The hydrophobic residues on the one side will embed between hydrophobic lipidic tails, while the hydrophilic residues on the other side will interact either with charged/polar head groups phospholipids and water [22]. From this stage on, different mechanisms are described in the literature. The main one involves the disruption and/or permeabilization of bacterial plasma membrane [4, 21, 24]. Other mechanisms involve the interaction of peptides with intracellular target, such as nucleic acids and phosphorylated proteins, ,or the interference with key cellular processes like DNA and protein synthesis, protein folding, enzymatic activity and cell wall synthesis [22, 24]. In figure 1.2 many of these modes of action (briefly described below) are schematized.

Membrane-active peptides. Most AMPs are thought to act by direct perturbation of the lipid membrane through pore-formation or detergent-like mechanisms [4, 15]. α-Helical peptides are the most extensively studied peptides among AMPs and many of the modes of actions described in the literature have been put forward on the basis of their behaviour. They can form transient pores through the 'toroidal pore' model (e.g. Magainin,) [25, 26] or 'the barrel-stave' model (e.g. Alamethicin) [26, 27]. Both these models involve peptide insertion into membranes, with a final orientation parallel to the membrane normal, and perturbing membrane permeability through pore-formation [4, 5, 15, 28]. The pore wall is constituted by a certain number of peptides or by the peptides and the lipids head group in the barrel-stave and toroidal wormhole model, respectively. Otherwise, AMPs activity can be described with the 'carpet model' (e.g. Cecropin) [26], on the basis of which they aggregate on the membrane surface and align parallel to the lipid bilayer surface, coating local areas in a carpet-like fashion, till they reach a threshold of high local concentration sufficient to destroy the membrane via a detergent-like mechanism [4, 5, 28]. Thus, being this route highly concentration dependent, it is likely to observe the carpet-like model with the high concentrations used during *in vitro* experiments, while there are few evidences for peptides actually following this mechanism at the relatively low concentrations encountered *in vivo* [4, 22]. In an attempt to unify the different mechanisms proposed for AMPs activity, the so called Shai-Matsuzaki-Huang (SMH) model has been proposed [1, 3]. It envisages an initial carpeting of the peptides on the outer leaflet, their insertion into the membrane and the consequent thinning of the outer leaflet, followed by the formation of transient pores and the

translocation of lipids and peptides into the inner leaflet. This would lead to eventual diffusion of the peptides through the membrane into the cell to finally interact with intracellular targets and/or causing the collapse of the membrane [1].

Another mechanisms involves the perturbation of membrane stability by the clustering of anionic lipids around the positively charged peptides. This process consists in the segregation of anionic charged lipids from zwitterionic/uncharged ones to form negatively charged domains (rafts) of lipids and peptides. Such a high concentration of anionic lipids in a restricted region of the membrane where cationic peptides can aggregate causing a breach in the bilayer, with consequently leakage of small organic molecules and/or membrane depolarization [19, 20, 22]. In addition, bacteria might be damaged by this redistribution of anionic lipids, leading to the disruption of functional domains of the membrane or the depletion of anionic lipids needed to interact with intracellular proteins [19, 20]. For this mechanism to be efficient, a high percentage of zwitterionic or uncharged lipids is required in order to have the anionic ones segregated in rafts. Hence, Gram-negative bacteria are, in general, more susceptible to this mechanism since are endowed with a higher percentage of zwitterionic lipids than Gram-positive ones [19–21]. This suggests that the anionic lipid clustering should be the preferred route depending on the phospholipid composition of the bacterial membrane, rather than to the bacterial species; indeed, even some Gram-positive bacteria characterized by a relatively high percentage of zwitterionic lipids, such as *Bacillus cereus*, are found to be susceptible to anionic lipid clustering [19, 20]. A good conformational flexibility was demonstrated to increase the anionic lipid clustering capability of peptides. For instance, GF-17, the longer fragment of LL-37 lost the characteristic amphipathic helical folding and the ability to release dyes from liposomes (pore formation) if three D-amino acids are introduced in different positions (GF-17D3). While GF-17 is toxic either for Gram-negative and -positive bacteria, GF-17D3 shows specificity against Gram-negative bacteria, suggesting lipid clustering as the principal mechanism [19, 20].

Non-membrane-active peptides. It is now well established that many AMPs can translocate inside the cell without damaging the plasma membrane and interact with several essential molecules and metabolic cycles leading to cell death. Thus, novel mechanisms were described involving interference with nucleic acid and protein synthesis, enzymatic activity and cell wall formation [4, 28]. The frog peptide Buforin II, in contrast to most α-helical peptides, does not perturb membrane integrity, but rather translocates and accumulates in the cytoplasm of *Escherichia coli* cells where it binds to DNA and RNA, interfering with their biochemical pathways [4, 22]. Also structurally different peptides like the β-sheet human

defensin hNP-1 and the extended peptide Indolicidin, interfere with nucleic acids cycle [4, 22]. The proline-rich insect peptides Pyrrhocoricin, Drosocin and Apidaecin were observed to cross plasma-membrane and to interact with intracellular proteins [4, 22, 24, 26].

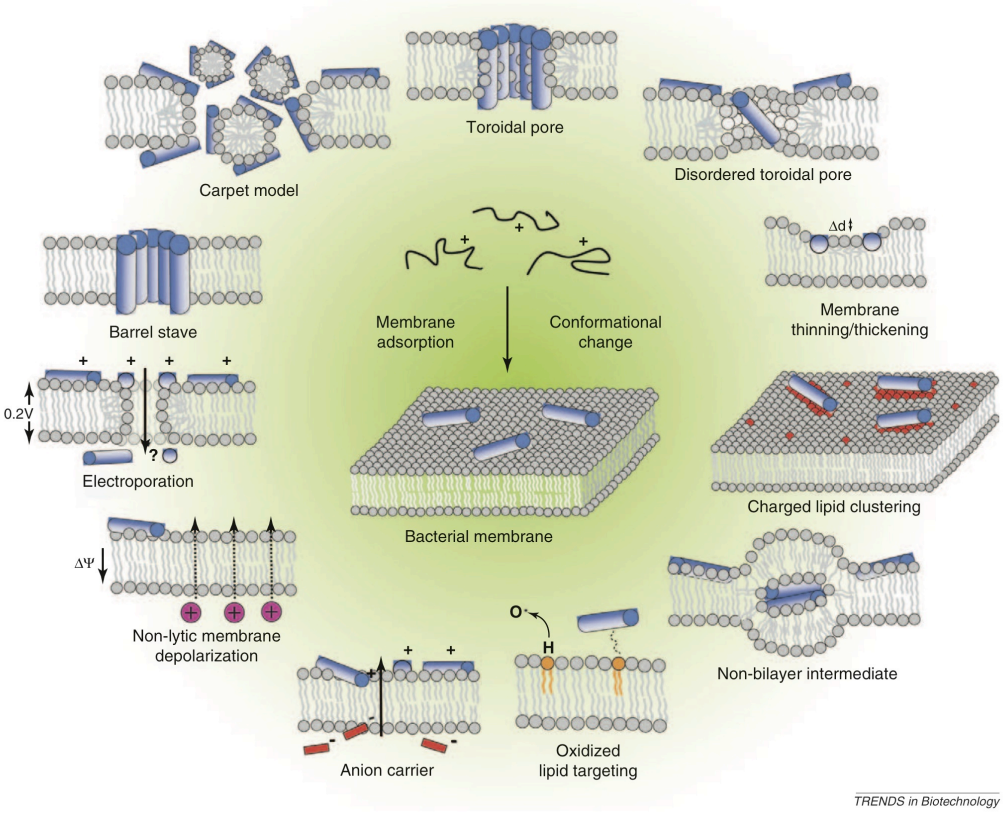

Figure 1.2. Events occurring once AMPs face bacterial plasma membrane. In the classical models of membrane disruption, the peptides lying on the membrane reach a threshold concentration and insert themselves across the membrane to form either pores (barrel-stave or toroidal pore models), or solubilize the membrane into micellar structures (carpet model). The thickness of the bilayer can be affected by the presence of the peptides, or the membrane itself can be remodelled to form domains rich in anionic lipids surrounding the peptides. In more specific cases, non-bilayer intermediates in the membrane can be induced; peptide adsorption to the membrane can be enhanced by targeting them to oxidized phospholipids; a peptide may couple with small anions across the bilayer, resulting in their efflux; the membrane potential can be dissipated without other noticeable damage; or conversely, in the molecular electroporation model, the accumulation of peptide on the outer leaflet increases the membrane potential above a threshold that renders the membrane transiently permeable to various molecules including the peptides themselves. These events are not necessarily exclusive of each other. Figure taken by Nguyen el al. 2011 [21].

AMPs can also interfere with the formation of structural components. This is the case of two lantibiotics produced by some bacteria species, namely Mersacidin and Nisin, that interfere with lipid II processes, necessary for the synthesis of the peptidoglycan [4, 5].

Immunomodulatory peptides. Beside the bactericidal activity of AMPs, HDPs also act by modulation of the immune response. The presence of many HDPs in immune circulating cells and in strategic sites where infections can start is consistent with this hypothesis. Moreover, an increase in the production of HDPs during infections was demonstrated [2]. Conversely, mutations affecting the production of HDPs cause increased susceptibility to infections [6, 8, 14, 28].

In some cases, it has been reported that HDPs with microbicidal effects might be actually present at too low concentration *in vivo* (with respect to the MIC value determined *in vitro*), and/or that the physiologic environment may inhibit their activity. This could be due to e.g. the presence of a high concentration of electrolytes, serum components, peptidases and polyanionic glysoaminoglycans. However it has been shown that they preserve their immunomodulatory properties in the same conditions [6, 8, 14, 28].

Many are the effects described for HDPs on the immune system. A primary function, among others, is the promotion of immune cells recruitment at the site of infection and, then, a direct contribution to the clearance of infections. Indeed, HDPs can promote recruitment of neutrophil, monocytes and immature dendritic cells (iDCs), either by direct recruitment acting as chemoattractors or by inducing the production of chemokines [8, 28].

It is noteworthy that many HDPs exert these effects at concentrations lower than those necessary to exploit a direct antimicrobial activity. This agrees with the recent observation that anti-infective potential of some HDPs is not only due to the bactericidal activity and supports the potential of some of these HDPs or their synthetic derivatives as therapeutic agents, despite they are devoid of direct antimicrobial activity but being good modulators of the immune system [6, 29]. This is the case of a 5-mer modelled peptide, called IMX942, in pre-clinical trial as immunomodulator by Inimex Pharmaceuticals (Vancouver, Canada) [28, 29].

Finally, HDPs have been shown to behave also as anti-inflammatory agents. Several peptides like cathelcidin LL-37, defensin hBD-2 and IDR-1 and IDR-1002, can modulate host immune inflammatory response induced by pathogens. They act by suppressing some pro-inflammatory processes, such as the induction of tumour necrosis factor TNF-α, pro-inflammatory cytokines like IL-1β, and nitric oxide in the presence of either infections or pro-inflammatory stimuli, through different specific mechanisms [8]. Many HDPs, like LL-37 and

IDRs peptides, inhibit dangerous pro-inflammatory response while still maintaining active the protective anti-infective response [8, 11].

Even if many of these positive effects are reported for HDPs, very little is know about the molecular mechanisms. It is clear that HDPs target multiple receptors and processes depending either on cell type and peptide sequence [6]. Generally speaking, the translocation of peptides inside the cells has been suggested as a necessary step [6], but whether it is a receptor-mediated route or a direct endocytosis process is not clear. Once inside the cell, HDPs can interact with several molecules (including nucleic acids) and/or receptors to modulate the response by inducing or suppressing mediators production.

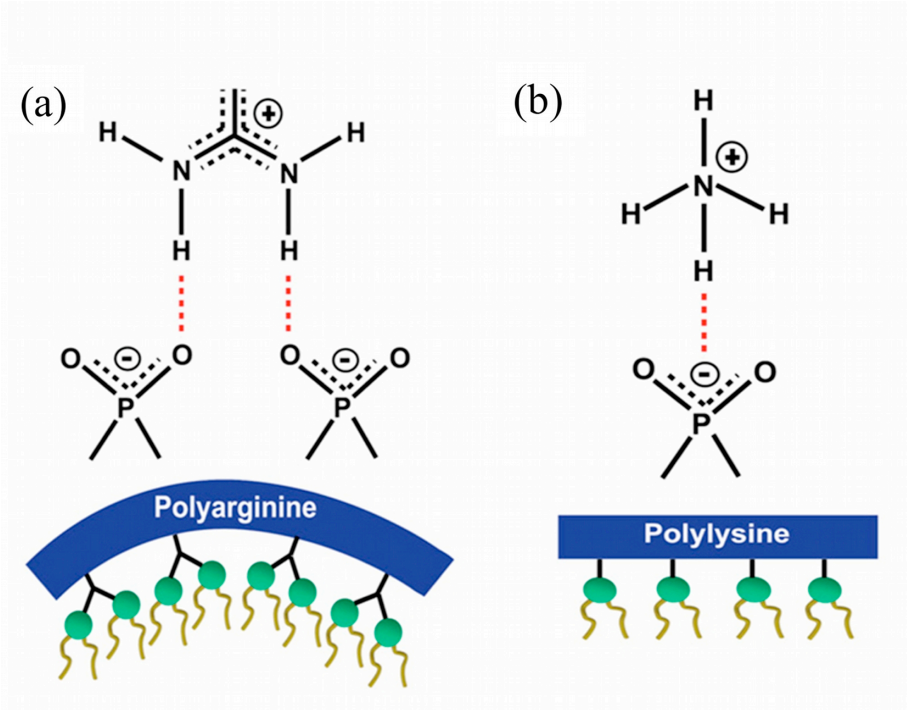

Figure 3. Representation of the different interactions of arginine and lysine residues with phosphate groups of phospholipids moieties. (a) Multidentate coordination of arginine's guanidinium side chain induces positive curvature strain along the peptide. (b) Monodentate coordination of lysine's amino side chain does not induce positive curvature. Figure taken by Mishra et. al 2011 [30].

As reported in section 1.1.2, despite the low sequence and secondary structure similarity, most HDPs share some distinctive features. Among these, the net positive charge (in particular for AMPs) and an amphipathic folding appear to be extremely important. Recently, some residues were identified as more necessary than others to enhance HDPs activity. In particular, lysine and arginine have been suggested as specifically required for the interaction with the lipids head group and for membrane insertion. These two basic residues,

have been described as promoters of negative Gaussian membrane curvature of the lipid bilayer, and as the main responsible of phenomena including pore formation, blebbing, budding, vesicularization and lipid clustering [30, 31]. Arginine and lysine side chain can form hydrogen bonds with the negatively charged head group and/or phosphate groups of phospholipids causing a negative curvature in the membrane [30–33] (figure 1.3). This should stabilize the presence of these basic (and charged) residues in the lipid moieties and allow either penetrating mechanisms and anionic lipid clustering. Arginine, in particular, is thought to be more effective than lysine, since it can form multiple hydrogen bonds thanks to bidentate guanidinium group. Lysine residues, on the other hand, need to be separated by hydrophobic amino-acids to exert the same action, as typically occurs in HDPs sequences [30, 33].

1.2 The role of HDPs in preventing the threat of bacterial drug-resistance

With the use of penicillin during the Second World War the therapeutic application of antimicrobial agents to treat microbial infections started. Since then, many drugs were developed that helped, together with the improvement of hygienical conditions, to reduce the morbidity of pathogenic attacks. However, recently there has been a decline of the new drugs discovery, with only three new chemical classes of antibacterial compounds entering the market in the last decades, namely lipopeptides, oxazolidinones and streptogamins [28]. On the other hand, more and more pathogens resistant to conventional antibiotics have been isolated, due either to the high rates of mutation inherent to the reproduction mechanism of these microorganisms and to the bad medical, zootecnic and agriculture practice which, during the last 50 years, misused antibiotics [34, 35]. It is estimated that infectious diseases account for one-third of all human deaths, with respiratory infections, HIV, malaria and tuberculosis as the principal killers [28]. The development of bacterial resistance typically consists in drug inactivation or target site modification/mutation, limited drug uptake or enhanced efflux outside the cell and phenotypic resistance owing to specific growth modes (e.g. biofilms). Definitely, the clinical impact of resistance is immense, characterized by increased costs, length of hospital stay, and mortality [34].

Due to the growing threat of drug-resistant microorganisms, HDPs were praised as novel candidates to develop a new class of anti-infective drugs since their discovery in insects and amphibians. They showed a broad spectrum activity against different classes of bacteria, fungi, virus, parasites and so on [4]. In addition, AMPs showed the tendency to target lipid bilayers, and the net positive charge should provide selectivity towards bacterial cells

preventing or limiting cytotoxicity. Moreover, the presence of cholesterol in eukaryotic bilayers interferes with the activity of AMPs by stabilizing the lipid bilayer or even interacting with the peptides themselves [3, 34]. Most importantly, the anionic bacterial-cell envelopes and the plasma-membranes are formed through evolutionarily well conserved biosynthetic processes and represent a non-selective target, making modifications by the microorganisms hard to be introduced and, thus, resistance onset unlikely [36].

Notwithstanding these assumptions, however, some mechanisms of resistance to AMPs activity are reported in the literature, such as modifications of negatively charged molecules of cell envelope by incorporating positive moieties [26, 36], efflux enhancement and the production of peptidases. Nevertheless, the evolutionary success of AMPs bolsters that they are able to overcome bacteria resistance by acting at high concentrations or by adopting different and synergistic modes of actions that do not necessarily involve perturbing membrane lipid bilayer [36].

In this scenario, the idea to stimulate host immunity response through HDPs-inspired immunoregulatory drugs is really attractive since the development of resistance by pathogens should be avoided because they not be directly targeted at all. Thus, this strategy might form the basis for broad spectrum therapeutics, since host immunity utilizes common mechanisms that are effective against a diverse array of pathogens. On the other hand, disadvantages might derive from the possibility of inappropriate dysregulation of immunity with consequent upregulation of inflammatory response [29]. Insufficient knowledge of the modes of action and the specific biological targets makes it hard to predict the positive and negative effects produced by new peptidic sequences used as immunomodulators. However, specific tests which correlate newly designed sequences with a desired immune response, like release of chemokines or reduction of LPS-stimulated TNF-α production, can be used to screen immunomodulatory properties of either natural and (semi-)synthetic peptides *in vitro* [6].

1.3 New developments (and limitations) in the use of HDPs as template for antimicrobial drugs

The growing threat of drug-resistant pathogens led researchers to look for candidates to develop new potential anti-infective drugs. Due to their interesting features, the attention was focused on cationic HDPs with the idea to use naturally occurring sequences as templates for the design of novel antibiotics. Despite efforts during last decades, very few sequences reached therapeutic use whereas several failed during clinical trials (e.g. the Genaera developed Pexiganan MSI-78) a synthetic 22-amino-acid variant of Magainin-2 administered

to treat diabetic foot ulcer) [5, 28]. Other HDPs continue to be designed and today many cationic peptides are still at different stages of clinical development. A significant case is MX-226 (Omiganan), a bovine Indolicidin homolog which revealed efficacy against catheter-associated infections [5, 28]. Examples of structurally different but successfully clinically used cationic peptides, include the Polymyxin B and Gramicidin S that are used in the topical treatment of infections, as well as the the lipopeptide daptomycin, an important antibiotic against multiply resistant Gram-positive bacteria. These are nonribosomally synthesized peptides, produced by microbes through the nonribosomal-peptide synthetases enzyme [5].

More recently, the study of synthetic peptides designed on the basis of the new knowledge on the immunomodulatory properties of HDPs, resulted in some interesting leads, like IDR-1. Even if devoid of direct antimicrobial activity, this peptide revealed to selectively modulate innate immune response, resulting in protection of mice models against multiple bacterial pathogens [28]. A 5-mer peptide based on IDR-1 sequence is at the phase II of clinical trial [6].

However, most of the HDPs inserted in clinical studies are being considered just for topical application, either because of the risk of systemic toxicity and/or of their sensitivity to physiological conditions (e.g. proteases in the blood stream, high concentrations of mono- and divalent ions, pH) [5, 6, 26]. Indeed, even if the selectivity of membrane-active AMPs towards bacterial membranes is ensured by the presence of the negatively charged molecules on prokaryotic membranes and of cholesterol in the eukaryotic cells, not-membrane active peptides exist that can easily enter the cell, both eukaryotic and prokaryotic, interacting with internal targets and thus representing a risk for the host organism [5]. This obviously prevent the development of such molecules for systemic administration (parenteral and oral). As far as the immunomodulatory properties of HDPs are concerned, the main risk associated with their practical use is an overstimulation of the innate immunity which can induce or exacerbate potentially harmful pro-inflammatory responses [5, 29].

The most obvious obstacle hampering the use of HDPs *in vivo* is their sensibility to proteolytic degradation. Proteases can hydrolyse peptides, particularly if they are not branched like almost all nature occurring peptides, resulting in reduced bioavailability at the infection site [4–6, 8]. Many strategies were suggested to overcome this problem. These include the acetylation of the N-terminus to block the activity of aminopeptidases [6], peptide cyclization through disulphide bridges or peptide N- and C-terminus joining [6], the insertion of non-natural D-amino-acids to change peptide stereochemistry and the alteration of peptide backbone while preserving the spatial orientation of the side chains (e.g. peptidomimetics, for

details see [34, 37]). All these approaches involve chemical modifications of the peptide sequence in order to mask them from proteases recognition.

A further strategy consists in the use of the multiple antigenic peptide approach (MAP) to synthetize multimeric-branched peptides [37, 38]. This approach, firstly introduced to prepare peptide immunogens in the ‘80s, led to the production of several dendrimeric peptides, where several copies of the selected sequence are bound to a core. This new design should promote an improvement of both antimicrobial activity (many copies of the functional units per mole) and proteolytic resistance (branched structure instead of a linear peptide) with respect to the monomeric counterpart [37, 39, 40]. The increased resistance of peptides to enzymatic cleavage is in this case likely due to either the steric hindrance of branched peptides, which limits their access to the cleavage site of enzymes, and to the possibility for dendrimeric peptide backbones to generate hydrophobic clusters, which contribute to the proteolytic resistance of the final products [38].

On the other hand, proteolytic sensitivity may be useful in the case of immunomodulatory peptides, since the fast degradation of the peptides should prevent the overstimulation of the immune system. Thus, it can be suggested that when moving from direct antimicrobial activity of AMPs to host immunostimulatory HDPs, peptide resistance to proteases may be of secondary importance [28].

Another issue in the systemic application of HPDs derives from the inherent conditions encountered *in vivo*. The antimicrobial activity of most cationic peptides is severely reduced in the presence of mono- and divalent cations, since they compete with peptides for the specific binding sites on the surface of cells [14]. HDPs activity is also influenced by the presence of anionic glysoaminoglycans, like heparin, which could bind and segregate cationic peptides [14]. Thus, it is extremely important to test antimicrobial properties in conditions as similar as possible to those encountered *in vivo*. Conversely, the immunomodulatory properties of most HDPs, usually tested in physiologic tissue culture media, are preserved despite they lose their direct antimicrobial activity [14].

Finally a not negligible aspect which contributed to the limited number of HDPs-AMPs sequences developed and tested in clinical settings, is the high cost of peptides manufacturing on a large scale. To overcome this problem, many attempts have been made to produce peptides by a variety of recombinant DNA methods using bacteria, fungi, plants and animal production systems, but they usually meet pharmaceutical companies requirements only poorly. Another strategy consists in the design of active sequences as short as possible:

the shorter the peptide, the cheaper the production. This strategy, for instance, was particularly successful in the case of the IDR-1 analog [5, 6, 8, 28].

1.4 Aim of the work

My project is focused on the characterization of the structure to function relationship of cationic HDPs using different biophysical techniques. In particular, I studied three different peptides having a different origin, different structural features and, the core of my thesis, a remarkably different behaviour. These three specific peptides have been chosen in order to span different categories of typical HDPs, from direct antimicrobial to immunomodulatory, from helical to β-structured, from natural to synthetic. The main aim was to characterize the three-dimensional structure of these representative cases in the presence of suitable membrane models and to correlate their structure to the mechanism of action. By collecting information from a wide arsenal of experimental techniques, the final goal was to possibly introduce some rational modification in the original sequences in order to improve or tune their activity. Particular emphasis has been placed on a proprietary dendrimeric peptide, which I believe is really promising, in the light of the evidences collected during my work, for further improvements.

Esculentin-1b(1-18) (Esc(1-18)) encompasses the first 18 residues of the N-terminal fragment of the 46-mer peptide Esculentin-1b which was isolated from the granular skin secretions of the European frog *Pelophylax* (*Rana*) *lessonae/ridibundus* [41–43]. It represents the 'classic' model for AMPs, folded as a α-helix and endowed with a good and broad spectrum antimicrobial activity [42–44].

Plasticin-L1 is a 25 amino acid residue peptide isolated from the skin secretions of a frog as well, namely, the South-American Santa Fe frog *Leptodactylus laticeps*. Its primary structure is quite atypical with respect to the other HDPs. It is devoid of a net positive charge and presents a rather high number of glycine and leucine residues [45, 46]. Plasticin-L1 is not a direct antimicrobial peptide, but an outstanding immunomodulatory activity has been revealed [46].

The last case presented in this work concerns a group of four analogous peptides. The original one, called SB056 is a lipidated dendrimeric peptide endowed with a good antimicrobial activity, characterized by two copies of the same peptide sequence (10 amino acid residues) attached to a central core and a lipophilic chain; overall the peptide is expected to fold as a β-type [47]. During my Ph.D. work, I investigated the original dendrimeric peptide and its monomeric counterpart, as well as two analogues (one dendrimeric and its

monomeric counterpart) with a rationally optimized sequence. These peculiar peptides represent an innovative case. A new class of semi-synthetic peptides whose structural features, three-dimensional folding and behaviour are almost completely unknown. To the best of my knowledge, similar examples are totally missing in the literature or, at least, only preliminary investigations are reported, mostly focused on the evaluation of the biologic properties without any attempt to investigate the structure to function correlations.
Different techniques have been employed, from typical biological assays, to biophysical methods and molecular spectroscopy techniques. A work with a marked multidisciplinary character on a topic at the interface of Chemical Physics, Biochemistry and Biology.

1.5 References

1. Giuliani, A., G. Pirri, A. Bozzi, A. Di Giulio, M. Aschi, et al. 2008. Antimicrobial peptides: natural templates for synthetic membrane-active compounds. Cell. Mol. Life Sci. 65: 2450–60.

2. Hancock, R.E., and G. Diamond. 2000. The role of cationic antimicrobial peptides in innate host defences. Trends Microbiol. 8: 402–10.

3. Zasloff, M. 2002. Antimicrobial peptides of multicellular organisms. Nature. 415: 389–95.

4. Jenssen, H., P. Hamill, and R.E.W. Hancock. 2006. Peptide antimicrobial agents. Clin. Microbiol. Rev. 19: 491–511.

5. Hancock, R.E.W., and H.G. Sahl. 2006. Antimicrobial and host-defense peptides as new anti-infective therapeutic strategies. Nat. Biotechnol. 24: 1551–7.

6. Haney, E.F., and R.E.W. Hancock. 2013. Peptide design for antimicrobial and immunomodulatory applications. Biopolymers. 100: 572–83.

7. Wang, G (ed). 2010. Antimicrobial peptides: discovery, design and novel therapeutic strategies. Cabi, Wallingford, Oxfordshire.

8. Choi, K.Y., L.N.Y. Chow, and N. Mookherjee. 2012. Cationic host defence peptides: multifaceted role in immune modulation and inflammation. J. Innate Immun. 4: 361–70.

9. Hancock, R.E., and R. Lehrer. 1998. Cationic peptides: a new source of antibiotics. Trends Biotechnol. 16: 82–8.

10. Sato, H., and J.B. Feix. 2006. Peptide-membrane interactions and mechanisms of membrane destruction by amphipathic alpha-helical antimicrobial peptides. Biochim. Biophys. Acta. 1758: 1245–56.

11. Zhang, L., and T.J. Fall. 2010. Potential therapeutic application of host defense peptides. In: Antimicrobial peptides. Methods and protocols. A. Giuliani and A.C. Rinaldi (eds.), Humana Press-Springer, New York, NY, USA, 303-27.

12. De Smet, K., and R. Contreras. 2005. Human antimicrobial peptides: defensins, cathelicidins and histatins. Biotechnol. Lett. 27: 1337–47.

13. Lehrer, R.I., A.M. Cole, and M.E. Selsted. 2012. θ-Defensins: cyclic peptides with endless potential. J. Biol. Chem. 287: 27014–9.

14. Bowdish, D.M.E., D.J. Davidson, and R.E.W. Hancock. 2005. A re-evaluation of the role of host defence peptides in mammalian immunity. Curr. Protein Pept. Sci. 6: 35–51.

15. Diamond, G., N. Beckloff, A. Weinberg, and K.O. Kisich. 2009. The roles of antimicrobial peptides in innate host defense. Curr. Pharm. Des. 15: 2377–92.

16. Blondelle, S.E., and R.A. Houghten. 1996. Novel antimicrobial compounds identified using synthetic combinatorial library technology. Trends Biotechnol. 14: 60–5.

17. Vogel, H.J. 2012. Lactoferrin , a bird' s eye view. 244: 233–244.

18. Wieczorek, M., H. Jenssen, J. Kindrachuk, W.R.P. Scott, M. Elliott, et al. 2010. Structural studies of a peptide with immune modulating and direct antimicrobial activity. Chem. Biol. 17: 970–80.

19. Epand, R.M., and R.F. Epand. 2011. Bacterial membrane lipids in the action of antimicrobial agents. J. Pept. Sci. 17: 298–305.

20. Epand, R.M., and R.F. Epand. 2010. Biophysical analysis of membrane-targeting antimicrobial peptides: membrane properties and the design of peptides specifically

targeting Gram-negative bacteria. In: Antimicrobial Peptides: discovery, design and novel therapeutic strategies. G. Wang (ed.), CABI, Wallingford, UK, 116 –27.

21. Arouri, A., V. Kiessling, L. Tamm, M. Dathe, and A. Blume. 2010. Morphological changes induced by the action of antimicrobial peptides on supported lipid bilayers. J. Phys. Chem. B. 115: 158–67.

22. Nguyen, L.T., E.F. Haney, and H.J. Vogel. 2011. The expanding scope of antimicrobial peptide structures and their modes of action. Trends Biotechnol. 29: 464–72.

23. Dathe, M., and T. Wieprecht. 1999. Structural features of helical antimicrobial peptides: their potential to modulate activity on model membranes and biological cells. Biochim. Biophys. Acta. 1462: 71–87.

24. Torcato, I.M., M.A.R.B. Castanho, and S.T. Henriques. 2012. The application of biophysical techniques to study antimicrobial peptides. Spectrosc. An Int. J. 27: 541–49.

25. Ludtke, S.J., K. He, W.T. Heller, T.A. Harroun, L. Yang, et al. 1996. Membrane pores induced by magainin. Biochemistry. 35: 13723–8.

26. Brogden, K.A. 2005. Antimicrobial peptides: pore formers or metabolic inhibitors in bacteria? Nat. Rev. Microbiol. 3: 238–50.

27. Bechinger, B. 1999. The structure, dynamics and orientation of antimicrobial peptides in membranes by multidimensional solid-state NMR spectroscopy. Biochim. Biophys. Acta. 1462: 157–83.

28. Jenssen, H., and R.E.W. Hancock. 2010. Therapeutic potential of HDPs as immunomodulatory agents. In: Antimicrobial peptides. Methods and protocols. A. Giuliani and A.C. Rinaldi (eds.), Humana Press-Springer, New York, NY, USA, 329-47.

29. Hamill, P., K. Brown, H. Jenssen, and R.E.W. Hancock. 2008. Novel anti-infectives: is host defence the answer? Curr. Opin. Biotechnol. 19: 628–36.

30. Schmidt, N.W., A. Mishra, G.H. Lai, M. Davis, L.K. Sanders, et al. 2011. Criterion for amino acid composition of defensins and antimicrobial peptides based on geometry of membrane destabilization. J. Am. Chem. Soc. 133: 6720–7.

31. Wadhwani, P., R.F. Epand, N. Heidenreich, J. Bürck, A.S. Ulrich, et al. 2012. Membrane-active peptides and the clustering of anionic lipids. Biophys. J. 103: 265–74.

32. Schow, E. V, J.A. Freites, P. Cheng, A. Bernsel, G. von Heijne, et al. 2011. Arginine in membranes: the connection between molecular dynamics simulations and translocon-mediated insertion experiments. J. Membr. Biol. 239: 35–48.

33. Mishra, A., G.H. Lai, N.W. Schmidt, V.Z. Sun, A.R. Rodriguez, et al. 2011. Translocation of HIV TAT peptide and analogues induced by multiplexed membrane and cytoskeletal interactions. Proc. Natl. Acad. Sci. U. S. A. 108: 16883–8.

34. Rotem, S., and A. Mor. 2009. Antimicrobial peptide mimics for improved therapeutic properties. Biochim. Biophys. Acta. 1788: 1582–92.

35. Laxminarayan, R., A. Duse, C. Wattal, A.K.M. Zaidi, H.F.L. Wertheim, et al. 2013. Antibiotic resistance—the need for global solutions. Lancet Infect. Dis. 13: 1057–98.

36. Peschel, A., and H.-G. Sahl. 2006. The co-evolution of host cationic antimicrobial peptides and microbial resistance. Nat. Rev. Microbiol. 4: 529–36.

37. Giuliani, A., and A.C. Rinaldi. 2011. Beyond natural antimicrobial peptides: multimeric peptides and other peptidomimetic approaches. Cell. Mol. Life Sci. 68: 2255–66.

38. Falciani, C., L. Lozzi, A. Pini, F. Corti, M. Fabbrini, et al. 2007. Molecular basis of branched peptides resistance to enzyme proteolysis. Chem. Biol. Drug Des. 69: 216–21.

39. Bracci, L., C. Falciani, B. Lelli, L. Lozzi, Y. Runci, et al. 2003. Synthetic peptides in the form of dendrimers become resistant to protease activity. J. Biol. Chem. 278: 46590–5.

40. Bruschi, M., G. Pirri, A. Giuliani, S.F. Nicoletto, I. Baster, et al. 2010. Synthesis, characterization, antimicrobial activity and LPS-interaction properties of SB041, a novel dendrimeric peptide with antimicrobial properties. Peptides. 31: 1459–67.

41. Simmaco, M., G. Mignogna, D. Barra, and F. Bossa. 1993. Novel antimicrobial peptides from skin secretion of the European frog Rana esculenta. FEBS Lett. 324: 159–61.

42. Mangoni, M.L., D. Fiocco, G. Mignogna, D. Barra, and M. Simmaco. 2003. Functional characterisation of the 1-18 fragment of esculentin-1b, an antimicrobial peptide from Rana esculenta. Peptides. 24: 1771–7.

43. Mangoni, M.L., G. Maisetta, M. Di Luca, L.M.H. Gaddi, S. Esin, et al. 2008. Comparative analysis of the bactericidal activities of amphibian peptide analogues against multidrug-resistant nosocomial bacterial strains. Antimicrob. Agents Chemother. 52: 85–91.

44. Manzo, G., R. Sanna, M. Casu, G. Mignogna, M.L. Mangoni, et al. 2012. Toward an improved structural model of the frog-skin antimicrobial peptide esculentin-1b(1-18). Biopolymers. 97: 873–81.

45. Conlon, J.M., Y.H.A. Abdel-Wahab, P.R. Flatt, J. Leprince, H. Vaudry, et al. 2009. A glycine-leucine-rich peptide structurally related to the plasticins from skin secretions of the frog Leptodactylus laticeps (Leptodactylidae). Peptides. 30: 888–92.

46. Scorciapino, M.A., G. Manzo, A.C. Rinaldi, R. Sanna, M. Casu, et al. 2013. Conformational analysis of the frog skin peptide, Plasticin-L1, and its effects on production of proinflammatory cytokines by macrophages. Biochemistry. 52: 7231–41.

47. Scorciapino, M.A., G. Pirri, A.V. Vargiu, P. Ruggerone, A. Giuliani, et al. 2012. A novel dendrimeric peptide with antimicrobial properties: structure-function analysis of SB056. Biophys. J. 102: 1039–48.

2.1 Materials

Peptides. The synthetic form of natural peptides, Esc(1-18) (GIFSKLAGKKLKNLLISG-NH_2) and Plasticin-L1 (GLVNGLLSSVLGGGQGGGGLLGGIL) were purchased from ANASPEC (Campus Drive Fremont, CA, USA) at a purity of 98%, while the purity. The different analogues of the semi-synthetic peptide SB056 were synthesized using a standard solid-phase peptide fmoc (9-fluorenylmethyoxy-carbonyl) strategy in the laboratories of the Institute of Biological Interfaces-2 (IBG-2) at the Karlsruhe Institute for Technology (KIT, Karlsruhe, Germany), where I have spent 6 months during the present PhD work.

Reagents. Amino-acids and a NovaPEG Rink Amide resin (0.67 mmol/g) were purchased from Sigma-Aldrich (St. Louis, MO, USA) and Novabiochem (Merck Chemicals Ltd., Nottingham, UK). Peptide synthesis grade N,N-dimethylformamide (DMF), N-methylpyrrolidone (NMP), trifluoroacetic acid (TFA), dichloromethane, diethyl ether and O-(Benzotriazol-1-yl)-N,N,N',N'-tetramethyluronium hexafluorophosphate (HBTU) were purchased from ChemImpex (Wood Dale, IL, USA) and Sigma-Aldrich.

All the perdeuterated solvents employed, such as methanol-d4, chloroform-d, trifluoroethanol-d6, and dimethyl sulfoxide-d6 were purchased from Sigma-Aldrich with a purity ≥99%. Perdeuterated SDS-d25 and DPC-d38, as well as 3-(trimethyl-silyl)-2,2',3,3'-tetradeuteropropionic acid (TSP-d4), were purchased from Cambridge Isotope Laboratories (Andover, MA, USA) with a purity of 98%. 1-Palmitoyl-2-oleyl-*sn*-glycero-3-phosphocholine (POPC) and 1-palmitoyl-2-oleyl-*sn*-glycero-3-phosphoglycerol (POPG) sodium salt were purchased from Avanti Polar Lipids (Alabaster, AL, USA). All other reagents and solvents were purchased from Sigma-Aldrich.

2.1.1 Solid-phase fmoc synthesis of the SB056 analogues

Both the monomeric [WKKIRVRLSA-NH_2] and [KWKIRVRLSA-NH_2], and the dendrimeric $[WKKIRVRLSA]_2$-K-8Aoc-NH_2 and $[KWKIRVRLSA]_2$-K-8Aoc-NH_2 analogues of SB056 were synthesized with the C-terminus amidated (figure 5.1 in Chapter 5). In the following, they will be referred to as SB056-lin, β-SB056-lin, SB056-den and β-SB056-den, respectively). Both the dendrimeric peptides were synthesized as a branched dimer on a lysine scaffold with the 8-aminoctanamide as a lipidic tail. A manual standard solid-phase peptide fmoc (9-fluorenylmethyoxy-carbonyl) strategy was employed, working under nitrogen flow. Peptides were purified through RP-HPLC on a Jupiter Proteo analytical

C12 column supplied by Phenomenex (Torrance, CA, USA), using 0.1% TFA/H_2O as solvent A, and 0.1% TFA/MeCN as solvent B. The monoisotopic molecular mass of each peptide was determined by MALDITOF MS (Bruker Daltonik, Bremen, Germany), using sinapinic acid as acidic matrix. For details on the synthesis and purification protocol see [1].

2.2 Characterization of the three-dimensional structure with Nuclear Magnetic Resonance spectroscopy

Currently, NMR spectroscopy, together with X-ray crystallography, is one of the most suitable techniques for determining the three-dimensional structure of macromolecules at atomic resolution [7]. As far as HDPs are concerned, their folding upon membrane contact is one of the fundamental steps in the recognized modes of action of these molecules. The investigation of their three-dimensional structure is thus of primary importance to clarify the effective mechanism. The central goal of my Ph.D. thesis has been the structural characterization of the peptides of choice when interacting with different membrane-mimicking environments, with liquid state NMR spectroscopy as the main investigation technique.

2.2.1 Liquid state NMR spectroscopy

Liquid state NMR spectroscopy was confirmed as a useful tool for structural investigations of biomolecules by Kurt Wüthrich, whose group solved the first protein structure in 1984-1985 [2–4].The standard set of 2D (^{1}H, ^{1}H) NMR experiments usually applied to determine the secondary structures of proteins and peptides includes *double-quantum-filtered correlation spectroscopy* (DQF-COSY) and *total correlation spectroscopy* (TOCSY), for resonances assignment of the amino-acid spin systems, and *nuclear overhauser effect spectroscopy* (NOESY) for their sequential assignment and to establish the through-space correlations. Also, the ^{13}C chemical shift values provide useful structural information and $^{13}C^{\alpha}$ and $^{13}C^{\beta}$ amino acids chemical shifts can be collected through ^{1}H-^{13}C-heteronuclear single quantum coherence (HSQC) experiments. The ^{13}C resonances are then assigned on the basis of the known proton resonances obtained from ^{1}H homonuclear 2D NMR experiments [7].

The intent of this section is not to present a deep dissertation on the basis of NMR spectroscopy, but, a very brief description of the various two-dimensional techniques employed will be reported, with the aim to provide the non-expert readers with the fundamental information needed to fully understand the results and their discussion. For the

sake of brevity, I won't go into the mathematical details, and also the very specific and technical aspects will be keep to the minimum. The interested readers can refer to books and literature [5-9] dedicated to describe the basis of the technique.

2.2.1.1 Double-quantum filtered spectroscopy (DQF-COSY).

In the ^{1}H-^{1}H COSY-type experiments, cross-peaks arise due to coherence transfer between scalar coupled nuclear spins, which is mediated by the bonding electrons. In practice, this through-bond coherence transfer is limited to protons separated by two to three chemical bonds. The pulse sequence consists of two 90° pulses separated by a variable delay (t1). The recycle delay precedes the first pulse, and the acquisition period (t2) follows the second pulse, as shown in figure 2.1.

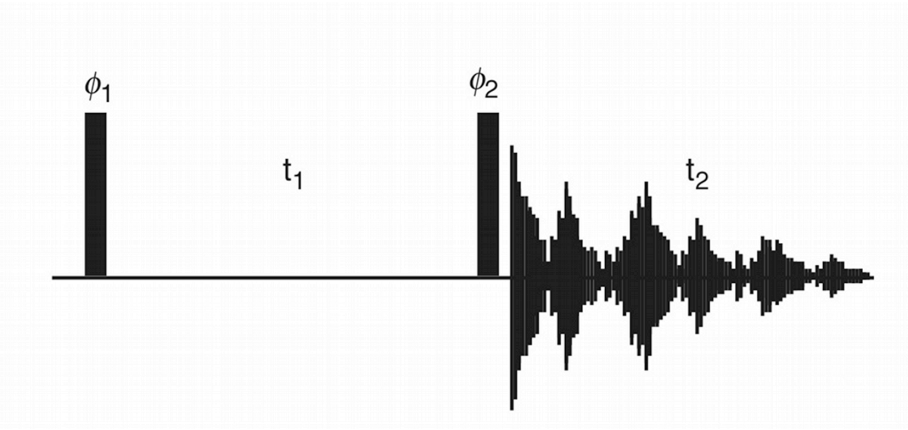

Figure 2.1. Pulse sequence of COSY experiment. Narrow bars represent 90° pulses. Figure from *Cavanagh et al.* [7]

The COSY spectrum is best used to identify correlations in the so-called fingerprint regions, usually containing well-resolved cross-peaks. The regions of interest are the $^{1}H^{N}$–$^{1}H^{\alpha}$ (the backbone fingerprint), the $^{1}H^{\alpha}$–$^{1}H^{\beta}$, the aromatic region comprising the resonances of phenylalanine, tyrosine, tryptophan, and histidine side chains, the aliphatic region with the valine, leucine, isoleucine, alanine and threonine methyl groups.

The double-quantum filtered COSY (DQF-COSY) experiment overcomes some of the drawbacks inherent to the standard COSY experiments. In particular, the narrower lineshape usually allows to observe cross-peaks close to the diagonal peaks, that might be obscured by the latter in a standard COSY spectrum. In addition, the multiplet fine structure of the cross-peaks is better resolved in DQF-COSY, allowing for the measurement of the corresponding $^{3}J_{HH}$ scalar coupling constants. The main disadvantage of using DQF-COSY is due to a twofold decrease in overall sensitivity and a longer phase cycle [7].

The scalar coupling constants are extremely important quantities since it can be related to the dihedral angle between the two couples nuclei through the Karplus equation (see below). Knowledge about dihedral angles provide valuable information, for instance, on the peptide backbone conformation and side chains orientation.

2.2.1.2 Total correlation spectroscopy (TOCSY).

Total Correlation Spectroscopy (TOCSY), also known by the acronym HOHAHA (homonuclear Hartmann–Hahn) spectroscopy, utilizes isotropic mixing to transfer in-phase magnetization between spins via the strong scalar coupling Hamiltonian. The result is that magnetization can be transferred through several couplings (thus, several chemical bonds) during the course of the mixing period. In the absence of relaxation, cross-peaks are potentially generated between all resonances within the same amino acid spin system. These observable cross-peaks are critical for successful completion of the spin system assignment.

The pulse sequence consists of two 90° pulses separated by a variable recycle delay (t1). Prior the acquisition period (t2) a Hahn echo is introduced to provide a flatter baseline. The mixing sequence between the two pulse blocks to allow magnetization transfer (figure 2.2).

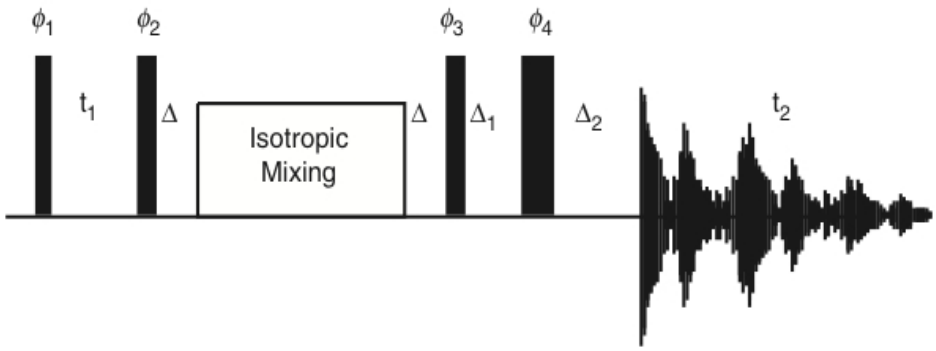

Figure 2.2. Pulse sequence of TOCSY experiment. The 90°-t1-90° block is followed by a mixing sequence and a Hahn echo, introduced prior to detection. Figure from *Cavanagh et al.* [7].

A fundamental aspect in experimental setting of a TOCSY experiment is the choice of a suitable mixing time. As the mixing time is increased, cross protons have even started to gain intensity. Thus, a maximization of transfer from $^1H^N$ to $^1H^\alpha$ will most likely be obtained with an isotropic mixing period of 35–45 ms in duration, while, in order to maximize transfer to protons distant from $^1H^N$, longer mixing times should be employed. Moreover, it is necessary to take into account also the relaxation processes since they reduce the intensity of all cross-peaks with increasing the mixing time and, thus, the pulse sequence overall length

[7]. In the case of proteins the size of ubiquitin, the maximal useful length of isotropic mixing is of the order of 100 to 120 ms; for larger proteins, this limit is shorter [7]. In the case of the peptides presented in this work, a mixing time of 80 ms represents a good compromise between reasonable magnetization transfer and minimum loss of signal intensity due to relaxation phenomenon.

2.2.1.3 Gradient Heteronuclear single-quantum coherence spectroscopy (gHSQC).

The statistical analysis of protein NMR chemical shifts revealed that also ^{13}C resonances are an important source of structural information. With respect to unfolded structures, $^{13}C^{\alpha}$ resonances shift at lower or higher frequencies in β-sheet and α-helical structures, respectively. Such empirical relationships enable the identification of specific secondary structural motives (α-helices or β-strands) in polypeptides. To collect ^{13}C chemical shifts it is necessary to apply heteronuclear spectroscopy. All multidimensional heteronuclear NMR experiments correlate the heteronuclear with ^{1}H resonances by a transfer of coherence (or polarization). In these experiments an indirect, or proton, detection is used in order to maximize sensitivity: ^{1}H spin polarization is initially transferred to the scalar coupled heteronucleus, the desired heteronuclear spin manipulations are performed, and the heteronuclear coherence is finally transferred back to the ^{1}H for detection. The two proton-detected heteronuclear correlation 2D experiments most commonly used are HSQC and HMQC, that differ for the kind of coherences evolving during the indirect evolution period and then transferred back to ^{1}H, i.e. single-quantum or multiple-quantum, respectively.

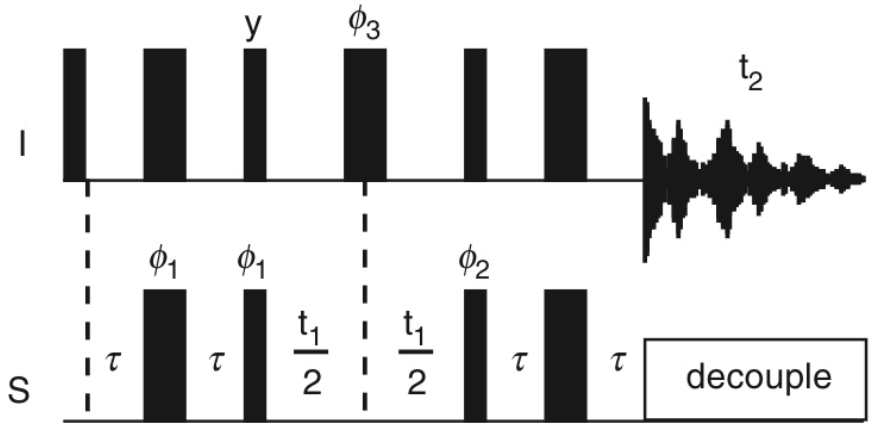

Figure 2.3. Pulse sequences for basic HSQC experiments. Thin bars represent 90° pulses and thick bars represent 180° pulses. Pulses are applied with x-phase unless the phase is indicated above the bar. Figure from *Cavanagh et al.* [7].

The pulse sequence of HSQC experiment is shown in figure 2.3. I and S represent two different nuclear spins. Two INEPT blocks are used to the transfer the I spin into single-quantum coherence before and back to ^{1}H magnetization for detection after the evolution period (t1). The 180° (I) pulse in the middle of the evolution period refocuses evolution of the 1H-heteronuclear J_{IS} scalar coupling interaction [7].

2.2.1.4 Nuclear overhauser spectroscopy (NOESY).

After all the resonances of the peptide's sequence have been assigned, every spin system is ascribed to a specific position in the polypeptide chain by using through-space dipolar coupling interactions, i.e. identifying the sequential connectivities between the spin systems. Dipolar coupled nuclei do not relax independently: cross-relaxation (relaxation between two spins) leads to magnetisation transfer between the spins and the resulting change in intensity is known as the nuclear overhauser effect (NOE). The population distribution of a nucleus can be affected by the population distributions of other nuclei that are nearby in space. Experimentally, the enhancement of the population difference of one nucleus can be observed by equalizing the levels population of a nearby one. An enhanced population difference gives rise to an enhanced NMR signal.

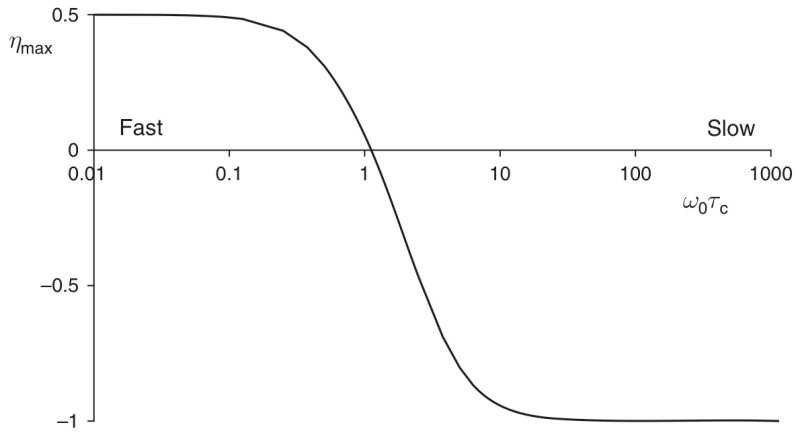

Figure 2.4. Dependence of NOE effect on molecular motions. The theoretical variation of the homonuclear NOE as a function of molecular tumbling rates as defined by $\omega_0\tau_c$, (where ω_0 is the spectrometer observation frequency, approximately equal to those of the hypothetical spins and τ_c is the correlation time of the molecule). Figure from Claridge's book, 2008 [9].

The rate of cross-relaxation, and thus the NOE enhancement factor is, among others, dependant on the inverse sixth power of the distance and on the motion of the molecule. The

NOE is caused by dipole–dipole interaction (through-space) of two nuclear magnets, modulated by the tumbling of the molecule in solution, ultimately affecting both the intensity and the sign of the NOE signal change [8]. For relatively small molecules, that tumble rapidly in solution (short τ_c), the NOE has a maximum possible value of +0.5 or 50%. At the other extreme, larger and/or immobilized molecules that tumble very slowly in solution experience negative NOEs. Between these two extremes is the intermediate region in which the NOE changes sign and even becomes zero. Within this region, the magnitude and sign of the NOE is highly sensitive to the rate of molecular motions and can be rather weak, possibly too weak to be observed (figure 2.4) [9].

Generally, the NOE can only be detected between ^1H nuclei that are separated by 5 Å or less. Thus, it is possible to correlate the so-called NOE intensity enhancement to the distance between the two nuclei. In a 2D NOESY experiments, it is the cross-peak intensity which provides information about inter-nuclear distances and these can then be used as distance restraints to determine accurate three-dimensional structures of proteins and peptides (see next section) [8]. Statistical analysis has shown that in proteins the majority of the short distance proton-proton couples are observed for residues adjacent in the primary sequence. Thus, identification of intense NOEs from $^1H^N$, $^1H^\alpha$, and/or $^1H^\beta$ of one spin system to $^1H^N$ of a second spin system suggests that the two spin systems are adjacent in the primary sequence, with the first spin system closer to the N-terminus of the peptide (i.e. the spin systems correspond to the amino acid residue *i* and *i+1*, respectively).

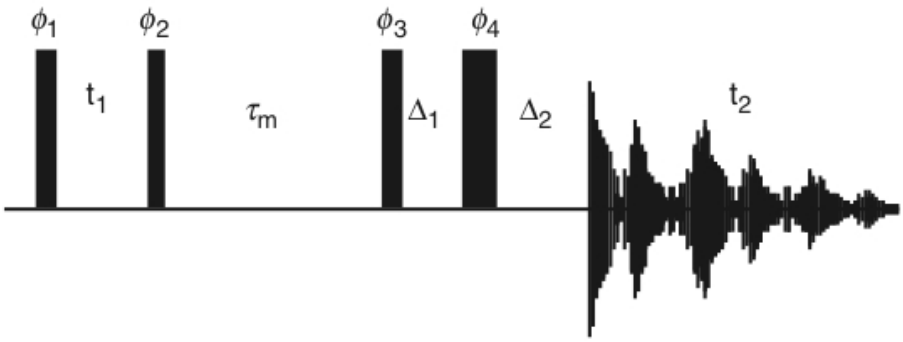

Figure 2.5. **Pulse sequence of NOESY experiment.** The 90°-t1-90° block is followed by a mixing sequence and a Hahn echo, introduced prior to detection. Figure from *Cavanagh et al.* [7].

The pulse sequence for the NOESY (figure 2.5) experiment involves a first 90°–t1–90° element to frequency label the spins and return the magnetization to the z-axis. Magnetization transfer occurs via dipolar coupling for a period τ_m (the mixing time) before observable transverse magnetization is created by the final 90° pulse. The final pulse can be

replaced by a Hahn echo sequence with a concomitant improvement in the flatness of the baseline. If NOESY mixing times are too short the cross-peaks will have a poor signal-to-noise ratio. At longer mixing times, on the other hand, the intensity of the NOESY cross-peaks will be no longer directly proportional to the distance between the interacting spins. This is due to the fact that time evolution of magnetization transfer is inherently exponential even for two isolated spins. In addition, magnetization might be transferred from the first 'receiving' nucleus to other nearby spins in complex molecule, with a probability that increases with increasing the mixing time. This multi-step magnetization transfer mechanism is known as 'spin diffusion' and is usually one of the most severe sources of deviation from linearity between NOE cross-peaks intensity and inter-nuclear distances. In the case of proteins and peptides, mixing times of 50–150 ms represent a good compromise between reasonable cross-peak intensities and intensity loss from spins relaxation and/or spin diffusion [7].

2.2.1.5 Experimental details

The above described types of experiments were applied for the NMR-characterization of peptides investigated in this work. NMR spectra were acquired at 298 K with a Unity Inova 500NB high-resolution spectrometer (Agilent Technologies, CA, USA) operating at a ^{1}H frequency of 500 MHz, equipped with a high-field indirect detection probe. All 2D experiments were recorded using 2048 complex points. In order to avoid the loss of cross-peaks due to relaxation or to insufficient transfer of magnetization, a mixing time of 80 ms (MLEV-17 spin-lock scheme) was applied for the acquisition of TOCSY experiments. The NOESY was recorded with a mixing time of either 50 or 100 ms, to avoid that signals were affected by spin diffusion. Since it revealed a better resolution of cross-peaks, heteronuclear spectroscopy was applied to collect chemical shifts of C^{α} and C^{β} atoms of peptides backbone through HSQC technique. Any change in the technical parameters is specified case by case in the text.

2.2.2 Solving peptide three-dimensional structure with NMR data

NMR data can be used to calculate the three-dimensional structure of biomolecules. The most important NMR-observables come from the NOESY experiments. In principle, the NOESY cross-peak intensity is proportional to the inverse sixth power of the distance between two interacting ^{1}H spins. Thus, observed could be converted in distance restraints to be included into a computer structure calculation, using a known reference distance such as between two methylenic or two aromatic ring protons. Anyway, such a linear relationship

between the cross-peak intensity and the inter-proton distance is rigorous for short mixing times, when spin diffusion and relaxation effects can be neglected. However, short enough mixing times are usually not feasible due to the resulting low signal to noise ratio. Longer mixing times have to be applied and deviation from cross-peak intensity / inter-proton distance linearity should be expected. Definitely, it has been found that it is better to give up the rigorous quantitative determination of the inter-proton distances and to group NOESY cross-peaks into different categories on the basis of their relative intensity (strong, medium and weak). An upper bound separation between the interacting spins is correspondingly associated to each category and used as restraint in the structure calculations..

Another important parameter is the ^{3}J coupling constant. Karplus [10] has shown that the magnitude of a ^{3}J scalar coupling constant is function of the dihedral angle formed by the three consecutive covalent bonds separating the two scalar-coupled spins:

(2.3) $$^{3}J_{H_i H_j} = A\cos^2\theta + B\cos\theta + C$$

The constants A, B, and C depend upon the particular nuclei involved, and θ is the dihedral angle defined for the two atoms i and j. The most important Karplus equation for proteins has been parameterized to relate for the backbone Φ dihedral angles to the corresponding $^{3}J_{H}{}^{N}{}_{H}{}^{\alpha}$ coupling constants.

The isotropic chemical shift values are also widely employed in peptide/protein structure determination. It is now well established that chemical shifts of backbone nuclei (e.g. $^{1}H^{\alpha}$, ^{13}CO, $^{13}C^{\alpha}$ and $^{13}C^{\beta}$) are sensitive to the molecular conformation. This correlation forms the basis for the chemical shift index (CSI) method, an useful tool to predict the presence of specific secondary structural motives in proteins. This is based on the difference between the observed chemical shift value and the one expected for the same residue in an unfolded peptide. Today, specific algorithm exist to couple the CSI method to known protein structures databases, allowing for a systematic comparison between the chemical shift values observed for the peptide/protein under investigation and those stored in the database for similar amino acid sequences. One of the most widely used is TALOS+ [11], that is able to provide an estimation of the most reliable values for the backbone Φ and Ψ angles given the experimental chemical shifts and the amino acid sequence.

2.2.3 Software calculation

Once all the possible experimental data are collected, they are converted into geometrical restraints and used as input parameters into the software for structure

calculations. These algorithms look for atomic coordinates able to satisfy the imposed restraints while exploring the protein/peptide conformational space. Structure calculations are usually repeated many times to finally identify an ensemble of low energy structures consistent with the peptide parameterized force-field and the input NMR data [7].

To determine the structures of peptides investigated in the present work, a simulated annealing protocol through Dynamo software (http://spin.niddk.nih.gov/NMRPipe/dynamo/) was applied. Dynamo uses molecular dynamics based simulated annealing to find sets of atomic coordinates that are consistent with the experimental and covalent (e.g. Van der Waals radius parameters for the atoms, expected bond distances and angles, and torsions) constraints. In a simulated annealing, the temperature of the system is initially rapidly increased, then kept at a high value for a given number of calculation steps, and finally slowly reduced to zero. Thus, in the early stages of the annealing procedure, the system has sufficient kinetic energy to overcome large potential energy barriers. As the system is cooled down its motions are gradually restricted to lower and lower energy structures until it is confined in the deepest energy minima. A sufficiently high starting temperature ensures that all the relevant conformational space is sampled, and a sufficiently slow cooling rate ensures that a very low energy structure is finally chosen. Cross-peaks NOE were grouped on the basis of their relative intensity as strong, medium, and weak, and an upper bound distance of 0.27, 0.33, and 0.50 nm, was respectively applied, to restraint the corresponding inter-proton distances. $^{3}J_{H^{N}H^{\alpha}}$ Coupling constants were collected from the one-dimensional ^{1}H spectra (when possible) and/or from the DQF-COSY and were used as restraints for Φ dihedral angles on the basis of Karplus equation (the following values were used as parameter in equation **2.2**: $\theta = \Phi - 60°$, A= 7.13, B= -1.31 and C= 1.56 [10]). Finally, the chemical shift values of $^{1}H^{\alpha}$, $^{1}H^{N}$, $^{13}C^{\alpha}$, and $^{13}C^{\beta}$ were analysed through the software TALOS+ [9], whose output was converted into torsion angle restraints for the structure calculations. In order to obtain statistically relevant results, one thousand structures were calculated in each case, and the 100 conformers with the lowest potential energy were selected for the analyses. The selected 100 conformers were aligned, and the RMSD of the backbone heavy atoms was calculated with respect to the average structure.

2.3 Biophysical and microbiological characterization

Despite liquid-state NMR was the primary technique of choice for the present work, in the light of the strong multidisciplinary character of the topic, many other different techniques

have been employed in order to complement the NMR structural characterization. In the following, a brief description of the methodologies I personally applied is provided.

2.3.1 Assessment of biological activity

Biological (antimicrobial) activity of SB056's analogues was tested *in vitro* using minimal inhibitory concentration (MIC) assays based on resazurin incorporation. Resazurin is an redox indicator used for the evaluation of cell growth, particularly in various cytotoxicity assays. It is a blue non-fluorescent and non-toxic dye that becomes pink and fluorescent when reduced to resorufin by oxidoreductases within viable cells [13].

2.3.1.1 Experimental details

The MIC of both linear and dendrimeric peptides was determined against four standard strains, *Escherichia coli* (*E. coli*) ATCC 25922, *Pseudomonas aeruginosa* (*P. aeruginosa*) ATCC 27853, *Staphylococcus aureus* (*S. aureus*) ATCC 25923 and *Enterococcus faecalis* (*E. faecalis*) ATCC 29212, two Gram-negative and two Gram-positive bacteria, respectively. The MIC tests were realized using a two-fold broth dilution assay modified from the method of *Amsterdam et al*. [14]. Moreover, in order to investigate the effect of the presence of electrolytes at physiologic concentration on peptides' antimicrobial activity, the same MIC assays have been performed in the presence of 150 mM NaCl. Bacteria were grown in several steps in Mueller-Hinton (MH) broth at 310 K with continuous shaking at 200 rpm, till the solution gained an optical density (OD) of 2.0 at 550 nm. Then, the culture was diluted with MH broth up to a final bacterial concentration of 10^6 CFU/mL. MIC values were determined in a sterile 96-well polystyrene microtiter plate (total volume 100 μL), where the peptide was added to each well by following a serial dilution of the peptide stock solution. Finally, 50 μL of bacterial suspension were inoculated in each well (final bacterial concentration = $5x10^5$ CFU/mL). In the case of added NaCl, no changes were applied to the bacteria grown method described above, but in each well of the microtiter plate we simply used a MH broth supplemented with the proper amount of NaCl.

2.3.2 Surface-pressure analyses

Surface-pressure analyses were performed to investigate peptide insertion into lipid monolayers. The technique measures the increase of lipid monolayer surface pressure (π) due to peptides intercalating between the phospholipids, mimicking peptide interaction and insertion in biological membranes. Briefly, starting from different initial monolayer surface pressures π_0, a fixed amount of peptide is injected in the monolayer subphase and the surface

pressure is monitored until plateau is reached. The difference between the final and the starting surface pressure $\Delta\pi$ is plotted vs. π_0 and the data are finally fitted with a straight line. Usually, the intersection point with both the x- and y-axis is taken into account for results interpretation and peptides comparison [1, 15–17]. The intersection point with the x-axis is referred to as *exclusion pressure* π_{ex}, i.e. the monolayer surface pressure preventing further peptide insertion. The intersection point with the y-axis is simply referred to as $\Delta\pi_{max}$, and is the maximum surface pressure difference extrapolated at a monolayer starting pressure of zero (see figure 2.6 for an example of data analysis). This technique is described in details in the reviews by *Maget-Dana* and *Brockman* [15, 16].

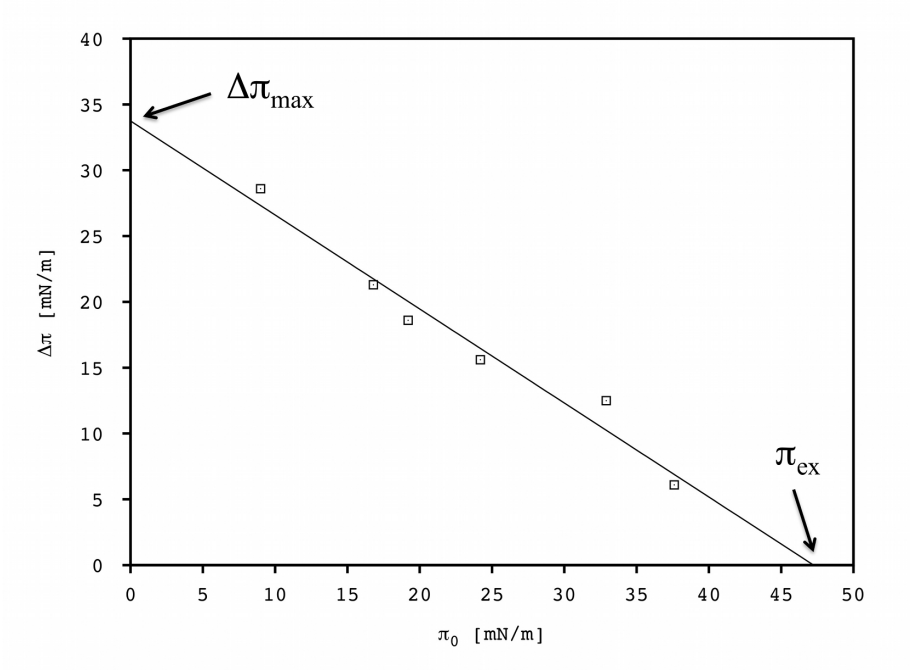

Figure 2.6. Example of surface-pressure analysis data. An example of data analysis for surface-pressure measurements is reported. Data of $\Delta\pi$ vs. π_0 are fitted with a least square procedure and then $\Delta\pi_{max}$ and π_{ex} values are taken into account for data interpretation and comparison.

2.3.2.1 Experimental details

Surface-pressure measurements were applied to investigate the intercalation properties of SB056 peptides analogues. The surface pressure was measured with a Wilhelmy wire attached to a microbalance (DeltaPi, Kibron Inc., Helsinki). Peptide penetration was monitored by recording the increase in surface pressure of the lipid film over the 35 min following peptide injection into the subphase.

2.3.3 Fluorescence spectroscopy

Fluorescence occurs when a molecule in the excited state returns to the ground state by loosing excitation energy as radiation instead of heat. Thus, fluorescence involves two processes: absorption and subsequent emission. The emission spectrum represents the variation of the fluorescence intensity with the wavelength of the emitted light. Fluorescence is very sensitive to the molecular environment, which can affect in different ways the various parameters (e.g. the position of the maximum in the emission spectrum, the quantum yield and the lifetime of the excitation state). This fluorescence's sensitivity to the environment makes this technique particularly useful to obtain information on different biophysical phenomena by changing the conditions of the system investigated. The main fluorophores used in biochemistry can be classified into natural fluorophores and fluorescent indicators, or probes. Natural fluorophores include aromatic amino-acids, allowing to extensively use fluorescence spectroscopy in the study of proteins and peptides. Tryptophan results to be the most sensitive standard amino acid with the highest quantum yields and, thus, it is the most used. However, due to the low number of natural fluorophores and their relative scarcity in natural sequences, many applications involve the addition of fluorescent probes or a suitable labelling reagents to the system under study [18]. In the present study, fluorescence spectroscopy was applied to characterize the biophysical behaviour of peptides. In particular, investigations on the membrane binding properties of SB056 peptides were performed.

2.3.3.1 Binding study.

Peptide binding to lipid vesicles can be investigated following the changes in the tryptophan emission spectra with the increasing of lipid concentration. Upon peptide binding, the tryptophan moves from the buffered water to the more hydrophobic environment of the lipid bilayer. Typically, this leads to a blue shift and an increase in the quantum yield of tryptophan fluorescence [19, 20]. Practically, peptide-lipids is monitored through titration of a fixed amount of peptide with increasing the lipids concentration. The variation of either tryptophan fluorescence intensity or position are reported vs. lipid concentration. If a low affinity binding is considered, experimental data can be fitted using the following equation:

(2.4)
$$F = (F_0 + F_1 K_a [L_{tot}]) \Big/ (1 + K_a [L_{tot}])$$

where F is the fluorescence intensity at a given lipid concentration, F_0 the fluorescence intensity at the beginning of the titration (absence of vesicles), F_1 the fluorescence intensity at the end of the titration (when plateau is reached), K_a is the association constant and $[L_{tot}]$ is

the total lipid concentration, which for low affinity binding can be assumed to be equal to the total lipid concentration [20]. This is an hyperbolic function, indicating the tendency of the binding process to reach a characteristic saturation value (see figure 2.7 for an example).

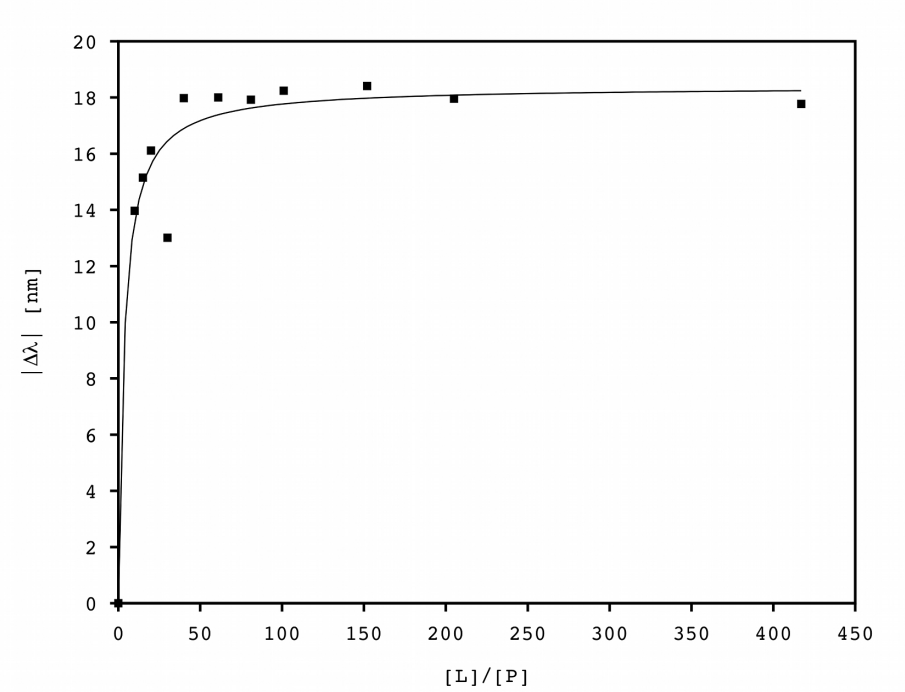

Figure 2.7. Example of binding fitting of fluorescence data. Tryptophan signal shifts with the increasing amount of lipids is plotted vs. lipid/peptide molar concentration (that is lipid concentration since peptide amount is fixed). Data describes a saturation curve which can be fitted with the model proposed from *Christiaens et al.* [20].

2.3.3.2 Experimental details

The binding experiments were performed with a LS55 Luminescence Spectrometer (Perkin-Elmer, Waltham, MA, USA) equipped with a thermostatic cuvette holder. Intrinsic fluorescence of tryptophan was measured at 300 K (i.e. above the phase transition temperature of 271 K for the lipids employed) by recording the emission spectrum between 300 and 450 nm. The excitation wavelength was set at 280 nm; beam entry and exit slit width was set at 5 nm. Peptide was added at a final concentration of 1 μM to the buffered liposomes dispersion. Proper aliquots of the liposomes stock solution have been diluted, in order to obtain lipid/peptide molar ratios ranging between 0 to 400. The LUV dispersion before peptide addition was used to perform spectrum background subtraction. For each peptide, the titration with lipids was performed either in the absence and in the presence of 150 mM NaCl in the phosphate buffer (pH 7.4), to investigate the effect of a physiologic electrolyte concentration on the binding process. An attempt to carry out the same measurements on

Esc(1-18) was performed by following the fluorescence of phenylalanine (this peptide is devoid of tryptophan residues) but, unfortunately, the quantum yield of this natural fluorophore was not sufficient to obtain spectra of good quality in this case.

2.3.4 Synchrotron radiation (SR) and conventional circular dichroism (CD)

Plane polarized light can be viewed as being made up of two circularly polarized components of equal magnitude, one rotating counter-clockwise (left handed, L) and the other clockwise (right handed, R). Circular dichroism (CD) refers to the differential absorption of these two components which results in a radiation with an elliptical polarization. A CD signal will be observed when a molecule has some chiral centers and thus it is optically active. CD is an useful tool to obtain information on secondary structure of peptides. One of the chromophores of interest is the peptide bond, which has a characteristic absorption in the range below 240 nm: a weak broad $n \rightarrow \pi^*$ transition centered around 220 nm and a more intense $\pi \rightarrow \pi^*$ transition around 190 nm. The different types of secondary structural motives found in proteins give rise to characteristic CD spectra in the far UV (figure 2.8) (for a detailed review on the technique see *Kelly et al. 2005* [21]).

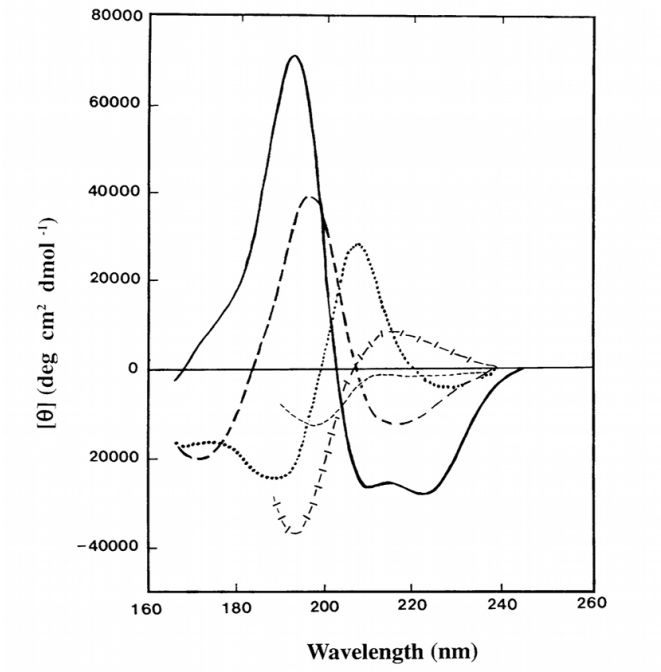

Figure 2.8. Far UV CD spectra of different types of secondary structures. Solid line, α-helix; long-dashed line, an anti-parallel β-sheet; dotted line, type II β-turn; cross dashed line, extended 3_{10}-helix or poly (Pro) II helix; short dashed line, irregular structure. Image taken from *Kelly et al. 2005* [21].

Conventional CD spectroscopy often shows severe spectral distortions when approaching 190 nm, making the resulting spectral shape difficult to interpret. These distortions are mostly due to insufficient incident radiation intensity below 190 nm and severe scattering artifacts when liposomes are employed as membrane-mimicking models.

Synchrotron radiation (SR) CD, on the other hand, offers different advantages over conventional CD [22]. At wavelengths below 190 nm synchrotron radiation is orders of magnitude more intense than that typically available in conventional instruments, allowing spectra to be obtained well into the vacuum ultraviolet region. Additional electronic transitions occur in that wavelength region, consequently the data acquired contain more information than conventional CD spectra. In addition, the greater intensity of the synchrotron light source provides a better signal-to-noise ratio (S/N) in the spectra collected with SRCD instruments.

2.3.4.1 Experimental details

Esc(1-18) folding propensity in water and in different mixtures with increasing amounts of TFE was investigated with conventional CD spectroscopy. Spectra were collected with a JASCO J-600 spectropolarimeter (Department of Biochemical Sciences ‘‘A. Rossi Fanelli’’, University of Rome ‘La Sapienza’) with a 1 mm path length cell. Spectra were recorded at 0.5 nm wavelength intervals in the 195–250 nm range, at 298 K, and at a peptide concentration of 100 μM. For each spectrum, CD data from eight scans were averaged.

SRCD (ANKA facilities-KIT, Karlsruhe, Germany) was used to investigate secondary structure of SB056’s analogues in the presence of lipid vesicles. Measurements were performed with 13.1 μm path length CaF_2 cells acquiring the spectrum between 180 and 260 nm. Spectra were recorded at 293 K. Three spectra were acquired and averaged for each sample.Weighted amounts of SB056 and analogues were dissolved in 10 mM PB to obtain stock solutions at a concentration of 25 mg/mL. Then, SRCD samples were prepared by adding a proper aliquot of peptide stock solution to the liposome dispersion in order to obtain a final lipid/peptide molar ratio of 25. The average spectrum was corrected by subtracting the corresponding spectrum of SUV dispersion in the absence of the peptide.

2.4 Membrane models

The interaction of HDPs with eukaryotic and prokaryotic plasmatic membranes is a fundamental step of their biologic activity. This interaction is favoured by the characteristic amphipathic structure adopted by these peptides. In order to better understand the mode of action of HDPs in defending the host from infections, it is necessary to deeply understand the structural properties and the biophysical behaviour of HDPs when they come into contact with lipid bilayers. Due to the extreme complexity of intact cells membranes, suitable models to mimic the lipid membranes are useful and sometimes necessary for biophysical

investigations. Many different membrane-mimicking models are reported in the literature with different complexity and characteristics, depending on the purposes and the specific technique to apply.

2.4.1 Surfactant micelles

Liquid state NMR has been the primary technique in the present thesis to obtain the atomic level three-dimensional structure of the membrane bound peptides. The main issue with this technique is the impossibility to work with peptide/membrane assemblies larger than 10^5 Da, since it would lead to slow molecular tumbling in solution and a consequently excessive broadening of the NMR resonances. Surfactant micelles represent a good compromise in this case, since they allow to study the peptide structure and obtain, still, physiologic relevant results [23, 24]. Surfactants are, generally speaking, amphipathic molecules consisting of a polar headgroup and a hydrophobic tail that spontaneously form compact structures above a specific critical micellar concentration (CMC). These structures are characterized by having the headgroups in contact with the external aqueous solvent, whereas the tails are packed in the micelle core [25]. The negatively charged sodium dodecylsulphate (SDS) and the zwitterionic dodecylphosphocholine (DPC) are the most widely used detergents in the field of antimicrobial peptides. Pure DPC micelles are usually used to mimic eukaryotic membranes, because DPC has exactly the same headgroup (e.g. phosphatidylcholine) of the predominant class of lipids in eukaryotic membranes. On the other hand, pure SDS micelles are used as models for bacterial membranes, in order to mimic the net negative charge of the typical prokaryotic lipid bilayers. However, since the latter are only rarely constituted only of negatively charged phospholipids [26, 27], for this study it was decided to use mixed DPC/SDS micelles at different molar ratios, thus tuning the net surface charge of this membrane model. In the literature there are only very few examples of application of such mixed micelles and, to the best of my knowledge, there are not systematic investigations aimed to ascertain whether mixed micelles are actually formed. Their use has been validated by one of our recent studies, where the CMC for different DPC/SDS mixtures has been determined. By applying both the RST and Motomura's formalism, we showed that these two surfactants are actually synergic and form mixed micelles in both deionised water and phosphate buffer solution (10 mM; pH 7.4) at 298 K, and thus it is possible to prepare mixed DPC/SDS micelles with different composition to be used as membrane-mimicking models [28].

2.4.1.1 Experimental details

In order to prepare these mixed micelles, proper amounts of SDS and DPC are weighted and solubilized in 10 mM phosphate buffer solution (PB) to obtain the desired DPC/SDS and L/P molar ratio (typically equal to 100). Micelles solution is then vortexed, sonicated for 10 min and left to equilibrate at room temperature overnight. Finally, the micelle dispersion is used to solubilise the peptide (powder). Typically, the final peptide concentration was 4 mM.

2.4.2 Lipid monolayers

If spread at the air/water interface, lipids form monolayers with the tails exposed to the air and the polar heads immersed in the polar solvent. The monolayer technique is particularly suitable to investigate the interactions of HDPs with lipids, since they act at the membrane/water interface. A detailed review on the biophysical properties of lipid monolayers can be found in the *Maget-Dana*'s work of 1999 [15].

2.4.2.1 Experimental details

In the present work, lipid monolayers have been used to investigate peptides ability/tendency to intercalate between the lipids by following the changing in the surface-pressure. In order to mimic the eukaryotic as well as different types of prokaryotic membranes (the former characterized by zwitterionic phospholipids, while the latter by a moderate to a large molar fraction of negatively charged lipids [26, 27]) different mixtures of the zwitterionic lipid POPC and the negatively charged lipid POPG were used. These were the lipids of choice because of their relatively low transition temperature (271 K). It was thus possible to work at room temperature, well above the lipids transition temperature. Proper amounts of lipids were dissolved in chloroform/methanol (1/1 V/V) and spread at the air/buffer (10 mM PB) interface of a 0.50 mL subphase in a circular glass well. After spontaneous organic solvents evaporation the lipid monolayer is formed and results to be stable, as it is shown by a fairly constant surface pressure reading. After this stabilization stage, the peptide was injected into the subphase at a final concentration of 1μM. All the measurements have been performed at room temperature.

2.4.3 Lipid vesicles (or liposomes)

One of the problems connected to the use of micelles in peptide-lipid investigations is represented by their excessive curvature. In this respect, micelles surface is certainly far from an ideal flat lipid bilayer, and such a high curvature might interfere with peptide native

folding [24]. In additon, micelles are not bilayered molecular assemblies. These are the two main reasons why liposomes, often called vesicles, are preferentially used as membrane model to study the peptide-membrane interactions. Liposomes are water-filled spherical assemblies characterized by one or more lipid bilayers (i.e. uni- or multilamellar vesicles, respectively). Compared to the detergent micelles, liposomes are more suitable to mimic the plasma-membranes since they are constituted by phospholipids and, being usually one or more order of magnitude larger, are characterized by a lower curvature.

2.4.3.1 Experimental details

In this thesis, vesicles were used to characterize the biophysical and structural behavior of selected HDPs, through fluorescence and CD spectroscopy.

Large unilamellar vesicles (LUV) and small unilamellar vesicles (SUV) were used for fluorescence and CD investigations, respectively. Proper amounts of POPC and POPG were dissolved in chloroform/methanol solutions (1/1 V/V). The solvents were evaporated under a gentle stream of nitrogen, followed by overnight vacuum pumping to remove any residual. The resulting lipid film was hydrated with 10 mM phosphate buffer solution (PB, pH 7.4) and multi-lamellar vesicles (MLV) were formed by vortexing for 5x1 min, followed by 5 freeze-thaw cycles. Afterwards, LUVs were prepared with the extrusion method, i.e. by passing the MLVs dispersion 11 times through two different pore-size (namely 400 and 100 nm) Nuclepore polycarbonate filters (Whatman Inc., Piscataway, NJ), using the Avanti® mini-extruder (Avanti Polar Lipids). SUVs were obtained by sonication of the MLVs dispersion for 4x4 min in a high-power ultrasonic cup horn bath (UTR 200, Hielscher, Germany).

For the structural investigations with SRCD spectroscopy, weighted amounts of SB056 and analogues were dissolved in 10 mM PB to obtain stock solutions at a concentration of 25 mg/mL. Then, SRCD samples were prepared by adding a proper aliquot of peptide stock solution to the liposome dispersion in order to obtain a final lipid/peptide molar ratio of 25. The average spectrum was corrected by subtracting the corresponding spectrum of SUV dispersion in the absence of the peptide.

2.5 References

1. Scorciapino, M.A., G. Pirri, A.V. Vargiu, P. Ruggerone, A. Giuliani, et al. 2012. A novel dendrimeric peptide with antimicrobial properties: structure-function analysis of SB056. Biophys. J. 102: 1039–48.

2. Havel, T., and K. Wüthrich. 1984. A distance geometry program for determining the structures of small proteins and other macromolecules from nuclear magnetic resonance measurements of intramolecular ^{1}H-^{1}H proximities in solution. Bull. Math. Biol. 46: 673–98.

3. Billeter, M., M. Engeli, and K. Wüthrich. 1985. Interactive program for investigation of protein structures based on ^{1}H NMR experiments. J. Mol. Graph. 3: 79–83.

4. Wang, G. 2010. Structural studies of antimicrobial peptides provide insights into their mechanism of action. In: Antimicrobial Peptides: discovery, design and novel therapeutic strategies. G. Wang (ed.), CABI, Wallingford, UK, 116 –27

5. Ernst, R.R., G. Bodenhausen, and A. Wokaun. 1987. Principles of Nuclear Magnetic Resonance in One and Two Dimensions. The International Series of Monographs on Chemistry, M.L.H. Green, et al (eds.). Oxford University Press.

6. Aue, W.P., E. Bartholdi, and R.R. Ernst. 1976. Two-dimensional spectroscopy. Application to Nuclear Magnetic Resonance. J. Chem. Phys. 64: 2229–46.

7. Cavanagh, J., W. Fairbrother, A.G. Palmer III, M. Rance, and N.J. Skelton. 2007. Protein NMR Spectroscopy–Principles and Practice. Elsevier Academic Press, Oxford.

8. Jacobsen, N.E. 2007. NMR spectroscopy explained. Simplified theory, applications and examples for organic chemistry and structural biology. John Wiley & Sons, Inc., Hoboken, NJ.

9. Claridge, T.D.W. 2009. High-resolution NMR techniques in organic chemistry. (Second edition), Elsevier, Amsterdam.

10. Karplus, M. 1959. Contact Electron-Spin Coupling of Nuclear Magnetic Moments. J. Chem. Phys. 30: 11–15 .

11. Shen, Y., F. Delaglio, G. Cornilescu, and A. Bax. 2009. TALOS+: a hybrid method for predicting protein backbone torsion angles from NMR chemical shifts. J. Biomol. NMR. 44: 213–23.

12. Habeck, M., W. Rieping, and M. Nilges. 2005. Bayesian estimation of Karplus parameters and torsion angles from three-bond scalar couplings constants. J. Magn. Reson. 177: 160–5.

13. Sarker, S.D., L. Nahar, and Y. Kumarasamy. 2007. Microtitre plate-based antibacterial assay incorporating resazurin as an indicator of cell growth, and its application in the in vitro antibacterial screening of phytochemicals. Methods. 42: 321–4.

14. Amsterdam, D. 1996. Susceptibility testing of antimicrobials in liquid media. In: Lorian V, editor. Antibiotics in Laboratory Medicine. Baltimore: Williams & Wilkins. 52–111.

15. Maget-Dana, R. 1999. The monolayer technique: a potent tool for studying the interfacial properties of antimicrobial and membrane-lytic peptides and their interactions with lipid membranes. Biochim. Biophys. Acta. 1462: 109–40.

16. Brockman, H. 1999. Lipid monolayers: why use half a membrane to characterize protein-membrane interactions? Curr. Opin. Struct. Biol. 9: 438–43.

17. Zhao, H., A.C. Rinaldi, A. Di Giulio, M. Simmaco, and P.K.J. Kinnunen. 2002. Interactions of the antimicrobial peptides temporins with model biomembranes. Comparison of temporins B and L. Biochemistry. 41: 4425–36.

18. Campbell, I.D., and R.A. Dwek. 1984. Fluorescence. In: Biological Spectroscopy. The Benjamin/Cummings Publishing Company, Inc., Menlo Park, CA, 91-125.

19. Zhao, H., and P. Kinnunen. 2002. Binding of the antimicrobial peptide temporin L to liposomes assessed by Trp fluorescence. J. Biol. Chem. 277: 25170–77.

20. Christiaens, B., S. Symoens, S. Vanderheyden, Y. Engelborghs, A. Joliot, et al. 2002. Tryptophan fluorescence study of the interaction of penetratin peptides with model membranes. Eur. J. Biochem. 269: 2918–26.

21. Kelly, S.M., T.J. Jess, and N.C. Price. 2005. How to study proteins by circular dichroism. Biochim. Biophys. Acta. 1751: 119–39.

22. Miles, A.J., and B.A. Wallace. 2006. Synchrotron radiation circular dichroism spectroscopy of proteins and applications in structural and functional genomics. Chem. Soc. Rev. 35: 39–51.

23. Damberg, P., J. Jarvet, and A. Gräslund. 2001. Micellar systems as solvents in peptide and protein structure determination. Methods Enzymol. 339: 271–85.

24. Mäler, L., and A. Gräslund. 2009. Artificial membrane models for the study of macromolecular delivery. Macromol. Drug Deliv. 480: 129–39.

25. Seddon, A.M., P. Curnow, and P.J. Booth. 2004. Membrane proteins, lipids and detergents: not just a soap opera. Biochim. Biophys. Acta. 1666: 105–17.

26. Shaw, N. 1974. Lipid Composition as a Guide to the Classification of Bacteria. Adv. Appl. Microbiol. 17: 63-108.

27. Epand, R.M., and R.F. Epand. 2009. Domains in bacterial membranes and the action of antimicrobial agents. Mol. Biosyst. 5: 580–7.

28. Manzo, G., M. Carboni, A.C. Rinaldi, M. Casu, and M.A. Scorciapino. 2013. Characterization of sodium dodecylsulphate and dodecylphosphocholine mixed micelles through NMR and dynamic light scattering. Magn. Reson. Chem. 51: 176–83.

3.1 Introduction and background

Among the different natural sources, the skin of amphibians is a particularly rich source of AMPs, with each species producing its own specific set of peptides. These are stored in granules of holocrine-type dermal glands and released into skin secretions as a reaction to stress, injury, or upon contact with microorganisms [1–3].

Four peptide families were extracted from the granular skin glands of the European edible frog *Pelophylax lessonae/ridibundus* (previously classified as *Rana esculenta*) (figure 3.1), with the Esculentin-1 family being the most potent one, against Gram-positive and Gram-negative bacteria as well as fungi, with negligible effects on eukaryotic cell membranes [4–6]. Several studies reported results on the Esculentin-1 family members' biologic activity. The 46-mer Esculentin-1b resulted to be the most promising peptide as a possible candidate to be developed as drug [4]. It was found that its antimicrobial activity is due to the N-terminal fragment encompassing the first 18 residues (Esc(1-18): GIFSKLAGKKLKNLLISG-NH_2) [1, 6, 7].

Esc(1-18) is active against different bacterial species, especially Gram-negative, while shows negligible effects on mammalian cells, such as erythrocytes [1, 6]. It was found to have a high binding affinity for lipopolysaccharides, the main constituents of Gram-negative bacteria outer membrane [8]. Remarkably, unlike other AMPs, it displays a comparable activity in the presence of human serum [1, 8], indicating that the peptide preserves its antibacterial activity also under conditions close to those encountered in vivo. The permeation of both the outer and inner membranes is thought to be responsible for the observed synergism of Esc(1-18) with conventional antibiotics, which is presumably exerted by increasing the intracellular influx of the drugs [8]. In addition, it has been shown for the first time how an amphibian AMP can affect the protein expression profile of its bacterial target [8]. However, while many data are available on the biologic activity side, detailed information on the structure-function relationships are still lacking. A canonical straight α-helix has been proposed for the entire peptide sequence on the basis of some CD spectra. Similarly to what is usually observed for most of the known AMPs, Esc(1-18) was found to be unstructured in water, while adopting a helical conformation when bound to lipid vesicles [8]. Clearly, these scarce structural information were not sufficient to elucidate Esc(1-18) mechanism of action at a molecular level and, eventually, to move ahead toward its optimization as a rationally designed drug.

Figure 3.1. *Pelophilax lessonae/ridibundus* (ex *Rana esculenta*). Frog species from which the Esculentin peptide families were isolated: on the left, *Pelophylax lessonae* (photo by © Jan van der Voort) and on the right, *Pelophylax ridibundus* (photo by © Denis Coso).

3.2 Results

3.2.1 Toward an improved structural model: Esculentin-1b(1-18) in 30% and 50% TFE solutions

Before using sophisticated membrane models, it is fundamental to investigate the inherent folding propensity of the peptide, solely due to its specific amino acid sequence, in order to obtain an element of comparison when changing the various chemico-physical parameters of the environment. Thus, first the primary structure of Esc(1-18) was analysed through several secondary structure prediction web-tools, then, 2,2,2-trifluoroethanol (TFE)/water mixtures were used as pro-folding environment to test the inherent tendency of Esc(1-18) sequence to some particular structural motif [9].

3.2.1.1 Sequence analysis

Figure 3.2a shows the hydropathicity plot for Esc(1-18), where amino acids are ranked according to their relative hydrophobic character. Values have been calculated according to the method of Kyte and Doolittle [10] and the scale has been normalized between 0 and 1. Thus, the higher the value, the more hydrophobic is the residue. Hydrophilic and hydrophobic residues appear to be not uniformly distributed along the peptide sequence, with the formers being concentrated from S4 to K12, while the presence of a hydrophobic cluster is evident from L14 to I16.

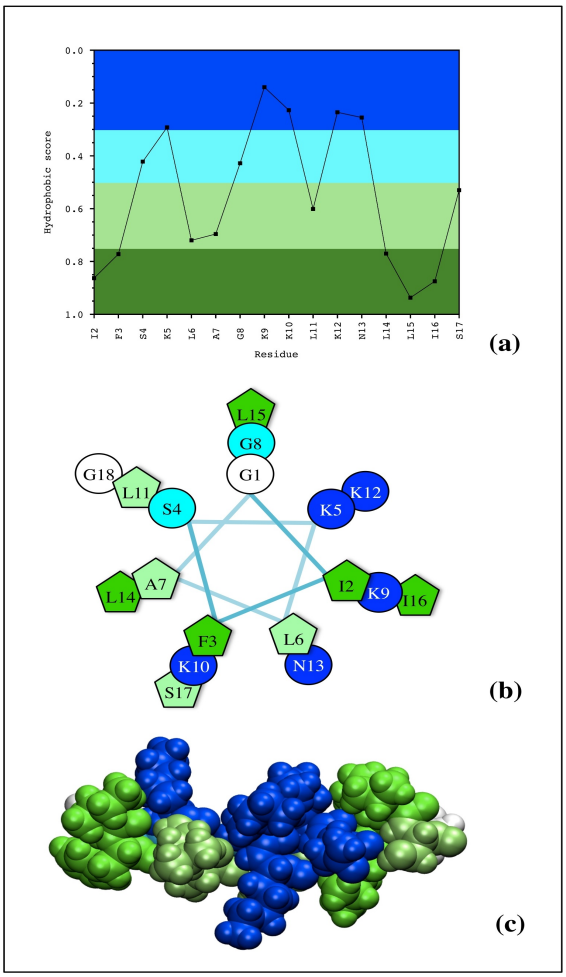

Figure 3.2. The α-helical model of Esc(1-18). (a) The hydropathicity plot calculated using the method of Kyte and Doolittle (window of three residues and a weight of 30% at the window edges) and then scaled between 0 and 1. The higher the value the more hydrophobic is the residue. The y-axis has been reversed in order to have hydrophobic residues located at the bottom and hydrophilic residues at the top of the graph. Residues have been divided in four categories: strongly hydrophobic (green), weakly hydrophobic (light green), weakly hydrophilic (cyan), and strongly hydrophilic (blue). The same colour scheme has been used in both (b) the helical wheel plot and (c) the corresponding 3D model. In the helical wheel plot (b), all the hydrophobic residues are represented as pentagons, while the hydrophilic ones are shown as circles. In (c) Van der Waals radii have been used to represent the atoms as spheres.

Figure 3.2b shows the helical wheel plot, where residues are arranged according to an ideal α-helical folding (top-view), comprising the whole peptide sequence as proposed in the literature [8]. On the basis of the values reported in figure 3.2a, residues have been classified as strongly hydrophobic, weakly hydrophobic, weakly hydrophilic, and strongly hydrophilic, and they have been accordingly colored in green, light green, cyan, and blue, respectively. Figure 3.2c shows the corresponding 3D picture (side-view). Even if a more hydrophilic side (and thus a more hydrophobic) can be guessed on the basis of the two-dimensional helical wheel plot (figure 3.2b and see also [8]), it can be seen that every side of the hypothesized α-helical conformation actually presents both hydrophilic and hydrophobic residues. Indeed, taking also the third dimension into account (figure 3.2c), it is clear that a canonical straight α-helix extending from the N- to the C-terminus does not provide, really, an amphipathic character to the Esc(1-18) as a whole, but rather the hydrophilic and the hydrophobic sides gradually ‘twist’ around the helix axis, to be finally turned upside down at the C-terminus.

When the Agadir algorithm (http://agadir.crg.es), [11–14] was used to predict the helical propensity of Esc(1-18) amino acid sequence, a helical fraction of only 42–46% of the sequence was obtained. A more detailed prediction could be obtained with the CFSSP server [15, 16] (http://www.biogem.org/tool/chou-fasman), resulting in a helical structure from I2 to K12 and an unfolded conformation for the rest of the sequence.

3.2.1.2 Structure investigation through CD and liquid state NMR spectroscopy

TFE is widely used in AMPs structural investigations [17] as an isotropic membrane-mimicking solvent, able to promote and facilitate peptide folding [18, 19]. Despite TFE forms neither a real lipid bilayer nor a detergent micelle in water, it is reported to act in the context of a pre-existing folded/unfolded equilibrium, shifting the latter toward a more structured conformation [18]. This effect would result from TFE clusters (in water) locally assisting peptide folding by both providing a solvent matrix that promotes interactions between the hydrophobic amino acid side chains, and favouring intra-molecular hydrogen bonds formation [19].

CD spectra of the peptide dissolved in water and in different water/TFE solutions are shown in figure 3.3. The spectra obtained both in pure water and in the 10% v/v TFE/water

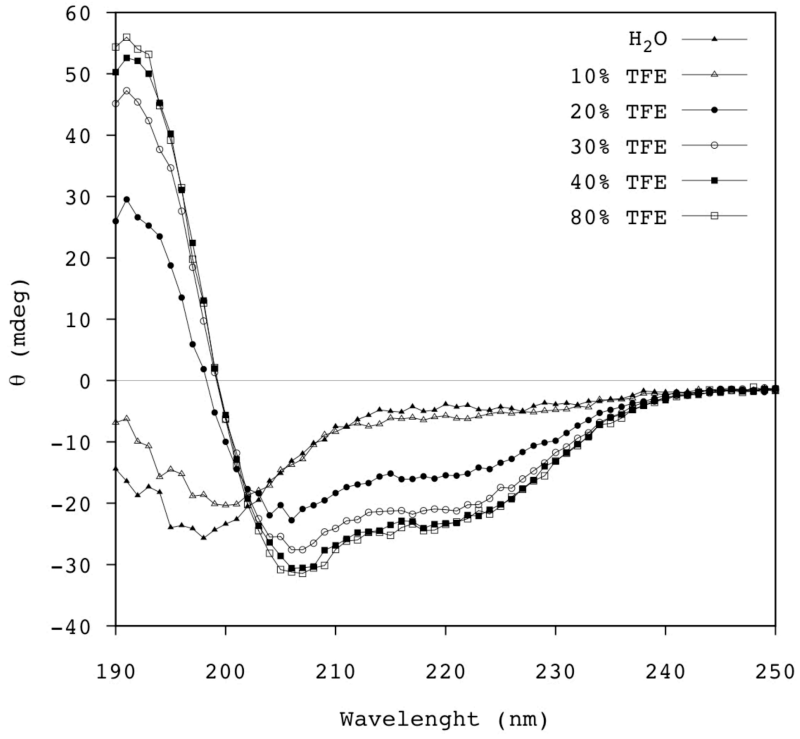

Figure 3.3. Circular dichroism spectra of Esc(1-18). CD spectra have been collected for Esc(1-18) in water and in different TFE/ water mixtures. TFE amount is reported as volume percentage.

solution show a minimum around 198 and 200 nm, respectively, and a negative ellipticity over the entire spectral range, which is a clear indication of a random coil conformation [20, 21]. Then, the helicity degree increased with increasing the TFE content, as it can be seen from the general rise in the ellipticity, the appearance of the characteristic positive band around 190 nm and the two negative bands at 207 and 220 nm [20, 21]. The maximum helicity was achieved in the 40% v/v TFE/water solution. The spectrum did not show any significant changes moving to higher TFE concentrations.

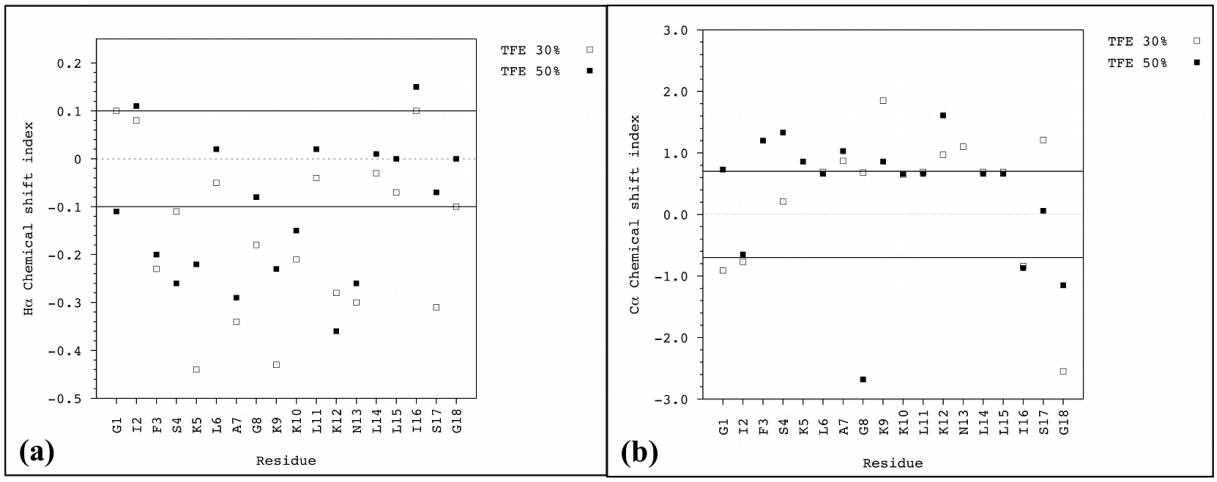

Figure 3.4. Carbon and proton chemical shift index. CSI values have been computed for the 1Hα (a) and 13Cα (b) resonances from Esc(1-18) in a 30% and 50% TFE/water solution, as the difference between the observed chemical shift and the so-called 'random coil' values used as references. Two straight lines define a CSI interval around the 0, corresponding to the random coil region of the plot.

On the basis of these results, a NMR investigation was carried out comparing the data obtained in pure water and in two selected TFE/water solutions, namely 30 and 50% v/v of TFE, i.e. below and above the minimal concentration to get maximum helicity (40%). ^{1}H and ^{13}C resonances were assigned as reported in Table A.1. The chemical shift index (CSI) values were calculated for both the alpha protons and carbons. Figure 3.4 shows the results of Esc(1-18) in the 30 and 50% TFE solutions. Data obtained in pure water are not reported for the sake of clarity, since chemical shift values were comparable to the corresponding random coil reference data for all of the amino acid residues. The CSI values obtained in the two TFE solutions are comparable and suggest a predominant helical conformation for the N-terminal part of the peptide until the $10^{th}/12^{th}$ residue, in agreement with secondary structure predictions.

Figure 3.5 summarizes the sequential assignments of the NOESY cross peaks observed in the 30% (figure 3.5a) and 50% (figure 3.5b) TFE solutions spectra.

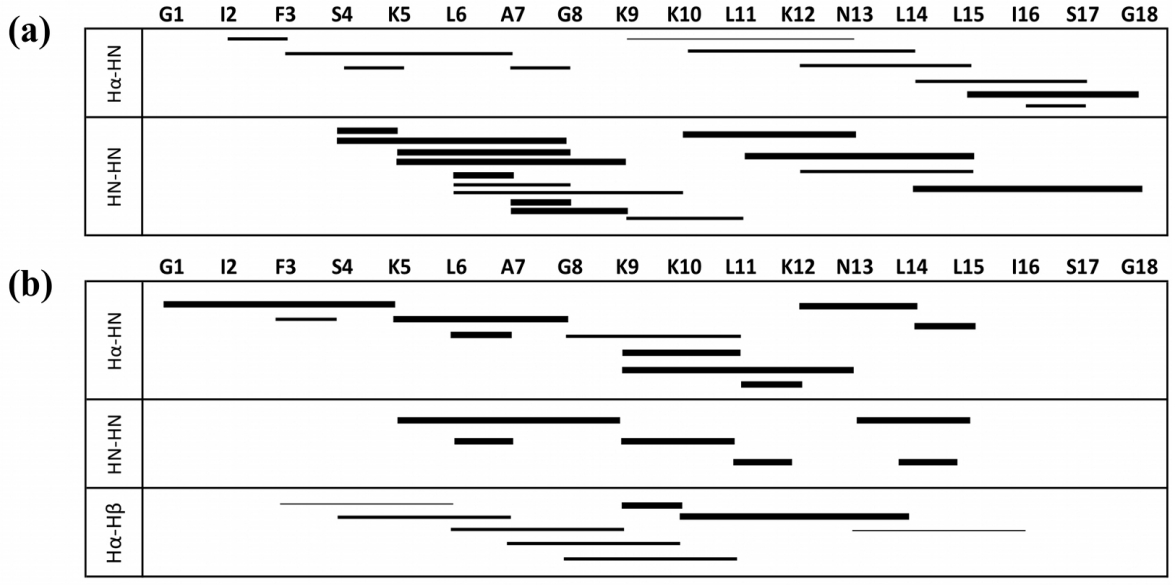

Figure 3.5. Short and medium-range interprotons NOEs. Dipolar interproton interactions found for Esc(1-18) in either (a) 30% and (b) 50% v/v TFE/water solution are reported as lines connecting the two residues involved. Lines thickness is proportional to the relative intensity of the corresponding NOESY cross peak.

A total of about 33 and 31 NOEs were unambiguously assigned in the former and the latter, respectively, and these have been the only ones used for structure calculations. In the 30% TFE solution (figure 3.5a), the most intense NOEs were observed in the H^N–H^N spectral region and mainly found to arise from dipolar coupling interactions between residues ranging from S4 to K10. With very few exceptions, the NOEs in the H^N–H^α region were all characterized by a significantly lower intensity. The number of cross peaks observed in the other spectral regions, such as the H^α–H^β, was negligible. In the case of the 50% TFE solution (figure 3.5b), a higher number of relatively strong medium-range NOEs have been observed in the H^N–H^N, H^N–H^α, and H^α– H^β regions. Mostly, these dipolar interactions were found to occur between residues ranging from S4 to K12. In the case of 30% TFE, the backbone root mean square deviation (RMSD) from the computed average structure was significantly higher than that obtained in the case of the 50% TFE solution, i.e., 1.4 ± 0.3 and 0.8 ± 0.4, respectively. Correspondingly, the standard deviation of the backbone angles distributions was significantly higher in the 30% than in the 50% TFE case. Indeed, in the former, a unique and well superimposable peptide conformation could not be obtained, but rather, both a set of

right- and a set of left-handed helical structures, covering almost the whole peptide length.

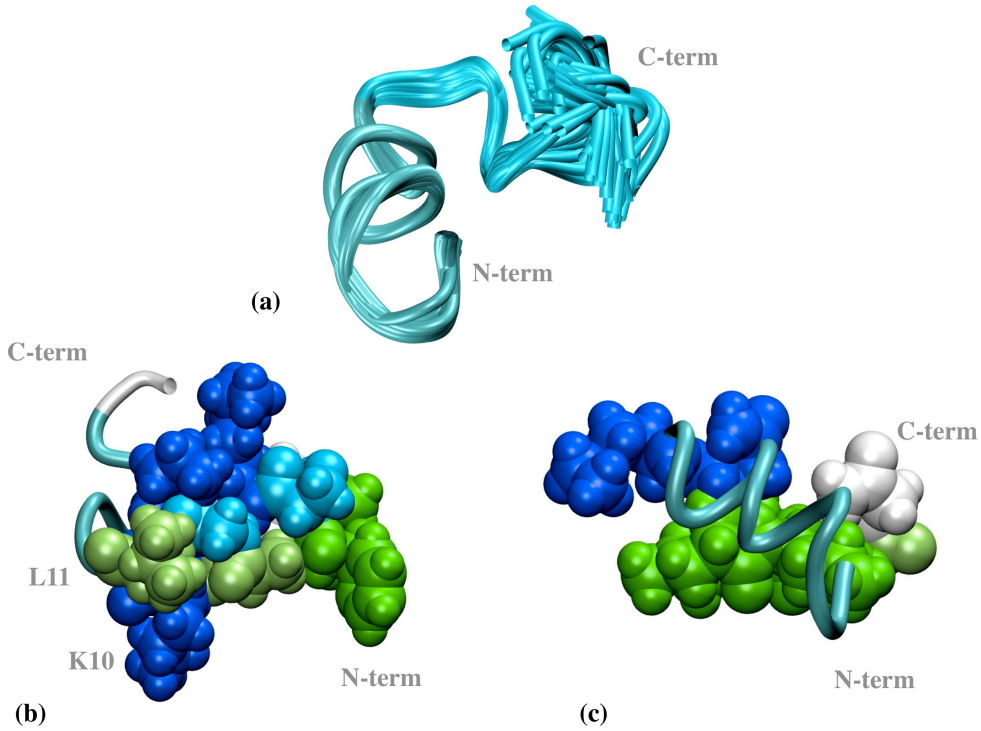

Figure 3.6. 3D structure of Esc(1-18) in a 50% v/v TFE/water solution. In (a), the 100 structures with the lowest potential energy are aligned on the basis of the backbone heavy atoms. Residues belonging to the helical N-terminal (b), and the unfolded C-terminal portion (c) are represented using the Van der Waals atomic radii and a different color on the basis of the hydropathicity values as in figure 3.2: the more intense is the green the more hydrophobic is the residue; the more intense is the blue the more hydrophilic is the residue

Figure 3.6a shows the backbone conformation of the Esc(1-18) structures obtained for the 50% TFE solution, aligned on the basis of the backbone heavy atoms. In this case, a unique cluster of structures was obtained, displaying a right-handed helical conformation for the N-terminal part of the peptide (residues ranging from F3 to L11), and a basically unfolded C-terminal portion. In the figures 3.6b and 3.6c, the structure corresponding to the lowest RMSD is shown. The helical N-terminal and the unstructured C-terminal segments are highlighted, respectively, using the Van der Waals atomic radii and coloring the residues on the basis of their corresponding hydrophobicity score as in figure 3.2. This particular peptide conformation is clearly amphipathic, with the hydrophobic and hydrophilic residues neatly arranged on the opposite sides. The only discrepancy in this amphipathic profile is observed right at the end of the helical part of the peptide, where residues K10 and L11 are located on

the opposite side with respect to the other hydrophilic and hydrophobic residues, respectively (figure 3.6b).

3.2.2 Moving to more realistic systems: DPC and DPC/SDS micelles through liquid state NMR

After the first characterization in TFE/water mixtures,the structure adopted by Esc(1-18) was investigated using a more realistic model: pure DPC and DPC/SDS mixed micelles at 3/1 molar ratio. First, it is important to note that the mixing time typically used for TOCSY experiments (80 ms) was not appropriate in the case of mixed micelles. Quite surprisingly, the TOCSY spectrum was devoid of cross-peaks. A possible explanation is that nuclear ^{1}H magnetization relaxed within a time shorter than the TOCSY mixing time applied. Thus, a trail spectrum was acquired with a shorter mixing time (40 ms), but this resulted to be too short for an efficient magnetization transfer, leading to a TOCSY spectrum characterized by the presence of cross-peaks only for those ^{1}H nuclei separated by a maximum of three consecutive bonds, i.e. a COSY-like spectrum. These results, together with the observation of

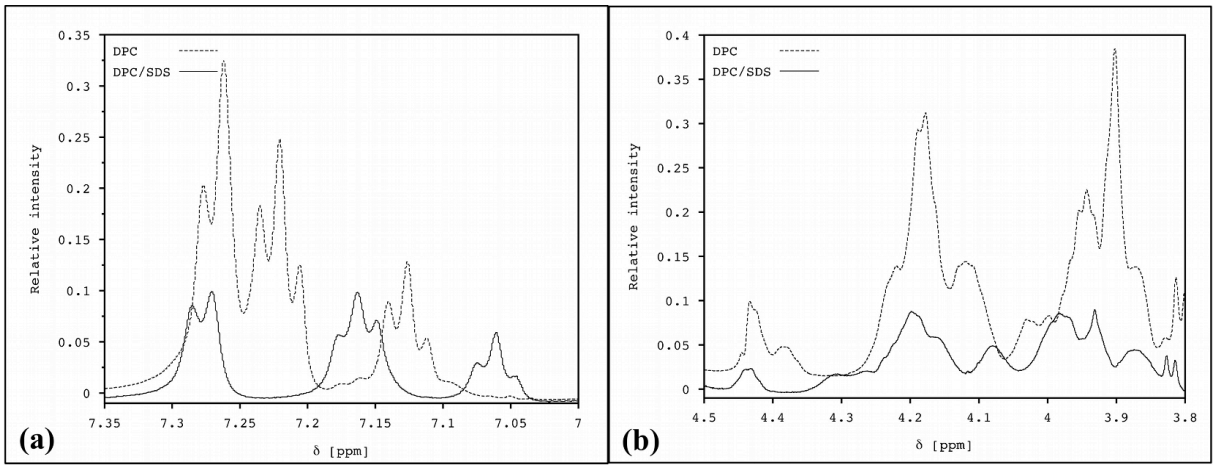

Figure 3.7. Comparison between 1H NMR spectra. Phenilalanine (a) and alpha protons (b) regions of 1D spectra for either DPC and DPC/SDS. To allow comparisons, signals intensities were normalized respect to TSP intensity.

broader ^{1}H resonances in the 1D spectrum in the presence of mixed micelles than pure DPC ones, bolster the hypothesis of a faster relaxation rate in the former case. Figure 3.7 shows both the aromatic and the H^{α} regions of the one-dimensional ^{1}H spectra of Esc1b(1-18) either in the DPC and DPC/SDS case. The samples were prepared at the same final concentration of both the peptide and the internal reference TSP. Spectra were normalized with respect to the intensity of the reference TSP resonance.

Such a faster relaxation might be due to a stronger binding between the peptide, which is positively charged, and the mixed micelle, which has a net negative charge. The tighter the binding, the slower the peptide dynamics, leading to longer rotational correlation times and, in turn, to faster relaxation, ultimately causing resonances broadening.

Chemical shift values for both the DPC and DPC/SDS case are reported in Table A.2. On the basis of the experimental chemical shifts, the software TALOS+ [22] was applied to predict the peptide secondary structure. In the presence of DPC micelles a helical conformation was predicted from the residue 5 to 17, whereas in the presence of the mixed micelles the helical conformation was interrupted at level of residues G8 and K9. However, Φ and Ψ backbone angles for G8 were not predicted with a sufficiently high consensus in both the cases and was not included in the successive structure calculations.

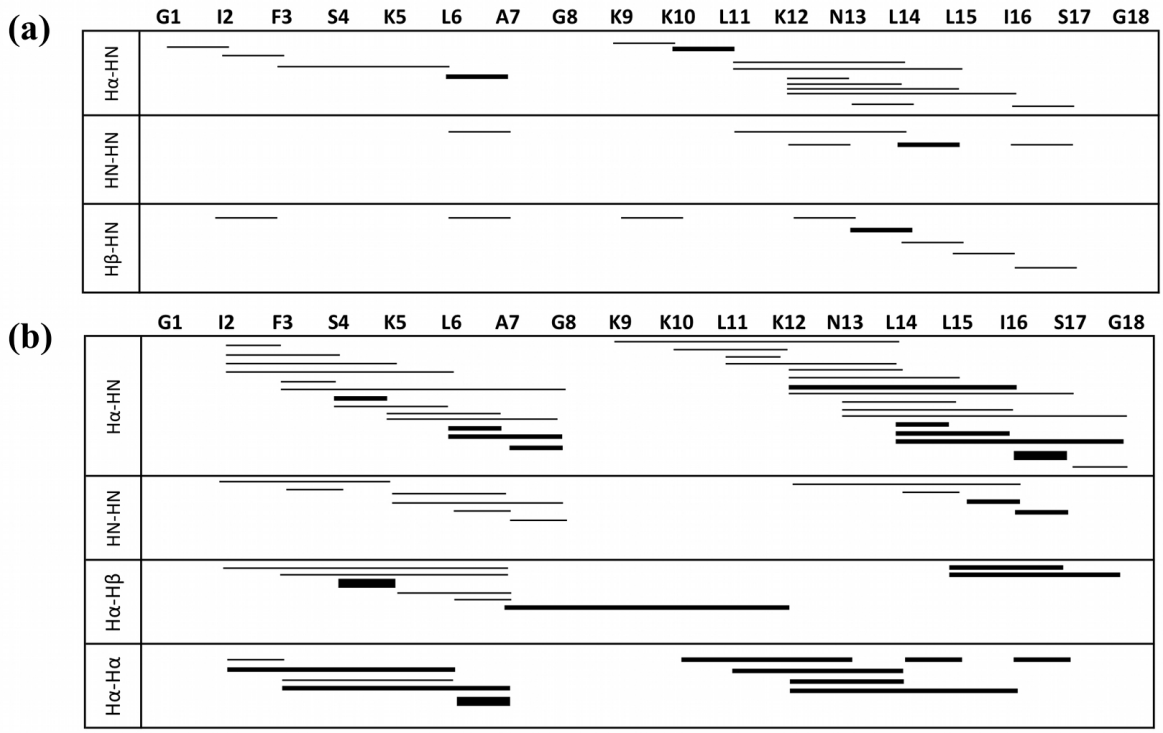

Figure 3.8. Short and medium-range interprotons NOEs. Dipolar interproton interactions found for Esc(1-18) in (a) DPC and (b) DPC/SDS 3/1 mol/mol ratio. Correlations are reported as lines connecting the two residues involved. Lines thickness is proportional to the relative intensity of the corresponding NOESY cross peak.

Figure 3.8 summarizes the sequential assignments of the NOESY cross peaks. In DPC (figure 3.8a) a total of 47 NOEs were unambiguously assigned, including intra-residue dipolar interactions. On the other hand, in DPC/SDS (figure 3.8b) the unambiguous NOEs were 83. In the light of the low number of NOEs observed in pure DPC micelles, a poorly defined

structure should be expected. This can be ascribed to a low binding affinity of Esc1b(1-18) for this purely zwitterionic membrane model, resulting in the equilibrium shifted towards the unbound and unstructured state.

On the other hand, the high number and the distribution of the sequential dipolar interactions strongly suggest the presence of two distinct helical fragments separated by residue G8.

Dynamo calculation for both cases was applied using unambiguously NOEs and TALOS+ [22] prediction as distance and torsional angle restraints, respectively.

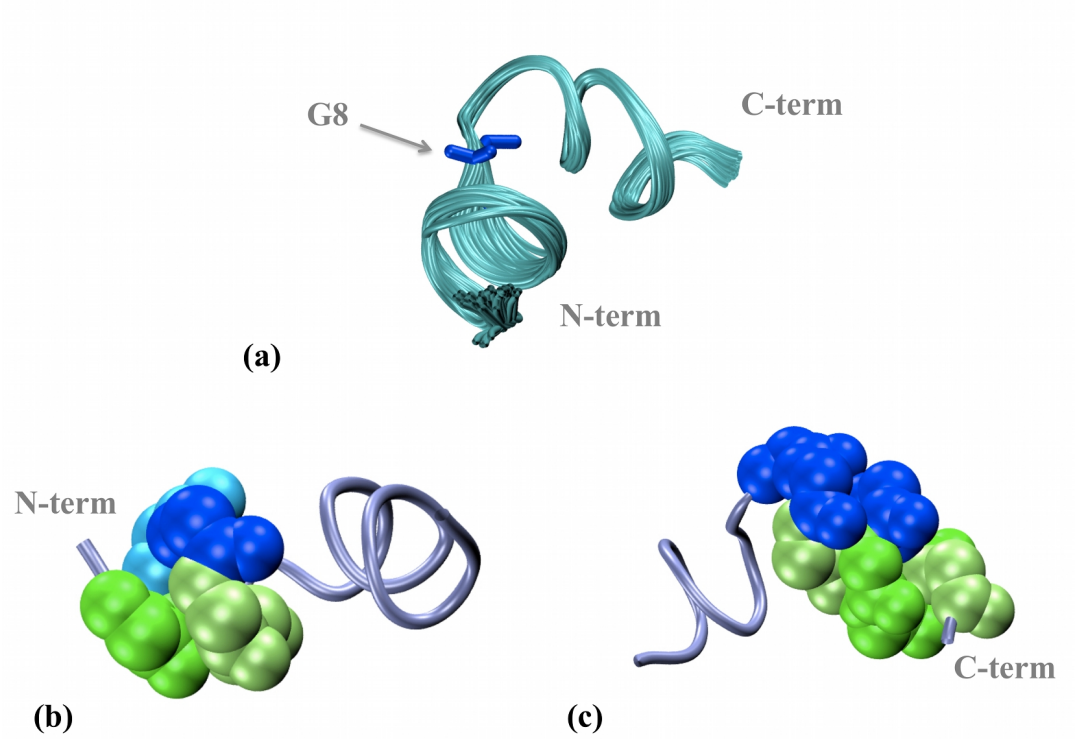

Figure 3.9. 3D structure of Esc(1-18) in DPC/SDS 3/1 mol/mol. In (a), the 100 structures with the lowest potential energy are aligned on the basis of the backbone heavy atoms. Residues belonging to the N-terminal (b), and the C-terminal helix (c) are represented using the Van der Waals atomic radii. The same color scheme as in figure 3.6 and 3.2 was used to facilitate comparison.

In DPC structure calculation resulted in a helical conformation for the C-terminal fragment, starting from the residue K9 (data not shown). Nevertheless, it is unlikely that the low number of NOEs observed produced such a structure and it is due to the strong weight given to torsional angles by Dynamo force field. The high dynamic character of this structure was confirmed by the high values of RMSD obtained, ranging between 0.15 to 0.25 nm.

Figure 3.9a shows the backbone conformation of the Esc(1-18) structures obtained in DPC/SDS, aligned on the basis of their backbone heavy atoms. Structures are characterized by two helical fragments separated by a kink at residue G8. Both the helical fragments are well defined, as shown by the alignment of 100 conformers with lowest potential energy used for the analysis. This is confirmed by the RMSD calculated with respect to the average structure, which ranges between 0.02 and 0.09 nm. Panel (b) and (c) show the structure corresponding to the conformer with the lowest RMSD, where the N- and the C-terminal helices are highlighted, respectively, using the Van der Waals atomic representation. Residues are coloured on the basis of the hydrophobicity following the same color-code as for the results obtained in the water/TFE mixtures (figure 3.2 and 3.6). The images clearly show the amphipathicity of the two helical fragments.

Overall, these findings suggest that Esc(1-18) affinity for the negatively charged micelles, used to mimic a prokaryotic membrane, is much higher than for the zwitterionic ones as expected, leading to a well defined 3D structure for the bound-state. Conversely, in the case of pure DPC micelles, used to mimic an eukaryotic membrane, the binding affinity appeared to be rather low. These results provide a convincing explanation for Esc1b(1-18) antimicrobial potency and the absence of any hemolytic activity [8].

3.2.2.1 Investigating Esc(1-18) insertion into micelles through paramagnetic probes

Mn^{2+} has been reported in literature as a useful probe to investigate the insertion of peptides into membrane models with liquid-state NMR. Indeed, the presence of the paramagnetic ions in the solvent leads to a strong enhancement of both the longitudinal and the transversal relaxation rate of the nuclei exposed to water with resultant intensity loss of the corresponding cross-peaks in a 2D NMR spectrum. This effect is both distance and concentration dependent so that the resonances will be progressively less affected as much as the nuclei are buried in the micelle. In practice, the intensity variation of the H^N-H^α cross-peaks is monitored by calculating the ratio between a TOCSY spectrum acquired in the presence and in the absence of the paramagnetic ions at different concentrations [23, 24]. Thus, this approach allows to distinguish the residues exposed to the solvent from those buried in the micelle, providing valuable information about peptide orientation and insertion with respect to the surface of the micelle, as it was in the case of Plasticin-L1, described in the next chapter (see Chapter 4).

However, in the present investigation of Esc1b(1-18), TOCSY spectra suffered from severe intensity loss as said, thus, NOESY spectra have been used to perform the analysis of

paramagnetic relaxation enhancement in the presence of Mn^{2+} ions. In particular, a series of NOESY spectra were collected in the presence of different concentration of Mn^{2+}, in the case of either DPC, and DPC/SDS micelles. Figure 3.10 summarizes the results.

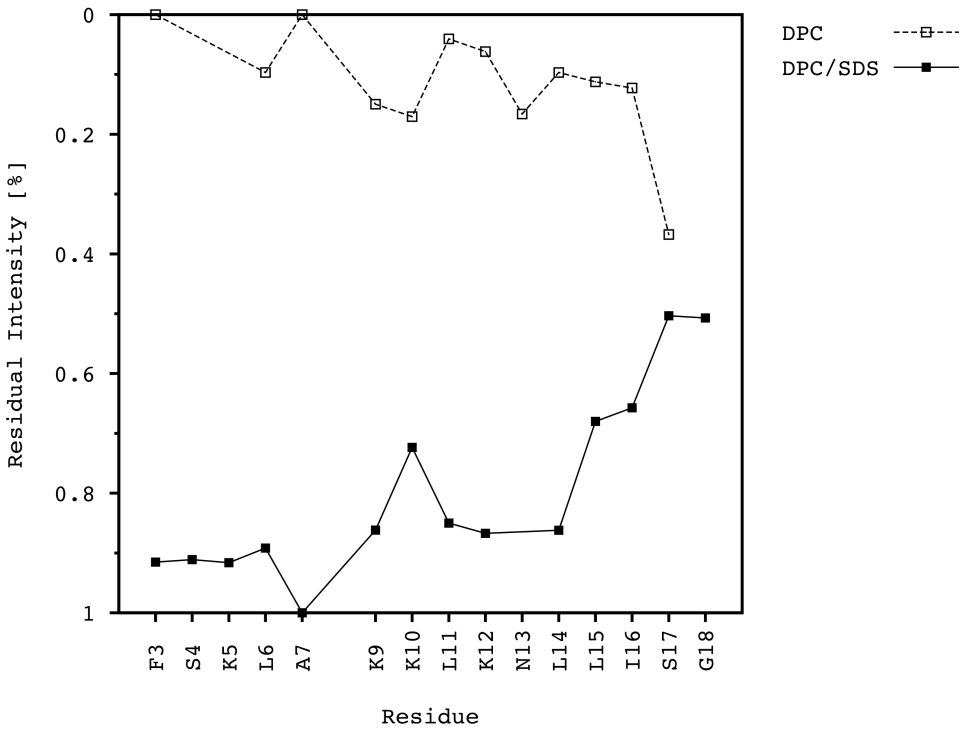

Figure 3.10. NMR experiments with Mn^{2+} as paramagnetic probe. Residual intensity of the NOESY cross-peaks in the H^N–H^α region is calculated as the ratio between data acquired in the presence and absence of Mn^{2+} 0.1 mM. An intra-residue cross-peak was used for each amino-acid. The y-axis has been reversed in order to have buried residues at the bottom and solvent exposed residues at the top of the graph, making this profile directly comparable to hydropathicity plot (figure 3.2 (a)).

In the presence of DPC micelles, a significant reduction of the NOESY cross-peaks intensity was observed for all the Esc(1-18) residues when the Mn^{2+} ions were added to the solution. These results clearly indicate that the peptide is weakly bound to the micelle and is almost entirely exposed to the solvent. Conversely, in the case of mixed DPC/SDS micelles, no significant reduction of signals intensity was observed, indicating that the peptide is deeply buried in the micelle. In the case of Plasticin-L1 (see Chapter 4), the folded peptide was found to be located at the micelle/water interface and, correspondingly, the TOCSY cross-peaks intensity-loss profile obtained with the use of Mn^{2+} was characterized by an alternate pattern of buried and solvent exposed residues, strictly following the peptide helical folding. In the case of Esc1b(1-18), despite an overall helical folding was found through a computational

simulated annealing coupled to experimental NMR restraints, a similarly alternate pattern is not observed in figure 3.10. This difference strongly suggest that Esc1b(1-18) is not just embedded between the detergents head groups, but rather it is actually vertically inserted in the micelle. Finally, these results bolster Esc(1-18) higher affinity for negatively charged micelles than for the neutral ones and suggest that its mechanism of action involves, similarly to other helical AMPs [25–28], peptide insertion into the negatively charged lipid membrane.

3.3 Discussion and conclusions

Most of the known natural AMPs show a helical folding when come into contact with membrane models. The amphipathic character of the resulting 3D structure represents the basis for the first stage of their mode of action, i.e. the interaction with lipid bilayers. The hydrophobic residue are embedded in the inner region of the bilayer, while the hydrophilic ones interact with the polar/charged lipid headgroups and the hydration waters. The same scenario have been put forward for Esc1b(1-18) just on the basis of some CD spectra [8]. However, both the hydropathicity and the helical wheel plots, and a close inspection of the hypothetic 3D structure corresponding to a canonical straight α-helix (figure 3.2), revealed that such a conformation of Esc(1-18) is not fully compatible with the picture of an amphipathic helix bound to a lipid bilayer. Some structural distortion should be expected to allow the potential energy of the peptide/membrane interaction going to a minimum. This incompatibility is also supported by the secondary structure prediction performed with both the Agadir (http://agadir.crg.es) [11–14] and CFSSP (http://www.biogem.org/tool/chou-fasman) [15, 16] web-tools.

In order to investigate the intrinsic folding propensity of the sequence, the peptide (in water) was titrated with increasing amount of TFE and the changes in secondary structure were monitored with CD spectroscopy (figure 3.3). In agreement with what previously observed in the presence of lipid vesicles [8], Esc(1-18) showed a clear tendency to fold into a helical conformation with increasing the TFE concentration, reaching the maximum helicity at 40% TFE. On the basis of these results, liquid state NMR has been employed to collect more detailed information about the structure adopted by Esc(1-18). In water, the $^{1}H^{\alpha}$ chemical shift values and the absence of inter-residue NOEs, confirmed that the peptide was unstructured. In the presence of either 30 or 50% TFE, both the $^{1}H^{\alpha}$ and $^{13}C^{\alpha}$ CSI values (figure 3.4) were comparable and indicative of a helical conformation encompassing the residues from F3 to K10/K12, in agreement with the CFSSP prediction. Nevertheless, these evidences were not taken into account during the detailed 3D structure calculations. The

simulated annealing algorithm Dynamo was applied using only the $^{3}J_{H}{}^{N}{}_{H}{}^{\alpha}$ scalar coupling constants (Table A.1) and the NOEs (figure 3.5) to restraint the backbone Φ angles and the interproton distances, respectively. It is also important to stress here that no TFE (or water) were present in the structure calculations, the latter only relying upon the NMR experimental restraints and the Dynamo force field. The relatively small number of NOEs and the relatively broad $^{1}H^{N}$ resonances (when compared with the other resonances in the same spectrum), indicated that a significant proton exchange between the peptide and the solvent was still present, thus, that the peptide structure continued to be characterized by a relatively high motional flexibility in such an isotropic, although amphiphilic, environment.

In the 30% TFE/water solution the tendency to a helical folding was evident but a set of right- and a set of left-handed helices were obtained, extending almost over the entire peptide length. In addition, about the 40% of the analyzed structures presented two different fragments, the N- and the C- terminal, one left- and the other right-handed, separated by a kink located around G8. In other words, 30% TFE appeared to promote a mainly helical conformation, as shown also by the corresponding CD spectrum, but this was not enough to shift the unordered/ordered equilibrium toward a sufficiently stable and well defined structure. On the other hand, moving from the 30 to the 50% TFE solution, the CD spectrum showed an increased ellipiticity and a highly self-consistent 3D structure was correspondingly found. A right-handed helix extending from F3 to L11 and an unfolded C-terminal region (figure 3.6) were observed under these conditions, in very good agreement with the CFSSP prediction. Moreover, in contrast to an ideal α-helical structure encompassing the whole peptide, the obtained conformation appears to be really amphiphilic. Hydrophilic and hydrophobic residues are actually well segregated on opposite sides of the global folding (figure 3.6b and c) providing a consistent picture for a peptide interacting with an amphipathic environment such as the lipid bilayer/water interface. The only interruption of this global amphipathicity occurs right at the end of the helical segment, where K10 and L11 appear to be dislocated.

On the basis of these preliminary results, the antimicrobial activity of an Esc(1-18) analog obtained by exchanging the position of these two residues was tested in-vitro, aiming at improving the peptide folding and, hopefully, its biologic activity. Unfortunately, the analog showed exactly the same antimicrobial activity of the original Esc(1-18) sequence (data not shown) and consequently this compound was no further investigated. Finally, it is also intriguing to note that the above-mentioned hydrophobic cluster of residues (L14-L15-I16) is located right in the middle of the unfolded C-terminal portion of the peptide, which is

expected to be functional, as suggested by the lack of antibacterial activity of the 1-15 N-terminal fragment of Esculentin-1 [29].

These interesting preliminary results encouraged us to move ahead using a more sophisticated membrane model to better mimic plasma membranes. To this end three-dimensional structure of Esc(1-18) was characterized through liquid state NMR spectroscopy in two different micelle systems, namely, pure DPC and DPC/SDS at 3/1 molar ratio, to model an eukaryotic and a prokaryotic plasma membrane, respectively [30–33]. When the purely zwitterionic micelle was employed, TALOS+ [22] prediction, which is based upon the experimental chemical shifts, resulted in a helical folding encompassing residues between K5 and S17. However, the NOESY experiments showed a very low number of homonuclear ^{1}H-^{1}H dipolar interactions (figure 3.8a), clearly indicating a flexible and poorly structured average conformation. Dynamo annealing protocol produced a structure characterized by a helical folding in the C-terminal region, but with a high dynamicity as confirmed by the high values of RMSD observed (data not shown). In the presence of the mixed micelles, on the other hand, TALOS+ [22] and NOEs agree in describing two folded fragments separated by a kink at the level of residue G8. Indeed, dipolar correlations were observed mostly between residues in two separate peptide portions, i.e. I2-A7 and K9-S17, and the presence of many sequential H^{α}-H^{N} and H^{N}-H^{N} suggests a helical folding. The structure calculations confirmed these observations, resulting in a well-defined structure characterized by two helical fragments separated by a kink at the G8. The two folded fragments of Esc(1-18) are perfectly amphipathic, while the overall structure amphipathicity depends on the relative orientation of the two fragments. The previously proposed straight helical conformation encompassing the entire peptide sequence [8] was shown to be not compatible with the picture of an amphipathic helix interacting with a lipid bilayer. However, the structural data collected during the present Ph.D. work demonstrated that the global amphipathicity can be “restored” when the kink at the G8 is taken into account. The presence of kinks or bends, usually observed where a glycine or proline residue is located, is a common feature of many amphipathic helical AMPs, like Cecropin A, Magainin2 [34], Caerin 1.1 and Maculatin 1.1 and its importance in the antimicrobial activity has been highlighted for many of them [35].

Mn^{2+} ions were finally used as paramagnetic probes to investigate peptide insertion into the micelle. These experiments proved that Esc(1-18) inserts deeply into the negatively charged micelle, providing also a valid explanation for the aforementioned issues in collecting suitable TOCSY spectra. Conversely, the peptide only weakly binds to the surface of the

zwitterionic micelles, strongly supporting the fundamental role played by the binding stage in determining the antimicrobial and hemolytic properties of a peptide sequence (figure 3.10).

For the sake of completeness, it has to be mentioned that an attempt to carry out a binding study of Esc(1-18) was actually performed. The idea was to follow the intrinsic fluorescence of the F3 residue, which is the only fluorescent amino acid present in the Esc(1-18) sequence. Unfortunately, the quantum yield of this aromatic amino acid was not sufficient to obtain spectra of good quality and a direct investigation of Esc(1-18) binding to the micelles employed in the present study was thus not possible. Nevertheless, the poor structuration and insertion observed in DPC micelles demonstrate that it interacts weakly with zwitterionic detergents. On the other hand, Esc(1-18) was shown to fold and insert deeply into the mixed micelles indicating a strong binding with their negatively charged surface. Thus, the presence of negative lipids in the bilayer appear to be necessary for Esc(1-18) to bind, fold in the right three-dimensional structure and, definitely, to exert its biological effects. Moreover, the presented results explain the selectivity of Esc(1-18) towards negative bacteria plasma membranes, indicating the binding as the major factor in determining a good antimicrobial activity while maintaining toxicity at the minimum.

Even if further studies are needed to achieve a complete understanding of the mode of action of Esc(1-18) interesting experimental findings reported here confirm that this peptide belongs to the large family of 'roughly' helical AMPs and thus some hypothesis can be put forward. Similarly to other known natural peptides of this class [25–28], the deep insertion in negatively charged membranes suggests a membrane-disruption mechanism of action, probably involving the formation of pores. Liposomes leakage experiments, for instance, and the use of more extended membrane models like bicelles in the NMR experiments might provide further information to definitely clarify Esc(1-18) mode of action. In particular, using bicelles, the peptide/lipid ratio could be increased allowing for the observation and investigation of concentration dependent oligomers.

3.4 References

1. Mangoni, M.L., G. Maisetta, M. Di Luca, L.M.H. Gaddi, S. Esin, et al. 2008. Comparative analysis of the bactericidal activities of amphibian peptide analogues against multidrug-resistant nosocomial bacterial strains. Antimicrob. Agents Chemother. 52: 85–91.

2. Conlon, J.M. 2011. The contribution of skin antimicrobial peptides to the system of innate immunity in anurans. Cell Tissue Res. 343: 201–12.

3. Conlon, J.M. 2011. Structural diversity and species distribution of host-defense peptides in frog skin secretions. Cell. Mol. Life Sci. 68: 2303–15.

4. Simmaco, M., G. Mignogna, D. Barra, and F. Bossa. 1993. Novel antimicrobial peptides from skin secretion of the European frog *Rana esculenta*. FEBS Lett. 324: 159–61.

5. Ponti, D., G. Mignogna, M.L. Mangoni, D. De Biase, M. Simmaco, et al. 1999. Expression and activity of cyclic and linear analogues of esculentin-1, an anti-microbial peptide from amphibian skin. Eur. J. Biochem. 263: 921–27.

6. Mangoni, M.L., D. Fiocco, G. Mignogna, D. Barra, and M. Simmaco. 2003. Functional characterisation of the 1-18 fragment of esculentin-1b, an antimicrobial peptide from *Rana esculenta*. Peptides. 24: 1771–7.

7. Simmaco, M., G. Mignogna, D. Barra, and F. Bossa. 1994. Antimicrobial peptides from skin secretions of *Rana esculenta*. 269: 11956–61.

8. Marcellini, L., M. Borro, G. Gentile, A.C. Rinaldi, L. Stella, et al. 2009. Esculentin-1b(1-18)-a membrane-active antimicrobial peptide that synergizes with antibiotics and modifies the expression level of a limited number of proteins in *Escherichia coli*. FEBS J. 276: 5647–64.

9. Manzo, G., R. Sanna, M. Casu, G. Mignogna, M.L. Mangoni, et al. 2012. Toward an improved structural model of the frog-skin antimicrobial peptide esculentin-1b(1-18). Biopolymers. 97: 873–81.

10. Kyte, J., and R.F. Doolittle. 1982. A simple method for displaying the hydropathic character of a protein. J. Mol. Biol. 157: 105–32.

11. Muñoz, V., and L. Serrano. 1994. Elucidating the folding problem of helical peptides using empirical parameters. Nat. Struct. Biol. 1: 399–409.

12. Muñoz, V., and L. Serrano. 1995. Elucidating the folding problem of helical peptides using empirical parameters. II. Helix macrodipole effects and rational modification of the helical content of natural peptides. J. Mol. Biol. 245: 275–96.

13. Muñoz, V., and L. Serrano. 1995. Elucidating the folding problem of helical peptides using empirical parameters. III. Temperature and pH dependence. J. Mol. Biol. 245: 297–308.

14. Lacroix, E., A.R. Viguera, and L. Serrano. 1998. Elucidating the folding problem of α-Helices: local motifs, long-range electrostatics, ionic-strength dependence and prediction of NMR parameters. J. Mol. Biol. 284: 173–91.

15. Chou, P.Y., and G.D. Fasman. 1974. Conformational parameters for amino acids in helical, beta-sheet, and random coil regions calculated from proteins. Biochemistry. 13: 211–22.

16. Chou, P., and G. Fasman. 1974. Prediction of protein conformation. Biochemistry. 13: 222–45.

17. Strandberg, E., and A.S. Ulrich. 2004. NMR methods for studying membrane-active antimicrobial peptides. Concepts Magn. Reson. Part A. 23A: 89–120.

18. Jasanoff, A, and A.R. Fersht. 1994. Quantitative determination of helical propensities from trifluoroethanol titration curves. Biochemistry. 33: 2129–35.

19. Reiersen, H., and A.R. Rees. 2000. Trifluoroethanol may form a solvent matrix for assisted hydrophobic interactions between peptide side chains. Protein Eng. 13: 739–43.

20. Whitmore, L., and B.A. Wallace. 2008. Protein secondary structure analyses from circular dichroism spectroscopy: methods and reference databases. Biopolymers. 89: 392–400.

21. Greenfield, N.J. 2006. Using circular dichroism spectra to estimate protein secondary structure. Nat. Protoc. 1: 2876–90.

22. Shen, Y., F. Delaglio, G. Cornilescu, and A. Bax. 2009. TALOS+: a hybrid method for predicting protein backbone torsion angles from NMR chemical shifts. J. Biomol. NMR. 44: 213–23.

23. Abbassi, F., C. Galanth, M. Amiche, K. Saito, C. Piesse, et al. 2008. Solution structure and model membrane interactions of temporins-SH, antimicrobial peptides from amphibian skin. A NMR spectroscopy and differential scanning calorimetry study. Biochemistry. 47: 10513–25.

24. Scorciapino, M.A., G. Manzo, A.C. Rinaldi, R. Sanna, M. Casu, et al. 2013. Conformational analysis of the frog skin peptide, Plasticin-L1, and its effects on production of proinflammatory cytokines by macrophages. Biochemistry. 52: 7231–41.

25. Wieprecht, T., O. Apostolov, M. Beyermann, and J. Seelig. 2000. Membrane binding and pore formation of the antibacterial peptide PGLa: thermodynamic and mechanistic aspects. Biochemistry. 39: 442–52 .

26. Zhao, H., A.C. Rinaldi, A. Di Giulio, M. Simmaco, and P.K.J. Kinnunen. 2002. Interactions of the antimicrobial peptides temporins with model biomembranes. Comparison of temporins B and L. Biochemistry. 41: 4425–36.

27. Mangoni, M.L. 2006. Temporins, anti-infective peptides with expanding properties. Cell. Mol. Life Sci. 63: 1060–9.

28. Sato, H., and J.B. Feix. 2006. Peptide-membrane interactions and mechanisms of membrane destruction by amphipathic alpha-helical antimicrobial peptides. Biochim. Biophys. Acta. 1758: 1245–56.

29. Roice, M., G. Suma, K. Kumar, and V. Pillai. 2001. Synthesis of Esculentin-1 antibacterial peptide fragments on 1,4-Butanediol Dimethacrylate cross-linked polystyrene support. J. Protein Chem. 20: 25–32.

30. Zasloff, M. 2002. Antimicrobial peptides of multicellular organisms. Nature. 415: 389–95.

31. Diamond, G., N. Beckloff, A. Weinberg, and K.O. Kisich. 2009. The roles of antimicrobial peptides in innate host defense. Curr. Pharm. Des. 15: 2377–92.

32. Epand, R.M., and R.F. Epand. 2010. Biophysical analysis of membrane-targeting antimicrobial peptides: membrane properties and the design of peptides specifically targeting Gram-negative bacteria. In: Antimicrobial Peptides: discovery, design and novel therapeutic strategies. G. Wang (ed.), CABI, Wallingford, UK, 116 –27.

33. Epand, R.M., and R.F. Epand. 2011. Bacterial membrane lipids in the action of antimicrobial agents. J. Pept. Sci. 17: 298–305.

34. Hwang, P.M., and H.J. Vogel. 1998. Structure-function relationships of antimicrobial peptides. Biochem. Cell Biol. 76: 235–46.

35. Haney, E.F., H.N. Hunter, K. Matsuzaki, and H.J. Vogel. 2009. Solution NMR studies of amphibian antimicrobial peptides: linking structure to function? Biochim. Biophys. Acta. 1788: 1639–55.

4.1 Introduction and background

The skins of frogs and toads contain an important array of HDPs and a large part of those reported in the literature has this origin. The first AMP was found in the skin of the European frog *Bombina variegata* some 30 years ago [1]. Vast number of such compounds have been isolated from skin secretions of anuran species and display a broad-spectrum antibacterial and antifungal activity, representing a key component of the animal's system of innate immunity [1–3].

Plasticin-L1 (GLVNGLLSSVLGGGQGGGGLLGGIL) is a 25 amino-acid-residue glycine/leucine-rich peptide originally isolated from norepinephrine-stimulated skin secretions of the South-American Santa Fe frog *Leptodactylus laticeps* (Leptodactylidae) (figure 4.1) [4]. Plasticin-L1 is a member of a structurally related family of gene-encoded, membrane-active host defense peptides that were first identified in the skin of phyllomedusid frogs from the family Hylidae. The Plasticins may be divided into two classes on the basis of their cytolytic activities. The strongly cationic peptides, Plasticin-B1 and -S1, that contain several lysine residues, show a potent broad spectrum antimicrobial activity but lyse erythrocytes, whereas the weakly cationic or neutral Plasticins, Plasticin-A1, -C1, -C2, and -DA1, are hemolytic only [5, 6]. On the hand, the biological role of Plasticin-L1 is unknown. This peptide does not inhibit the growth of either *E. coli* or *S. aureus* at concentrations up to 500 μM and, unlike the other neutral Plasticins from phyllomedusid frogs, lacks hemolytic activity. Plasticin-L1 stimulates the rate of release of insulin from rat clonal BRIN- BD11 cells without affecting the integrity of their plasma membrane, but it seems improbable that this observation has any physiological significance [4]. In common with other members of the Plasticin family, the conformation of Plasticin-L1 is markedly solvent dependent, with the peptide displaying a random coil conformation in water, a β-sheet structure in methanol, and an α-helical folding in 50% trifluoroethanol (TFE)−water, as it was observed with circular dichroism spectroscopy [4].

Figure 4.1 ***Leptodactylus laticeps* (Leptodactylidae).** The South-American Santa Fe frog from which Plasticin-L1 has been isolated. Photo: by Jordi Camardons Caralt

4.2 Results

4.2.1 Structural characterization of Plasticin-L1

4.2.1.1 Sequence analysis and liquid state NMR experiments

Before an in-depth characterization of the three-dimensional structure of Plasticin-L1, the hydropathicity profile of the amino acid sequence was analysed through the ProtScale [7] tool available on the ExPaSy server (http://expasy.org/). The method of Kyte and Doolittle [8] was applied and the results are presented in figure 4.2. The hydropathicity plot shows the residues ranked on the basis of their hydrophobic character. On a scale from 0 to 1, higher the score more hydrophobic the residue and vice-versa. The N- and C-terminal (residues 1-12 and 19-25, respectively) fragments of Plasticin-L1 are characterized by a pattern of alternating hydrophilic and hydrophobic residues, resembling an amphipathic helical motif, whereas only hydrophilic residues are present in the central region, suggesting that this might be an unfolded portion of the amino acid sequence.

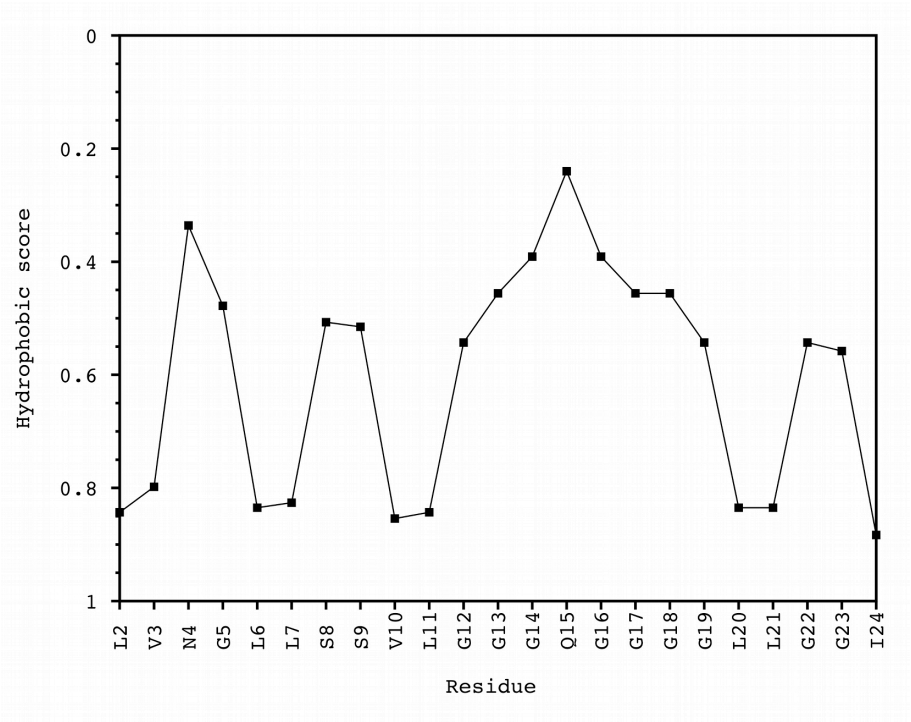

Figure 4.2. Hydropathicity plot. Hydropathicity plot of Plasticin-L1 obtained with the method of Kyte and Doolittle [8] with scores normalized on a scale between 0 and 1. The higher the score, the higher the residue hydrophobicity. The y-axis has been reversed to make this profile directly comparable to those obtained from MD simulations (figures 4.7 and 4.8).

Earlier circular dichroism studies indicated marked solvent dependent malleability with Plasticin-L1 adopting a disordered or random coil conformation in water but a well-defined β-sheet structure in methanol and a helical structure in 50% TFE-water [4]. The peptide concentration required for NMR characterization (mM range) is usually three order of magnitude higher than that required for circular dichroism (μM range) especially when working with non-isotopically labelled samples as in this case. Due to poor peptide solubility in the solvents previously employed for circular dichroism investigation [4], the NMR characterization in the same media was not practicable. However, Plasticin-L1 resulted to be highly soluble in micellar dispersions, allowing for an in-depth NMR structural investigation of the three-dimensional structure adopted when the peptide is bound to these models of the cell membrane. Liquid state NMR analysis was performed in two different micellar environments, namely, pure DPC and a mixed system with DPC and SDS at 1/1 molar ratio. The peptide and the detergents were dissolved at a molar ratio of 1:100 in both cases. The experimentally derived NMR geometrical restraints were used to determine the most energetically favourable conformation.

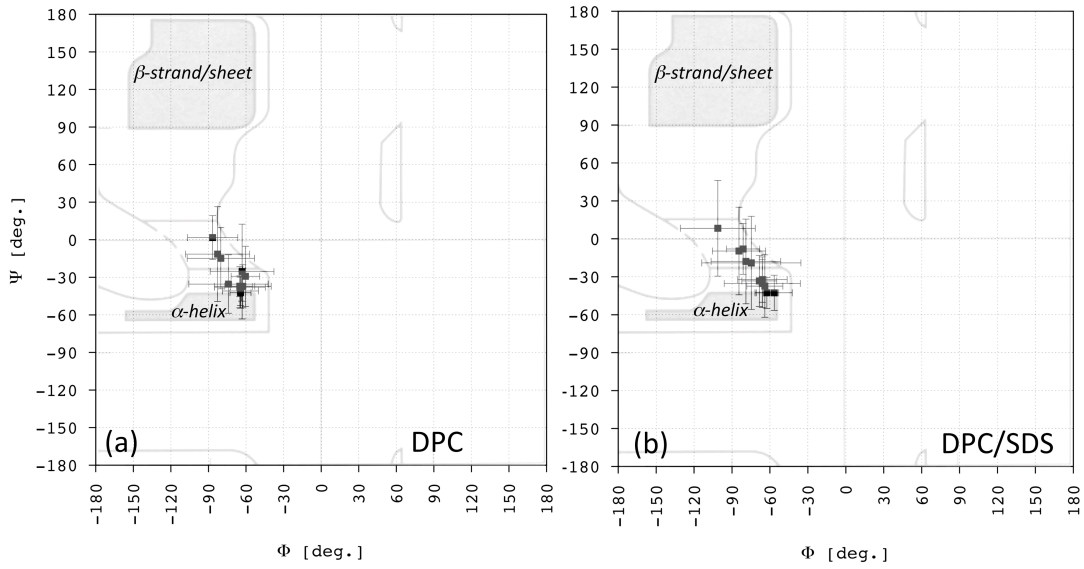

Figure 4.3. Ramachandran plot of Plasticin-L1**.** The TALOS+ [9] high-consensus predictions (residues from 2 to 11 and 20 to 22) are shown on the Ramachandran plot with the corresponding uncertainty. Results are shown for either (a) DPC or (b) DPC/SDS 1:1 mol/mol micelles.

The sequential resonance assignments were performed through a series of 2D experiments and Table A.3 (in the Appendix chapter) reports the NMR chemical shifts and the $^{3}J_{H}{}^{N}{}_{H}{}^{\alpha}$ coupling constants of Plasticin-L1 in the presence of micelles formed by either DPC or DPC/SDS. On the basis of the experimental chemical shifts, the application of the

software TALOS+ [9] predicted a helical conformation for both the N-terminal and C-terminal peptide fragments, separated by an unstructured loop. In both kind of micelles, a helical conformation is predicted for the region between residues 2 and 11, and between residues 20 and 22. The only exceptions were residue G5, in both the cases, and G22 in DPC/SDS whose backbone angles are not predicted with a sufficiently high consensus and so were not included in the successive structure calculations.

Figure 4.3 shows the Φ and Ψ angles obtained with TALOS+ [9], together with their uncertainties, on the Ramachandran plot. Only the high-consensus predictions are shown. Results obtained in the two cases are comparable, although, in DPC, the points are less dispersed and the uncertainties are slightly smaller than in DPC/SDS, suggesting that the two helical fragments are more defined and stable when the peptide is bound to a pure DPC micelle.

Figure 4.4 schematically shows the sequential $^{1}H-^{1}H$ NOE through-space connections observed for Plasticin-L1 in the two membrane-mimetic environments. Lines of different thickness are used to indicate strong, medium and weak NOEs, respectively. The total number of dipolar interprotons interactions is higher in DPC than in DPC/SDS. Moreover, the number

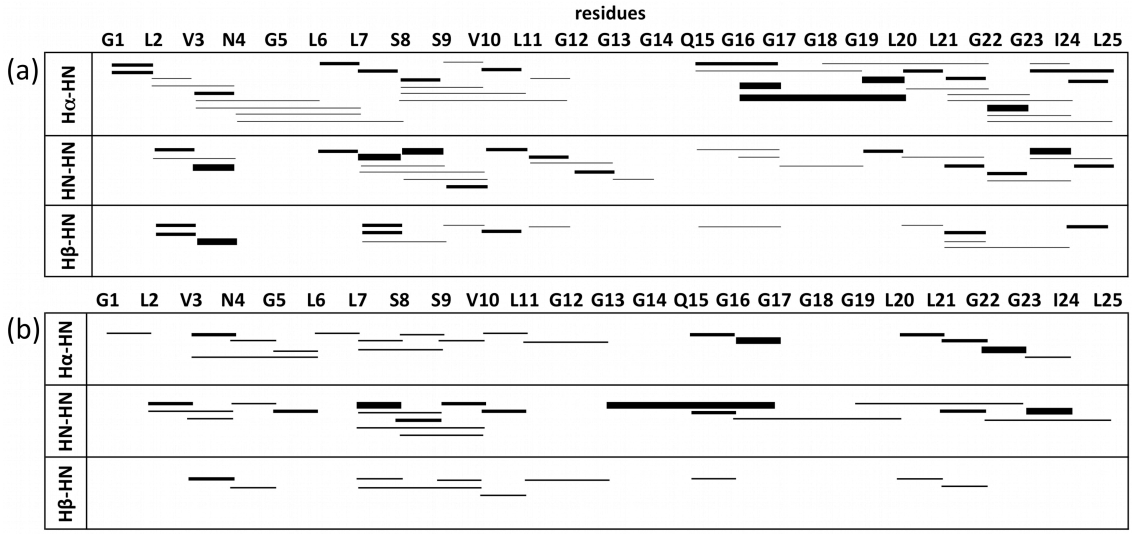

Figure 4.4 ^{1}H-^{1}H NOEs. Short and medium-range interproton NOEs found for Plasticin-L1 in presence of either (a) DPC or (b) DPC/SDS 1:1 mol/mol micelles. NOEs are reported as lines connecting the two residues involved. The thickness of the lines is proportional to the relative intensity (strong, medium, weak) of the corresponding NOESY cross-peak.

of strong NOEs is higher in DPC and a larger number of H_i-H_{i+3} and H_i-H_{i+4} interactions are also observed. This is consistent with the conformation based upon TALOS+ [9] predictions and the hydropathicity plot: two distinct helices are at the N- and C-terminal regions of the

peptide separated by an unstructured loop wherein the highest number of glycines is localized. However, in light of the lower number of NOEs observed in DPC/SDS, both helical fragments are predicted to have a higher conformational plasticity, with the C-terminal one showing the greater plasticity. Figure 4.5 shows the peptide structure obtained through the Dynamo (http://spin.niddk.nih.gov/NMRPipe/dynamo/) simulated annealing procedure applied with the NMR-derived geometrical restraints.

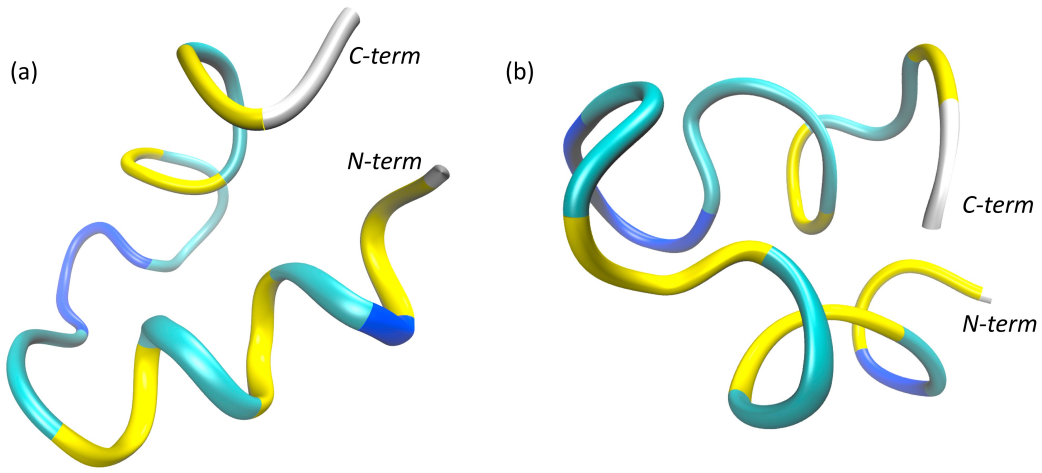

Figure 4.5 NMR-based structure of Plasticin-L1 in presence of either (a) DPC or (b) DPC/SDS 1:1 mol/mol micelles. This is the minimum backbone RMSD structure obtained among the 100 conformers with the lowest potential energy. For the sake of clarity, only the backbone trace is shown, without side chain residues. Amino acid residues are differently colored on the basis of their hydropathicity score (figure 4.2): markedly hydrophilic (blue), weakly hydrophilic (cyan), and hydrophobic (yellow).

The two helical segments are evident in both structures, either in the presence of DPC (figure 4.5a) or DPC/SDS (figure 4.5b) micelles. However, in DPC, the N-terminal domain comprises a regular and straight α-helix whereas the C-terminal helix is slightly distorted. As expected, the conformation obtained in the presence of the mixed micelles is even less regular: a distorted helix is clearly observed for the N-terminal segment, whereas the helical coil at the C-terminus is extremely loose. In the case of DPC micelles, the backbone RMSD calculated from the average structure for the 100 conformers with the lowest potential energy ranged between 0.2 and 0.4 nm. The analyses showed that this quite high deviation between the selected conformers is not due to poor secondary structure definition but to a difficult overall structures alignment. All the conformers are comparable to that shown in figure 4.5, the high RMSD arising from the extremely variable conformation of the unfolded loop between the two helical segments and, in turn, their relative orientation. The situation in the

case of DPC/SDS micelles is the same. The RMSD range was even larger (0.25−0.55 nm), because the secondary structure of the C-terminal segment is not as well-defined as in the presence of DPC micelles.

4.2.1.2 Investigating Plasticin-L1 insertion into micelle through relaxation enhancement experiments

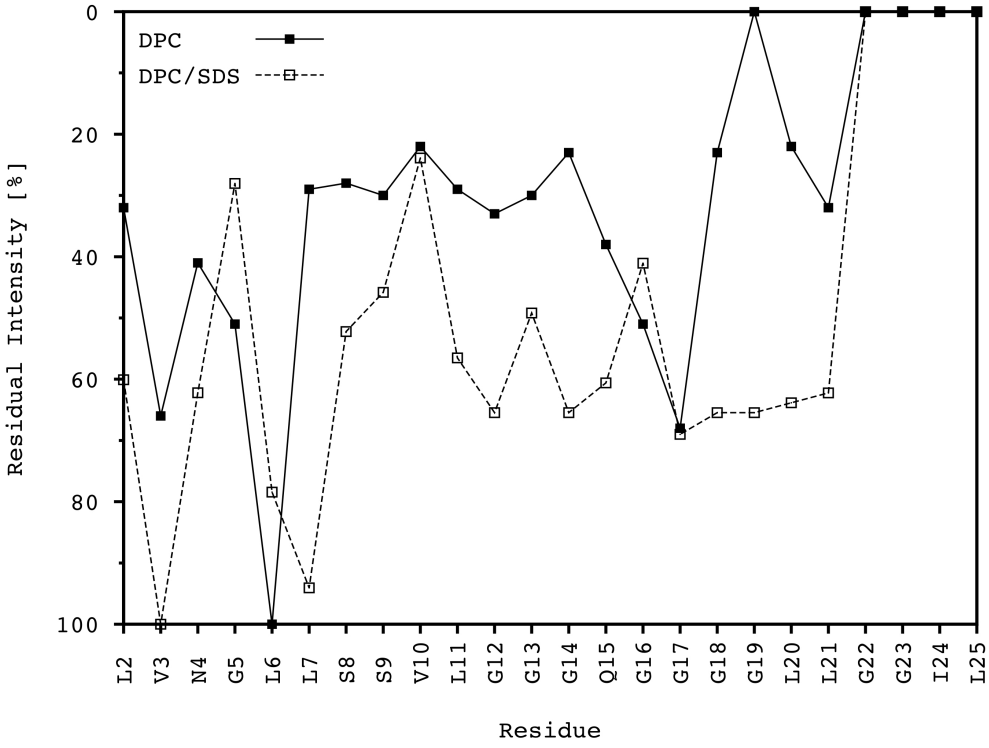

Figure 4.6 NMR experiments with Mn^{2+} as paramagnetic probe. Residual intensity of the TOCSY cross-peaks in the H^N–H^α region, calculated as the ratio between data acquired in the presence and absence of Mn^{2+} 0.1 mM. The y-axis has been reversed to make this profile directly comparable to those obtained from MD simulations (figures 4.7 and 4.8).

A series of TOCSY spectra were collected in the presence of different concentration of Mn^{2+} used as a paramagnetic probe. The relaxation enhancement, produced by this paramagnetic ion in the solvent, was followed for each of the amino acid residues by monitoring the intensity loss of the corresponding H^N–H^α TOCSY cross-peaks. This method has been previously employed to investigate other peptides [10]. Because the paramagnetic relaxation enhancement is distance (and concentration) dependent, this approach allows to distinguish the residues exposed to the solvent from those buried in the micelle, thus

providing information about peptide orientation and insertion with respect to the surface of the micelle.

Figure 4.6 shows the resulting profile for both micelle cases. The y-axis has been reversed to make these results directly comparable with the distance profiles obtained from MD simulations presented in next section. Plasticin-L1 appeared to be located at the micelle/water interface in both the cases, because the residual intensity profile oscillated throughout the peptide sequence. No completely buried regions were observed, and only the last four residues were found to be fully exposed to the solvent. The alternating profile observed for the N-terminal fragment of the peptide strongly supports the aforementioned helical folding, with the most hydrophobic residues interacting with the tails of the detergent molecules, whereas the hydrophilic residues are directed toward the solvent and are probably embedded within the head groups of the detergents. Similarly, the C-terminal region is characterized by an alternating pattern in the case of DPC, supporting the helical conformation found with Dynamo. In the presence of DPC/SDS, on the other hand, a flat profile is observed in this region, which is compatible with a less rigid conformation. However, in this case, the C-terminal segment and the central loop appear to be more buried than observed in the presence of DPC micelles.

4.2.2 Molecular dynamics (MD) simulations

Because Dynamo simulated annealing was applied '*in vacuo*', we decided to carry out further structural analyses through MD simulations, using explicit solvent and detergent micelles, to complement the NMR data and characterize better the three-dimensional structure adopted by the peptide when interacting with the micelles. I did not personally performed the computer simulations but I took part in the results analysis.

The radial distribution function (RDF) has been computed for different chemical groups of both detergents with respect to the center of mass of the micelle. RDFs have been separately calculated for the micelle equilibration stage in the absence of peptide and the production run in the presence of Plasticin-L1. No significant differences were observed. In the case of DPC, the RDF profiles and the time averaged radius of gyration (1.66 nm) are comparable to those previously reported [11]. On the other hand, there are no reports for mixed DPC/SDS micelles. The RDF profiles and the radius of gyration (1.59 nm) are in this case comparable to those obtained for DPC micelles. This is in agreement with one of our study where the hydrodynamic diameter of mixed DPC/SDS micelles has been measured with dynamic light scattering and no significant variations have been observed by varying their

composition [12]. The MD simulations protocols and technical details are reported elsewhere [13].

It is important to stress that the folding process itself was not investigated; MD was used to refine the equilibrium three-dimensional structure obtained on the basis of NMR results and the restraints obtained from NMR analysis were applied also to MD simulations. From our current data, we cannot state whether folding is completed prior to or after peptide binding to the micelle.

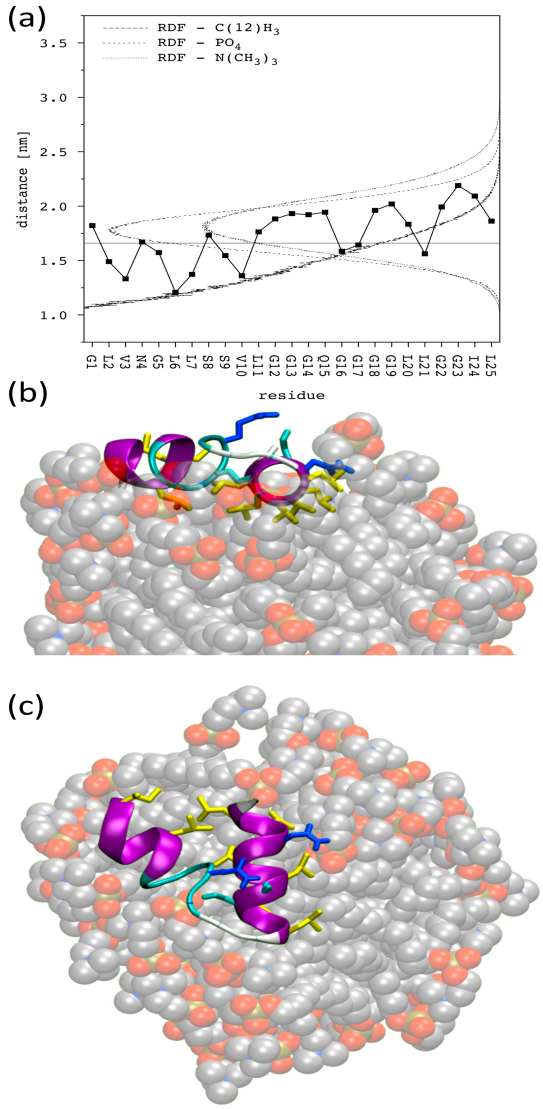

Figure 4.7. Equilibrium conformation of Plasticin-L1 in DPC micelles. Central structure of main peptide conformation cluster among 100 ns MD simulation in presence of DPC micelles. This cluster pertains to simulation time from ~60 to 100 ns. (a) The residues center of mass distance (time averaged) from the center of mass of the micelle is shown (filled squares). The solid horizontal line is reported as a reference for the radius of gyration of the micelle. The differently dashed curves are the radial distribution functions obtained for three different chemical groups of DPC. The corresponding 3D side- and top-views are shown in (b) and (c), respectively, where residues are differently colored according to their hydropathicity scores (figure 4.2): markedly hydrophilic (blue), weakly hydrophilic (cyan), and hydrophobic (yellow).

In the presence of DPC micelles, a stable α-helix was found encompassing residues 1−11, an unstructured loop from residue 12 to 18, and a more flexible helical conformation for the C-terminal region. As expected from the NMR results, the backbone RMSD spans about 0.3 nm, indicating that the peptide adopts different conformations along the MD, whose difference is mostly due to the central unfolded loop and the relative orientation of the two

helical fragments. Figure 4.7 shows side- and top-view images of the final equilibrium conformation reached by Plasticin-L1 during a 100 ns long MD simulation. In addition, a plot of the distance between the center of mass of the amino acid residues and that of the micelle was produced to provide a quantitative comparison of the insertion depth of the different regions of the peptide.

During the starting equilibration stage, the peptide approaches and starts to interact with the surface of the DPC micelle. The first residues to bind the micelle were V10 and L11, which are the most hydrophobic according to the hydropathicity plot (figure 4.2). The N-terminal and C-terminal helices were almost parallel. During the first ~2 ns of the production run, the entire N-terminal helix resided on the micelle's surface, inserted between DPC head groups and rotated along its main axis., in order to direct the hydrophobic residues toward the micelle interior. Then, the C-terminal helix followed the N-terminal one, binding the micelle surface during the next stage of the simulation. The global peptide conformation did not change significantly, with the two helical segments remaining parallel. Finally, at ~60 ns, Plasticin-L1 found its equilibrium conformation, which did not change further up to the end of the simulation (figure 4.7). This conformation is characterized by a helix-loop-helix super-secondary motif approximating to a 'V'. Both helices are localized at the micelle/water interface, with the N-terminal helix being slightly more buried than the other. As expected, the hydrophilic central loop never inserted into the micelle.

In the presence of DPC/SDS micelles, a stable α-helix was found encompassing residues (1-11) as in the case of DPC micelles. However, the central unfolded portion of the peptide was two residues longer (i.e., from residue 12 to 20). As a consequence, only one helical turn was observed at the C-terminal region. As expected from NMR results, backbone RMSD spanned a larger interval, about 0.5 nm instead of 0.3 nm, indicating that overall conformation of the peptide is more unstable in DPC/SDS. In contrast to the DPC model, the starting equilibration stage was not sufficient to observe any peptide-micelle close-contact interaction. After ~7.6 ns of the production run, the peptide bounded to the micelle surface with the N-terminus approaching first. The peptide took another ~1.5 ns to lie on the micelle surface with a helix-loop-helix super-secondary motif, arranged in an 'L' conformation. During the rest of the simulation, Plasticin-L1 slowly orientated between detergent head groups but was always localized at the micelle/water interface, as in the case of DPC. Finally, the most populated conformation was reached (figure 4.8), characterized by an 'L' global shape. This is the main difference with respect to the equilibrium conformation obtained in

DPC micelles, whereas the global insertion depth was comparable in the two membrane models.

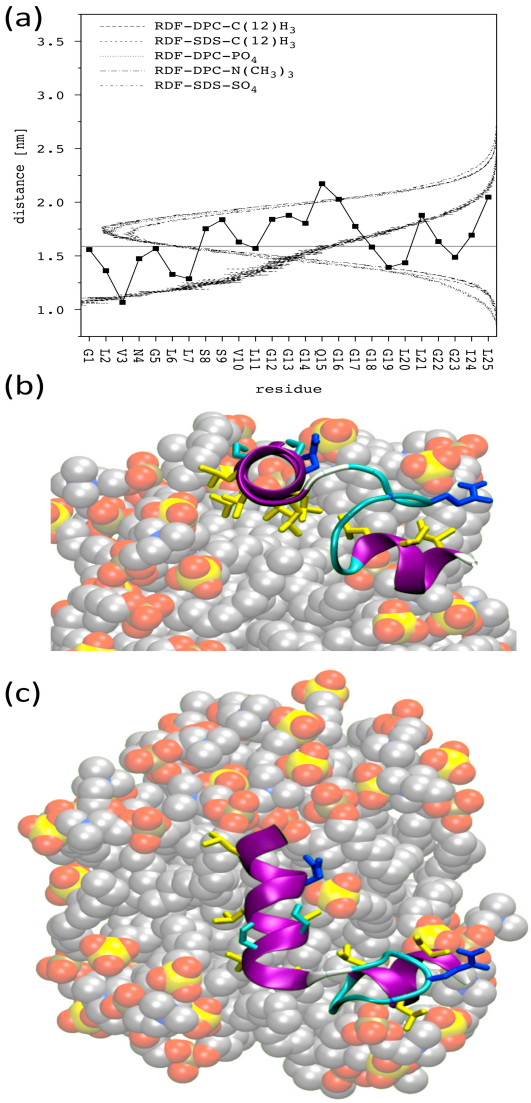

Figure 4.8. Equilibrium conformation of Plasticin-L1 in DPC/SDS micelles. Central structure of the main peptide conformation cluster among 100 ns MD simulation in the presence of DPC/SDS 1:1 mixed micelles. This cluster pertains to simulation time from ~77 to 100 ns. (a) The residues center of mass distance (time averaged) from the center of mass of the micelle is shown (filled squares). The solid horizontal line is reported as a reference for the radius of gyration of the micelle. The differently dashed curves are the radial distribution functions obtained for different chemical groups of DPC and SDS. The corresponding 3D side- and top-views are shown in (b) and (c), respectively, where residues are differently colored according to their hydropathicity scores (figure 4.2): markedly hydrophilic (blue), weakly hydrophilic (cyan), and hydrophobic (yellow).

In DPC, the most hydrophilic residue Q15 was always observed to interact with water, whereas in the case of DPC/SDS, Q15 strongly interacted with the sulfate head groups of SDS, often forming H-bonds. In DPC, (Q15)−Nδ−H···O− PO3(DPC) H-bonds were observed only during the first 30 ns, suggesting that they are important during the initial stage of peptide binding but, as soon as the equilibrium conformation is reached, Q15 preferentially interacts with water molecules. In DPC/SDS, (Q15)−Nδ−H···O−PO3(DPC) H-bonds have a lower frequency than in DPC and, again, were observed only during the initial stage of binding. On the other hand, the occurrence of (Q15)−Nδ−H···O−SO_3(SDS) H-bonds was observed throughout the simulation. This stronger interaction between Q15 and the sulfate head groups forced the central unfolded loop to “adhere” to the surface of the mixed micelle.

This is compatible with the NMR paramagnetic relaxation enhancement experiments (figure 4.6), where the central peptide portion was less exposed to the solvent than observed in DPC. This might also explain the different peptide global shape observed. In the DPC micelle, the flexible loop is not "anchored" to micelle surface, allowing for the two helices to come closer to each other and to form a more compact 'V-shaped' conformation.

4.2.3 Effect of Plasticin-L1 on the release of cytokines

Thanks to the collaboration with colleagues from the Center for Molecular Medicine of the University of Kragujevac (Kragujevac, Serbia), the effect of Plasticin-L1 on the release of cytokines from mice macrophages (of both C57BL/6 and BALB/C mice) was tested. Experimental details are described in [13]. Incubation with Plasticin-L1 (20 μg/mL; approximately 9 μM) significantly increased the release of the proinflammatory cytokine IL-1β from unstimulated peritoneal macrophages from both mice cells and potentiated the stimulation produced by lipopolysaccharide (LPS), but the last effect was not dramatic. Plasticin-L1 also increased the release of the proinflammatory cytokines IL-23 from both BALB/C and C57BL/6 mice and of TNF-α from C57BL/6 mice. The effect was significant for the unstimulated macrophages only. macrophages only. Treatment with the peptide significantly increased the release of the proinflammatory cytokine IL-12 from unstimulated macrophages from both C57BL/6 and BALB/C mice, whereas release of IL-6 was significantly increased from both unstimulated and LPS-stimulated macrophages from BALB/C mice. In the case of macrophages from C57BL/6 mice, the effect was significant only for the unstimulated cells. The release of the anti-inflammatory cytokine IL-10 from either unstimulated or LPS-stimulated cells was not affected. Lower peptide doses (1 and 10 μg/mL) did not induce any significant change in cytokine production).

4.3 Discussion and conclusions

Analysis of the structural and lipid affinity properties of Plasticin-L1 has revealed a marked affinity for both the neutral and the anionic membrane models employed, thus with no apparent discrimination between eukaryotic or prokaryotic cells, as it should be expected for peptides with low positive or zero net charge The final equilibrium peptide structure was found to be located at the micelle/water interface in both DPC and DPC/SDS micelles (figures 4.7 and 4.8), and its insertion depth and orientation with respect to the micellar surface resulted to be comparable and in agreement with the results from NMR paramagnetic enhanced relaxation experiments (figure 4.6). Since Plasticin-L1 is a highly hydrophobic

peptide, the main driving force for its interaction with micelles is the need to minimize the contacts between hydrophobic residues and the water molecules. At the same time, the presence of hydrophilic residues throughout the molecule allows the peptide to fold into an overall amphipathic three-dimensional structure. The hydrophobic residues interact with the nonpolar tails of the detergent molecules while the hydrophilic residues interact both with water and the polar head groups. In particular, the alternate pattern of two hydrophilic and two hydrophobic residues in the N-terminal fragment (residues 1-11) leads to a very stable α-helical conformation. In the C-terminal region, the same alternate pattern of hydrophobic/hydrophilic amino acids is present but involves fewer residues, leading to a helical folding with a higher conformational plasticity. The presence of multiple glycines in the central and the C-terminal regions makes these portions less amphipathic than the N-terminal helix. The central region of Plasticin-L1 is characterized by a relatively long, glycine rich, markedly hydrophilic and unstructured loop. Its conformational plasticity endows the peptide with the possibility of adopting multiple conformations with a different relative orientations of the two helical 'domains'. In both DPC and DPC/SDS micelles, the most hydrophilic residue Q15, located right in the middle of the central loop, establishes H-bonding interactions with the detergent head groups. However, although H-bonds were observed with SDS throughout the MD simulation, those formed with DPC were present only during the initial stage of binding. Q15 showed a strong and preferential interaction with SDS head groups despite its lack of net positive charge. Thus, in the case of mixed micelles, the central loop is forced to stay anchored to the micelle surface, in turn, a more "extended" helix-loop-helix super-secondary structure is found in mixed DPC/SDS micelles while a compact 'V-shaped' conformation is observed in the case of DPC.

Previous studies revealed that Plasticin-L1 is devoid of direct antimicrobial activity [4]. However, the present study demonstrated that this peculiar peptide has a stimulatory effect on the release of proinflammatory cytokines from mouse peritoneal macrophages, suggesting an immumodulatory role for this peptide *in-vivo*. A similar behaviour has been demonstrated, for instance, for IDR-1 (KSRIVPAIPVSLL-NH_2), a 13 amino acids long peptide, which showed no direct antimicrobial activity but the ability to modulate innate immune responses thereby providing potential prophylaxis/treatment of a wide range of infections [14]. A 5-mer peptide modelled on IDR-1 sequence, namely IMX942, is in pre-clinical trial as immunomodulator by Inimex Pharmaceuticals (Vancouver, Canada) [15, 16]. Similarly to Plasticin-L1, IDR-1 is characterized by a flexible conformation and a poor net positive charge (+3, all localized at the N-terminal region of the sequence) [14]. Thus, the

absence of direct antimicrobial activity in the case of Plasticin-L1 can be ascribed to this lack of positive charge, supporting the essential role exerted by basic residues in AMPs activity [17–20].

Another similarity between Plasticin-L1 and IDR-1 peptide is the high conformational plasticity. An increasing number of studies have convincingly demonstrated that structural versatility of peptides in the vicinity of membranes may lead to alternative mechanisms of action [5, 21]. This might suggest that either Plasticin-L1 and IDR-1 may act through different mechanisms thanks to the many conformations they can adopt.

Recently, a neutral peptide structurally unrelated to Plasticin-L1 has been isolated from norepinephrine-stimulated skin secretions of the Tyrrhenian painted frog *Discoglossus sardus*, named frenatin-2D. It was found to be devoid of antimicrobial activity but able to alter cytokines production of mouse peritoneal macrophages in a manner similar (but not identical) to that observed for Plasticin-L1 [22]. Overall, these findings and evidences from the literature raise the possibility that a fairly general mechanism exists whereby these neutral peptides act on macrophages in frog skin to produce a cytokine-mediated stimulation of innate and/or adaptive immunity, thus protecting the animal against invading microorganisms. It is not known whether stimulation of cytokine production by Plasticin-L1 (or Frenatin-2D) arises from a nonspecific interaction of the peptide with the macrophage membrane or from interaction with a specific receptor.

The Plasticin-L1 sequence contains three GXXXG motif repeats (where X denotes any amino acid), suggesting that the peptide may fold as a trans-membrane helix and possibly oligomerize into bundles. Indeed, GXXXG is the most common structural motif found at the interface between interacting trans-membrane helices [23, 24]. However, leucine, valine, and isoleucine are commonly found in the GXXXG motif of such helices bundles, as the presence of these hydrophobic residues ensures high affinity for the hydrophobic inner membrane region while the small (and weakly hydrophilic) glycines make insertion easier and facilitate different trans-membrane helices to come into close contact and assemble into bundles [23, 24]. In Plasticin-L1, the GXXXG motifs in the central and the C-terminal regions contain additional glycines probably making the peptide too hydrophilic to insert in the cell membrane. Moreover, the absence of arginine residues, recognized as fundamental for peptides penetration into the membrane [17–20], make unlikely the translocation of Plasticin-L1 inside the cell.

Although generation of high levels of pro-inflammatory cytokines may lead to toxicity, enhancing their selective release through a rational optimization of peptide sequence

may represent a possible therapeutic application of neutral frog skin peptides. Pro-inflammatory cytokines function as immunostimulatory agents, and several compounds that stimulate cytokine release are in clinical practice [25]. Immunostimulatory peptides may have an enhancing effect on the innate immune response to microbial infection and tumorigenesis.

Further investigations are needed to elucidate the precise mechanism of action of Plasticin-L1, but the present work forms the basis for a deeper understanding of structure-function relationships of immunomodulatory HDPs and represents an interesting starting point for further studies. In the future, these peptides may provide suitable templates to develop a new immunomodulatory class of molecules to be used in concert with other antimicrobial and/or anticancer drugs.

4.4 Reference

1. Rinaldi, A.C. 2002. Antimicrobial peptides from amphibian skin: an expanding scenario: Commentary. Curr. Opin. Chem. Biol. 6: 799–804.
2. Conlon, J.M. 2011. The contribution of skin antimicrobial peptides to the system of innate immunity in anurans. Cell Tissue Res. 343: 201–12.
3. Conlon, J.M. 2011. Structural diversity and species distribution of host-defense peptides in frog skin secretions. Cell. Mol. Life Sci. 68: 2303–15.
4. Conlon, J.M., Y.H.A. Abdel-Wahab, P.R. Flatt, J. Leprince, H. Vaudry, et al. 2009. A glycine-leucine-rich peptide structurally related to the plasticins from skin secretions of the frog Leptodactylus laticeps (Leptodactylidae). Peptides. 30: 888–92.
5. El Amri, C., and P. Nicolas. 2008. Plasticins: membrane-damaging peptides with “chameleon-like” properties. Cell. Mol. Life Sci. 65: 895–909.
6. Bruston, F., C. Lacombe, K. Zimmermann, C. Piesse, P. Nicolas, et al. 2007. Structural malleability of plasticins: preorganized conformations in solution and relevance for antimicrobial activity. Biopolymers. 86: 42–56.
7. Gasteiger, E., C. Hoogland, A. Gattiker, S. Duvaud, S., M.R. Wilkins, et al. 2005. Protein identification and analysis tools on the ExPASy server. In: The Proteomics Protocols Handbook, J.M. Walker (ed.), Humana Press, Totowa, NJ, USA, 571-607.
8. Kyte, J., and R.F. Doolittle. 1982. A simple method for displaying the hydropathic character of a protein. J. Mol. Biol. 157: 105–32.

9. Shen, Y., F. Delaglio, G. Cornilescu, and A. Bax. 2009. TALOS+: a hybrid method for predicting protein backbone torsion angles from NMR chemical shifts. J. Biomol. NMR. 44: 213–23.

10. Abbassi, F., C. Galanth, M. Amiche, K. Saito, C. Piesse, et al. 2008. Solution structure and model membrane interactions of temporins-SH, antimicrobial peptides from amphibian skin. A NMR spectroscopy and differential scanning calorimetry study. Biochemistry. 47: 10513–25.

11. Tieleman, D.P., D. van der Spoel, and H.J.C. Berendsen. 2000. Molecular dynamics simulations of dodecylphosphocholine micelles at three different aggregate sizes: micellar structure and chain relaxation. J. Phys. Chem. B. 104: 6380–6388.

12. Manzo, G., M. Carboni, A.C. Rinaldi, M. Casu, and M.A. Scorciapino. 2013. Characterization of sodium dodecylsulphate and dodecylphosphocholine mixed micelles through NMR and dynamic light scattering. Magn. Reson. Chem. 52: 176-83.

13. Scorciapino, M.A., G. Manzo, A.C. Rinaldi, R. Sanna, M. Casu, et al. 2013. Conformational analysis of the frog skin peptide, Plasticin-L1, and its effects on production of proinflammatory cytokines by macrophages. Biochemistry. 52: 7231-41.

14. Scott, M.G., E. Dullaghan, N. Mookherjee, N. Glavas, M. Waldbrook, et al. 2007. An anti-infective peptide that selectively modulates the innate immune response. Nat. Biotechnol. 25: 465–72.

15. Hamill, P., K. Brown, H. Jenssen, and R.E.W. Hancock. 2008. Novel anti-infectives: is host defence the answer? Curr. Opin. Biotechnol. 19: 628–36.

16. Jenssen, H., and R.E.W. Hancock. 2010. Therapeutic potential of HDPs as immunomodulatory agents. In: Antimicrobial peptides. Methods and protocols. A. Giuliani and A.C. Rinaldi (eds.), Humana Press-Springer, New York, NY, USA, 329-47.

17. Schow, E. V, J.A. Freites, P. Cheng, A. Bernsel, G. von Heijne, et al. 2011. Arginine in membranes: the connection between molecular dynamics simulations and translocon-mediated insertion experiments. J. Membr. Biol. 239: 35–48.

18. Mishra, A., G.H. Lai, N.W. Schmidt, V.Z. Sun, A.R. Rodriguez, et al. 2011. Translocation of HIV TAT peptide and analogues induced by multiplexed membrane and cytoskeletal interactions. Proc. Natl. Acad. Sci. U. S. A. 108: 16883–8.

19. Schmidt, N.W., A. Mishra, G.H. Lai, M. Davis, L.K. Sanders, et al. 2011. Criterion for amino acid composition of defensins and antimicrobial peptides based on geometry of membrane destabilization. J. Am. Chem. Soc. 133: 6720–7.

20. Wadhwani, P., R.F. Epand, N. Heidenreich, J. Bürck, A.S. Ulrich, et al. 2012. Membrane-active peptides and the clustering of anionic lipids. Biophys. J. 103: 265–74.

21. El Amri, C., F. Bruston, and P. Joanne. 2007. Intrinsic flexibility and structural adaptability of Plasticins membrane-damaging peptides as a strategy for functional versatility. Eur. Biophys. J. 36: 901–9.

22. Conlon, J.M., M. Mechkarska, J.M. Pantic, M.L. Lukic, L. Coquet, et al. 2013. An immunomodulatory peptide related to frenatin 2 from skin secretions of the Tyrrhenian painted frog Discoglossus sardus (Alytidae). Peptides. 40: 65–71.

23. Russ, W.P., and D.M. Engelman. 2000. The GxxxG motif: a framework for transmembrane helix-helix association. J. Mol. Biol. 296: 911–9.

24. Fink, A., N. Sal-Man, D. Gerber, and Y. Shai. 2012. Transmembrane domains interactions within the membrane milieu: principles, advances and challenges. Biochim. Biophys. Acta. 1818: 974–83.

25. Chatzidakis, I., and C. Mamalaki. 2010. T cells as sources and targets of TNF: implications for immunity and autoimmunity. Curr. Dir. Autoimmun. 11: 105–18.

5.1 Introduction and background

Despite the intense research on the AMPs during the last decades, little practical outcome has been generated. Multiple hurdles exist related to the fact that naturally occurring AMPs present serious drawbacks that limit their direct development into clinically applicable antibiotics. These include, for instance, high costs of manufacture, susceptibility to protease degradation and a reduced activity in the presence of salts at physiological concentrations [1–3]. Given the inherent limitations of naturally occurring AMPs, two general approaches have emerged to overcome these major obstacles, i.e. the modification of existing peptide sequences or the de-novo synthesis of peptides, and the development of synthetic molecules mimicking the properties and activities of AMPs (see Chapter 1 and references quoted therein). Among the latter, dendrimeric peptides have received large attention. These are radial or wedge-like branched macromolecules consisting of a branching core and a certain number of covalently attached functional units [4]. Usually, dendrimeric peptides display increased activity compared to their monomeric counterparts, probably because of the higher local concentration of the bioactive units. Moreover, they have a greater stability to peptidases and proteases, possibly due to the steric hindrance of the branching core that would limit the cleavage rates of plasma peptidases, thus increasing the peptides' pharmacokinetics properties [5].

Starting from a linear AMP sequence, originally identified by selecting a random phage library against whole *E. coli* cells, a rational modification and optimization led to the tetra-branched peptide known as SB041, found to be especially active against Gram-negative strains and able to strongly bind *E. coli* and *P. aeruginosa* lipopolysaccharide (LPS) in vitro [6]. Further modifications of the primary sequence led, more recently, to the so-called SB056, a novel AMP with a dimeric dendrimer scaffold. SB peptides are also characterized by the presence of a relatively short lipophilic tail, which was specifically added to improve membrane anchoring. SB056 showed high activity against Gram-negative bacteria, with a potency comparable to that of colistin and polymyxin B, but a broader spectrum of activity, with some limited activity also against Gram-positive bacteria [7]. A biophysical characterization through circular dichroism (CD), nuclear magnetic resonance (NMR), molecular dynamics (MD) simulation, and membrane affinity assayed through lipid monolayer surface pressure experiments, revealed that this interesting peptide is membrane-active, and tends to fold into a β-type conformation in lipid environment [7]. The primary

sequence [WKKIRVRLSA] of the peptidic branches of SB056 is characterized by a striking pattern of alternating hydrophilic and hydrophobic amino acids (with the only exception of the first two residues), thus being compatible with an extended β-strand conformation on the membrane surface, with the hydrophobic residues embedded between the lipids tail and the hydrophilic ones directed towards the head groups / water interface.

From this point of view, SB056 sequence is clearly reminiscent of the model peptide $[KIGAKI]_3$, which was specifically designed as an amphiphilic β-strand and is endowed with a high antimicrobial activity [8]. This interesting peptide has been suggested as a model system for studying membrane-induced formation of β-amyloid fibrils and plaques. Recently, by electron microscopy and CD, it has been shown to assemble as cross-β-sheet amyloid fibrils even in solution [9], and, by solid-state NMR, to form immobilized β-stranded aggregates in the membrane bound-state [10]. The antimicrobial activity of this model peptide seems to be related to the formation of such aggregates on the bilayer, which, in turn, was found to be strictly dependent on the peptide length [11]. A series of peptides composed of KIGAKI repeats with chain length between 6 and 30 residues have been studied. The β-content of the bound peptides showed a sigmoidal increase with the sequence length, with the midpoint at ~10-12 amino acids [11]. Peptides with a chain length >10 easily formed β-structures, while a poor β-structuration was observed in shorter peptides.

The peptidic part of the SB056 dendrimeric peptide has only 10 residues, thus being only a half-length of the model peptide $[KIGAKI]_3$ and representing the lower limit for β-structuration. As said, the amino acid sequence of the peptidic functional unit of SB056 [WKKIRVRLSA] presents a pattern of alternating charged/polar and hydrophobic residues but the first two amino acids at the N-terminus (figure 5.1). Inspired by the KIGAKI peptides, a rational optimization of SB056 amphipathic profile was carried out during a six months stay in the prof. Anne S. Ulrich labs at the Karlsruhe Institute of Technology (KIT), Germany. SB056 sequence was modified by exchanging the position of the first two residues [KWKIRVRLSA] (figure 5.1). During the present Ph.D. work the dendrimeric peptide and the monomeric counterpart of either the original peptide and its optimized analogue (SB056-den, SB056-lin, β-SB056-den and β-SB056-lin, respectively) were investigated. A wide arsenal of techniques has been employed, in order to characterize their biologic activity and biophysical behavior.

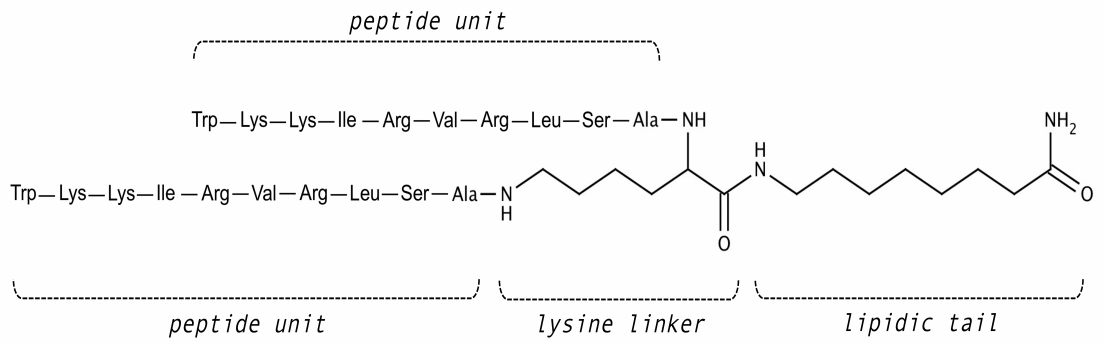

Figure 5.1 The SB056-den peptide. Schematic representation of the characteristic dendrimeric structure of the SB056 peptide. In the case of the β-SB056 analogues, the position of Trp-1 and Lys-2 is inverted. Most of the hydrogen atoms are not explicitly reported for the sake of clarity.

5.2 Results and Discussion

5.2.1 Dendrimeric peptides retain their antimicrobial activity at physiological electrolytes concentration

Minimal inhibitory concentration (MIC) assay was performed for all the four analogues. Table 5.1 reports MIC values determined against four standard bacteria strains. *E.coli* and *P.aeruginosa* were chosen as Gram-negative, *S.aureus* and *E.faecalis* as Gram-positive bacteria. In order to take into account the different molecular weight of the linear and dendrimeric analogues, MIC values are expressed in μM.

One of the main drawbacks of applying AMPs *in vivo* is the strong reduction of their antimicrobial activity in the presence of electrolytes [1, 12]. Counter-ions tend to dramatically attenuate the electrostatic interaction between the cationic peptide and the negatively charged bacterial membrane, reducing the binding and, in turn, the overall antimicrobial activity [13–15]. For the present investigation, MIC values have been determined either in the absence and in the presence of 150 mM NaCl in the buffered medium, in order to evaluate the salt effect on the antimicrobial activity of the peptides under investigation. The concentration value of 150 mM have been chosen on the basis of the literature, where this is reported to be the typical electrolytes concentration in biological fluids at physiologic conditions [16].

The results (Table 5.1) show that in the absence of added salt to the medium, SB056-den resulted to be more active than its linear counterpart, as previously reported [7]. Thus, the original idea behind the dendrimeric peptides design [6, 17] seems to be confirmed. This increased activity is usually attributed to the higher local concentration of the bioactive units due to the branched dendrimeric structure. β-SB056-lin, showed an improved antimicrobial activity against all the tested strains when compared to the SB056-lin. It resulted to be

comparable to the SB056-den, supporting the success of the structure optimization we performed. However, the dendrimeric optimized β-SB056-den showed higher MIC values than its linear counterpart. These results suggest that the extremely good amphipathic structure adopted by the β-SB056-lin is somewhat disturbed by the introduction of the branched core and the lipophilic tail.

In presence of 150 mM NaCl, both SB056-lin and β-SB056-lin showed a significant reduction of antimicrobial activity as expected. This is likely due to the charge shielding produced by the counter-ions cloud on both the peptide and the membrane surface, thus reducing their electrostatic interaction and, ultimately, peptide binding. On the other hand, both the dendrimeric peptides retained their antimicrobial activity (in some cases it improved), clearly showing that the dendrimeric structure is somehow able to overcome the electrolytes shielding effect.

Finally, it is interesting to note that, despite a general difference in the content of negatively charge lipids is known between Gram-positive and Gram-negative bacteria (it is significantly higher in the former [18, 19]), the relative antimicrobial activity observed for the four peptides investigated was the same against all the tested strains.

Table 5.1 MIC of four SB056 analogues against two Gram-negative and two Gram-positive standard strains. Values were determined either without and with 150 mM NaCl added to the medium.

	Microorganism/Strain							
	E. coli ATCC 25922		*P. aeruginosa* ATCC 27853		*S. aureus* ATCC 25923		*E. faecalis* ATCC 29212	
MIC (μM)	0 mM NaCl	150 mM NaCl	0 mM NaCl	150 mM NaCl	0 mM NaCl	150 mM NaCl	0 mM NaCl	150 mM NaCl
SB056-lin	45	178	45	45	45	89	178	178
SB056-den	10	3	10	10	5	5	20	20
β-SB056-lin	3	6	11	22	6	11	45	89
β-SB056-den	20	5	20	5	20	10	20	10

5.2.2 Dendrimeric peptides preserve high affinity for negatively charged membrane models at physiological electrolytes concentration

Upon binding, peptide's tryptophan moves from the buffered water to the more hydrophobic environment characterizing the lipid bilayer. Typically, this leads to a blue shift and an increase in the quantum yield of tryptophan fluorescence [20, 21]. However, fluorescence intensity ultimately depends on many different factors, hard to be quantitatively

taken into account. For instance, after the binding, if peptide oligomerization occurs, tryptophan residues could result in close proximity with each other leading to fluorescence self-quenching. Another source of quenching might be the interaction between tryptophan and the positively charged peptide residues [22], like the tryptophan flanking lysines in the peptides under investigation. Moreover, quenching could also be due to the charged head group of POPG interacting with tryptophan π-orbitals [20]. All of these contributions strictly depend upon the specific secondary structure adopted by the peptide, possible oligomerization and peptide orientation with respect to the bilayer. Insertion depth is also clearly fundamental, as well as the specific position of the tryptophan along the peptide sequence. In addition, the bilayer composition should exert an important influence on the observed fluorescence intensity. Thus, even if, in principle, intensity as a function of the lipid/peptide ([L]/[P]) ratio can be related to the peptide binding constant [21], no attempt was made in the present work to quantitatively estimate the latter, since accurate structural information about the vesicles-bound state of SB056 peptides is still lacking.

Nevertheless, tryptophan blue shift is able to provide important qualitative information about the relative binding strength/affinity of different analogues for the same membrane model. Similarly, the relative binding affinity of a peptide for differently charged membrane models can be evaluated. Emission wavelength (λ) decreases with increasing [L]/[P] until saturation is usually reached [20, 21]. Despite the maximum difference ($\Delta\lambda_{max}$) between saturation and the starting λ (in the absence of lipids) might depend upon several factors similarly to fluorescence intensity, the higher the peptide binding affinity, the lower the saturation [L]/[P].

The four SB056 analogues were investigated with increasing POPG/POPC molar ratio, since it is known that eukaryotic membranes are characterized by a very low content of negatively charged lipids, while this is remarkably higher in bacterial plasma membranes [23, 24]. In addition, Gram-negative bacteria typically have a content of negatively charged lipids around 30%, while it is 70% or more in the Gram-positive ones [18, 19]. Moreover, as already pointed out for the MIC assays, the effect of physiological electrolytes concentration on the peptide binding affinity was also investigated by performing the experiments either in the absence and presence of 150 mM NaCl in the 10 mM phosphate buffer employed for liposomes preparation. Figure 5.2 and 5.3 show the results obtained without and with NaCl, respectively. The absolute value of Δλ is plotted as a function of the [L]/[P] molar ratio. In all investigated cases, binding affinity increased with increasing the POPG content of vesicles. This was not surprising, since electrostatics plays a major role in peptide binding, determining

peptide selectivity for bacterial membranes.

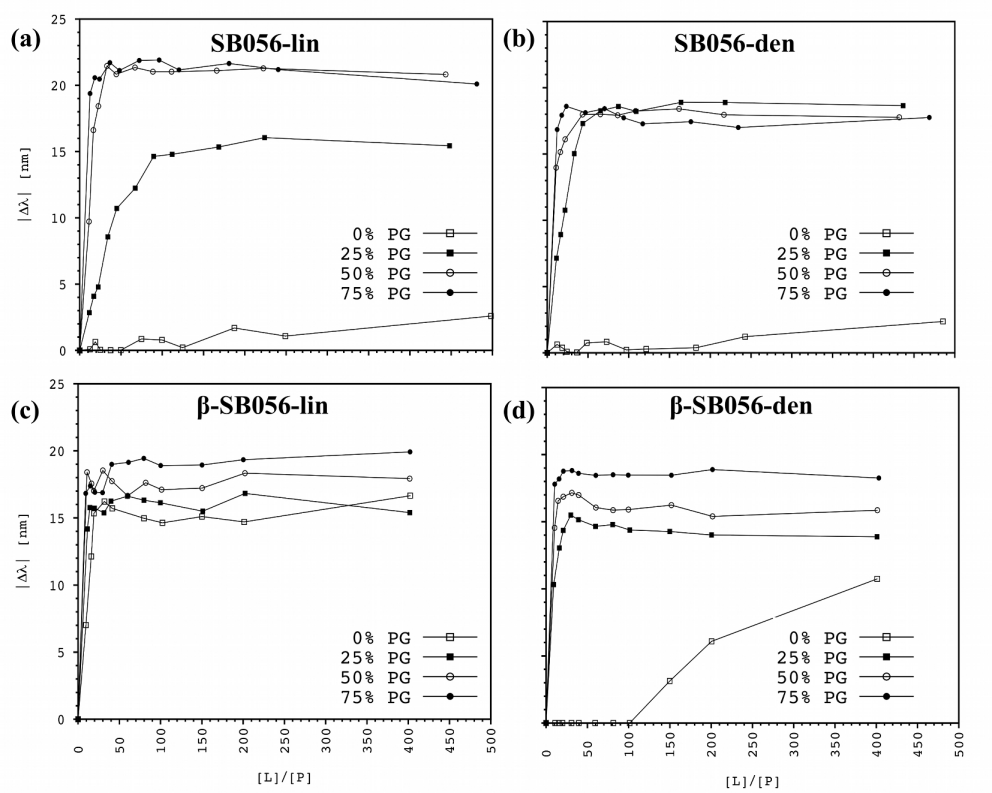

Figure 5.2 Peptide binding without added NaCl. The blue shift of tryptophan fluorescence emission |Δλ| is plotted as a function of [L]/[P] ratio for the four SB056 analogues in the presence of differently charged POPC/POPG LUVs. The lower the [L]/[P] ratio needed to reach saturation, the higher the peptide binding affinity. Measurements were carried out in 10 mM PB with no added NaCl.

In the absence of added NaCl (figure 5.2), SB056-lin showed a remarkable binding affinity starting from 50%PG (figure 5.2a), while its dendrimeric counterpart SB056-den from 25%PG only (figure 5.2b). Neither the linear nor the dendrimeric peptide showed a significant affinity for the 100% POPC liposomes as expected. This might be simply explained by the dendrimeric peptide having twice the positive charge per mole. The other dendrimeric peptide β-SB056-den (figure 5.2d) showed a comparable trend, even if it resulted to have a not-negligible, although low, affinity for the 100% POPC membrane. Finally, β-SB056-lin was the peptide with the highest binding affinity for all the investigated lipid compositions (figure 5.2c), as shown by the tryptophan fluorescence shift going to saturation faster than observed for all the other analogues. Binding was extremely strong even for the 100% POPC membrane. This is not compatible with the binding being driven only by electrostatics, since the linear peptide has half the positive charge per mole with respect to the dendrimeric one and, in addition, our sequence optimization consisted simply in exchanging the first two

residues, thus leaving the total charge unaffected. Nevertheless, SB056-lin and β-SB056-lin showed a remarkable difference in their relative binding affinity, the lowest and the highest, respectively, among the four peptides investigated.

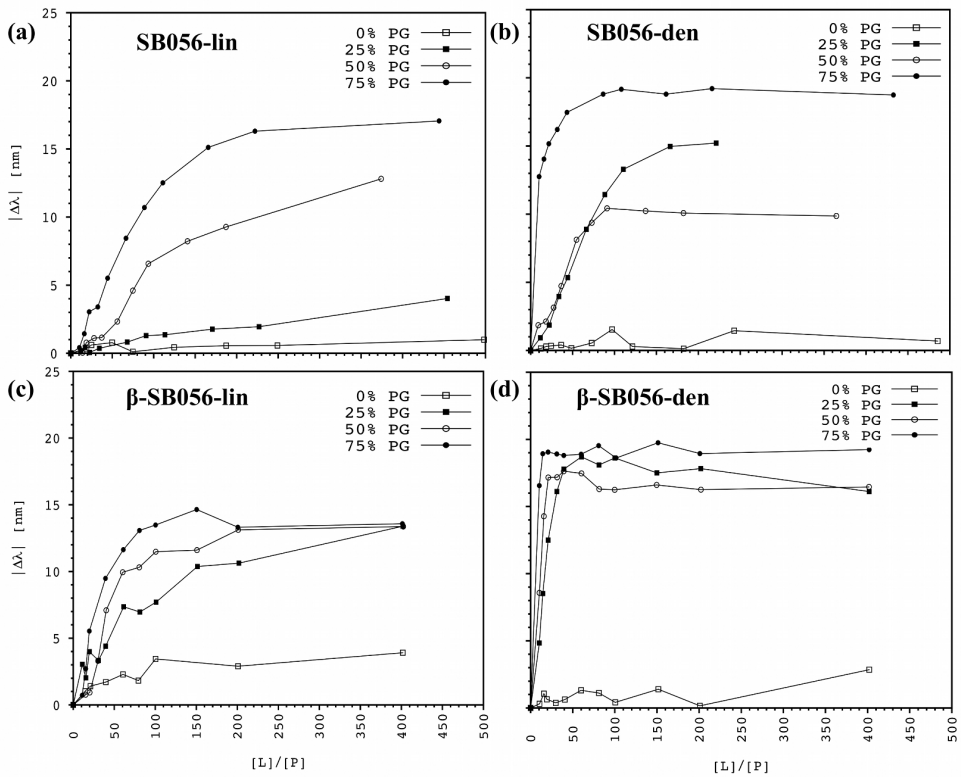

Figure 5.3 Peptide binding in the presence of added NaCl. The blue shift of tryptophan fluorescence emission |Δλ| is plotted as a function of [L]/[P] ratio for the four SB056 analogues in the presence of differently charged POPC/POPG LUVs. The lower the [L]/[P] ratio needed to reach saturation, the higher the peptide binding affinity. Measurements were carried out in 10 mM PB + 150 mM NaCl.

Electrolytes addition decreased binding affinity of all the peptides as expected (figure 5.3), confirming the fundamental role of the electrostatics. Nevertheless, similarly to what was observed for the antimicrobial activity, while salt effect was dramatic for both linear peptides, dedrimeric ones were less affected. These results suggest that the dendrimers' two-fold positive charge is less effectively shielded by counter-ions than for linear peptides and/or that the lipophilic tail plays a fundamental role in stabilizing the peptide bound-state. It is also possible to speculate that, upon approaching the membrane, the counter-ions density in the solvent volume between the membrane and pre-folded peptide should be higher in the case of the dendrimeric peptides. This might cause a higher entropic increase due to counter-ions (and polarized water) release upon peptide binding [25].

Finally, by comparing the two dendrimeric peptides, it is interesting to note that β-

SB056-den retains binding affinity in the presence of salt more than SB056-den, despite they bear exactly the same net positive charge, further showing that charged/polar (thus, also hydrophobic) residues distribution along the sequence is very important as peptide behavior determinant.

5.2.3 Excessive negative charge in the membrane worsens peptide insertion

The ability of the four analogues to insert into lipid monolayers was investigated with surface pressure analysis. Monolayer surface-pressure increases upon peptide insertion within phospholipids because of their lateral packing being augmented. Usually, the intersection point with both the x- and y-axis is taken into account for results interpretation and peptides comparison [26–29]. However, since it is known from literature that physiological membranes tend to maintain a specific lipid packing density on the order of 30 mN/m [27, 29–31], $\Delta\pi$ obtained at this specific value of π_0 were compared for the different SB056 analogues in the various monolayers employed. Anyway, the trend observed was the same for the corresponding π_{ex} values. Results are shown in figure 5.4 as a function of monolayer POPG molar percentage.

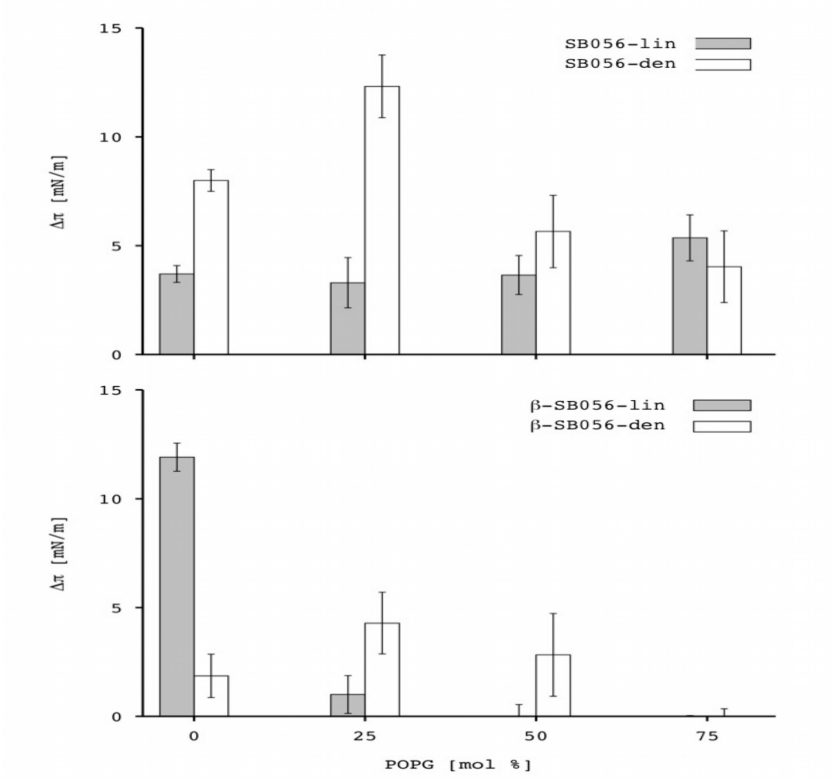

Figure 5.4 Insertion of SB056 analogues in lipid monolayers. Values of $\Delta\pi$ extrapolated at π_0 = 30 mN/m are shown for both linear and dendrimeric (**a**) SB056 and (**b**) β-SB056 peptides as a function of POPG content in the monolayer.

It is important to stress here that the final observed surface pressure might be highly case-specific. The value ultimately depends upon the dimension and orientation of the inserting peptide and, in addition, to the size of the oligomers if they are formed. As said, detailed structural information are still lacking for these novel peptides and similarity cannot be *a priori* assumed. Thus, in order to avoid possible misleading interpretations about the values obtained for the different analogues, let us focus on the trend as a function of the monolayer negative charge for each of the peptide under investigation separately.

From a general point of view, an increase in insertion capability have been observed for all the peptides investigated up to a certain monolayer PG content. However, insertion efficacy decreased with further increasing monolayer negative charge. Nevertheless, a strong correlation with binding affinity was observed for insertion. Indeed, strictly depending on the intrinsic membrane binding affinity of the specific peptide under investigation, as soon as membrane negative charge became too high, peptide insertion was prevented. For the sake of clarity, let us follow the order of binding affinity observed in the absence of added NaCl: SB056-lin < SB056- den < β-SB056-den < β-SB056-lin.

SB056-lin was the peptide with the lowest general binding affinity. Indeed, Δπ did not change significantly with varying monolayer PG content (figure 5.4a).

The two dendrimeric analogues showed a comparable binding affinity and, indeed, the same Δπ trend as a function of %PG (figure 5.4a, b). Δπ reached the maximum at 25% PG, then decreasing with further increasing the monolayer negative charge.

Finally, β-SB056-lin was the analogue with the highest general binding affinity. It showed a remarkable insertion in the 0%PG model but Δπ dropped as soon as 25% PG was present in the monolayer.

5.2.4 Excesive negative charge in the membrane worsens peptide structural order: a SRCD study

Peptide secondary structure adopted in the presence of differently charged membrane models (with increasing POPG/PC molar ratios) was investigated through SRCD spectroscopy and the measured spectra are shown in figure 5.5. Due to remarkable intensity difference, y-scale has been properly set for each peptide in order to make spectral shape clearly observable. Results show that all the SB056 analogues have a clear tendency for β-type folding in the presence of lipid vesicles. This is in agreement with a previous work about SB056 folding propensity in water/trifluoroethanol [7]. The characteristic positive band at 190-200 nm and the negative one at 210-220 nm are clearly distinguishable on the majority of

the spectra. However, relatively low intensity and deviations from an ideal β-type spectrum have been sometimes observed. These data suggest that structural order and/or peptide aggregation depends on the negative charge of the bilayer, that the original and sequence optimized SB056 analogues are differently sensitive to membrane charge variation, and that they probably fold/aggregate in different ways.

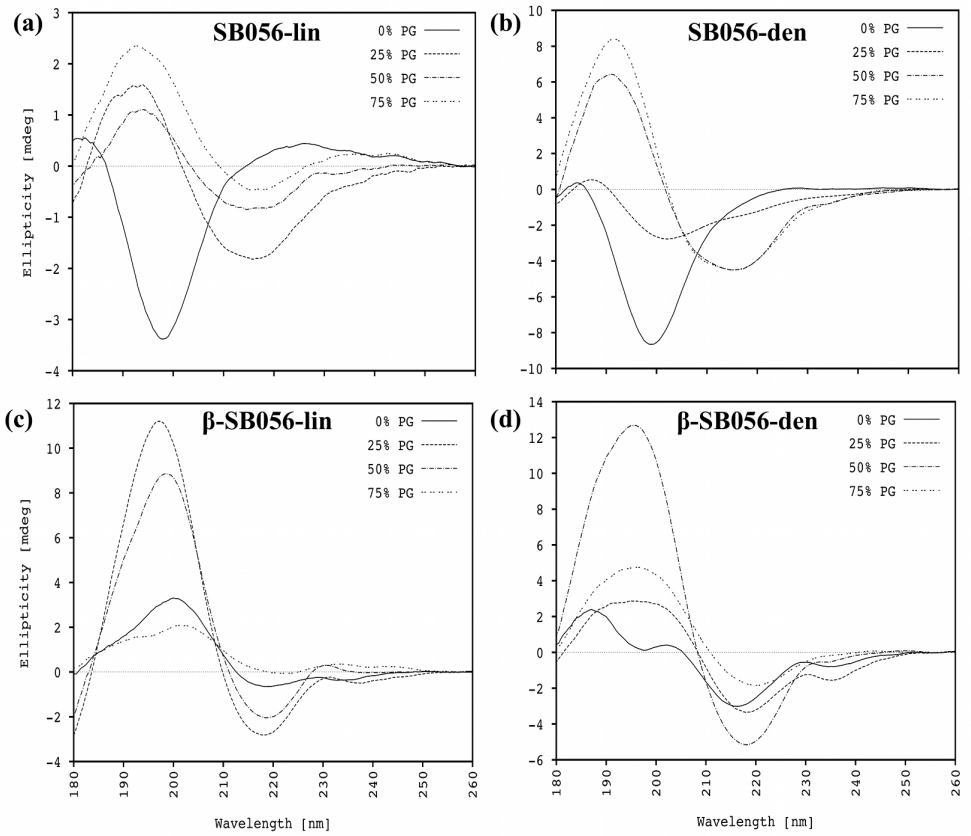

Figure 5.5 Characterization of the secondary structure of SB056 analoues. SRCD spectra of the four SB056 analogues in the presence of differently charged SUVs. The y-scale has been properly chosen in each case to make spectral shape clearly observable.

The spectrum of SB056-lin in pure POPC vesicles (that is 0%PG in figure 5.5a) presents an intense negative band at ~198 nm and a small positive band around 225 nm. These two spectral features are attributable to a random coil peptide, although they are very similar to those characterizing PPII secondary structure [32]. However, while PPII peptides are usually characterized by negative ellipticity in the range 180-190 nm, random coil is distinguished by positive ellipticity in the same range [32]. Since, synchrotron radiation allows to obtain suitable CD spectra below 190 nm, it is possible to unambiguously confirm that SB056-lin is actually random coil in the presence of 0% POPG vesicles (figure 5.5a). This is absolutely compatible with the negligible binding observed with fluorescence spectroscopy (figure 5.3a). Although peptide binding was found to increase with increasing

the negative charge in the bilayer, CD data revealed that structuration of SB056-lin (figure 5.5a) is poor in all the investigated cases, up to 100%PG vesicles. Spectral shape indicates some kind of β-type structure, as said, with a positive band at ~195 nm and a negative one at ~217 nm, but the relatively low intensity of these bands suggest to rule out the formation of regular β-strands on the bilayer.

Similarly, SB056-den shows the typical random coiled spectral shape in 0%PG vesicles, for which it had a negligible binding affinity indeed (figure 5.5b). However, SRCD spectrum dramatically changes moving to 25% and 50% PG, until β-structure shape was clearly observed. Ellipticity further increased with increasing the vesicles' content of negatively charged lipids up to 75%.

β-SB056-den showed a not negligible binding to 0%PG liposomes; the corresponding SRCD spectrum resulted to be difficult to be straightforwardly interpreted. Surely peptide structure was not ordered at all but, differently from the two SB056 peptides, it was not purely random coiled (figure 5.5d). Similarly to the other dendrimeric peptide, SRCD spectrum dramatically changed moving to 25% and 50% PG, until β-structure shape was observed with the maximum ellipticity in this case. However, with further increasing the PG content, ellipticity significantly decreased.

Finally, the sequence optimized β-SB056-lin peptide showed a strong binding affinity even for pure POPC vesicles. In agreement with fluorescence spectroscopy data, the corresponding SRCD spectrum (figure 5.5c) is clearly not indicative of a random coil structure. The SRCD spectrum obtained in the presence of 25%PG vesicles (figure 5.5c) is very intense and clearly indicates the peptide folding as well-ordered β-strands. However, similarly to its dendrimeric counter-part, as soon as vesicles' negative charge is increased distortions from the canonical β-type spectral shape are visible.

5.2.5 Towards the three-dimensional structure of SB056's peptides through liquid state NMR

A first atomic-level structural characterization was attempted for these novel peptides through liquid state NMR in the presence of detergent micelles. The same conditions used for SRCD spectroscopy were employed, that is a [L]/[P] molar ratio equal to 25 and a proper DPC/SDS molar ratio in order to maintain the overall system electroneutrality. In particular, from SRCD spectroscopy, electroneutrality appeared to be fundamental for the peptides to achieve a high degree of structuration. However, moving from SRCD to NMR, a three order of magnitude difference in the species concentration has to be taken into account (μM vs. mM range), as well as the dramatic reduction in size of the membrane model employed, small

unilamellar vesicles and micelles, respectively. Indeed, the former have a typical diameter of ~20 nm, the latter are characterized by a diameter of ~3-4 nm and, in turn, a higher curvature. For the sake of clarity, results will be presented in the same order as in the previous sections, i.e.: SB056-lin, SB056-den, β-SB056-den and β-SB056-lin.

5.2.5.1 SB056-lin

SB056-lin was investigated in the presence of mixed micelles constituted by DPC/SDS at 3/1 molar ratio, at a [L]/[P] of 25. Chemical shift values and the $^{3}J_{HNH_{\alpha}}$ coupling constants are reported in table A.4 (in the Appendix). The J coupling constants >8 Hz suggest a β-type folding [33] in agreement with the SRCD results. However, the application of TALOS+ [34], which make use of the experimental chemical shifts, predicted a helical structure from residues K3 to S9. This apparent contradiction might be explained by considering that the Karplus relationship between H^{N}-H^{α} J-couplings and the backbone Φ angle is parameterized for proteins [33] and some deviations should be envisaged for very short peptides like the SB056-lin. In addition, the relationship allows to estimate the value for the backbone Φ angle but does not tell us everything about the correspondent Ψ angle. A close inspection of the Ramachandran plot reveals that the region characteristic for right-handed helices covers a relatively wide range of Φ values, which is comparable to that for β-type structures [35]. Actually, the main discrimination is provided by the value of the Ψ angles that are not directly accessible from the measure of H^{N}-H^{α} J-couplings. Thus, one possible explanation for our results should be that SB056-lin folded in a helical conformation characterized by less usual but energetically and sterically accessible backbone Φ angles [35].

This was absolutely unexpected in the light of the SRCD results but the analysis of the sequential NOEs, summarized in figure 5.6, bolstered this hypothesis. The presence of several H^{α}_{i}-H^{N}_{i+n} and H^{N}_{i}-H^{N}_{i+n} strongly suggest a helical folding, especially in the middle of the peptide sequence. However, no attempt was made to calculate a 3D structure with the software Dynamo (http://spin.niddk.nih.gov/NMRPipe/dynamo/) at this stage. For the sake of completeness it has to be reported that a sort of white filament was found to have precipitated in the test-tube at the end of the NMR measurement series (figure 5.7), which took about one week. It is not known whether some micelle-bound or –unbound peptide aggregates precipitated but it was a clear indication for sample instability. Moreover, a slight although significant shift of the ^{1}H resonances was observed comparing the first with the last acquired spectra, clearly due the peptide equilibrium shifting towards the aggregated state.

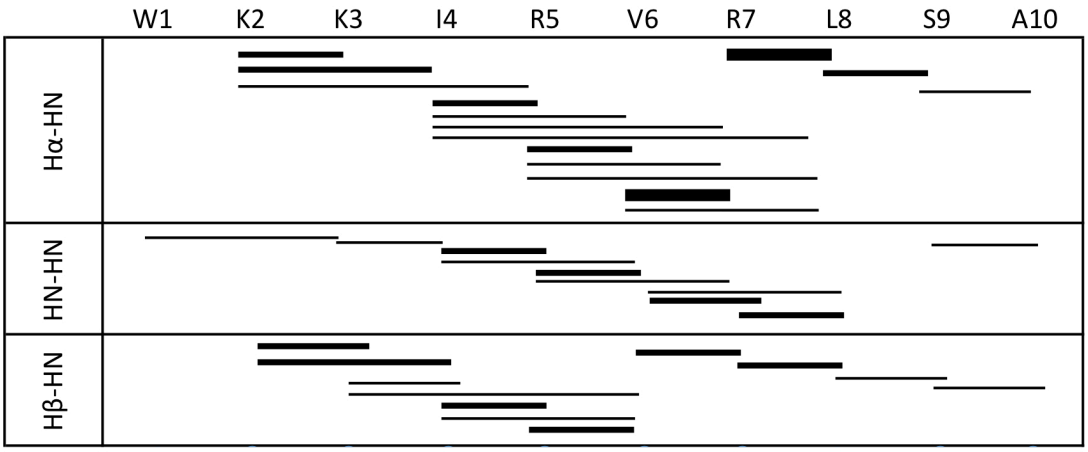

Figure 5.6 Short and medium-range interproton NOEs observed for SB056-lin. Dipolar interproton interactions found for SB056-lin in DPC/SDS 3/1 mol/mol are reported as lines connecting the two residues involved. Lines thickness is proportional to the relative intensity of the corresponding NOESY cross peak.

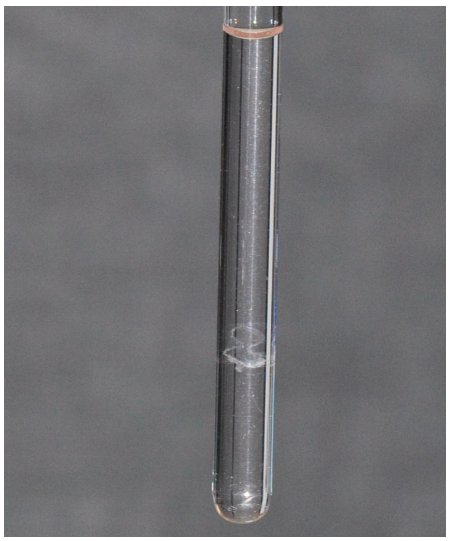

Figure 5.7 SB056-lin NMR sample after one week of measurements. Either some micelles-bound or –unbound peptide aggregates precipitated in the test-tube forming a sort of filament.

Further experiments would be needed to elucidate SB056-lin structure but these first data clearly indicate a very complicated and unusual behavior. In particular, it seems that the membrane model is able to significantly affect the folded structure, which was found to be β-like in the presence of lipid vesicles and helical in the presence of detergent micelles. It is thus possible that we observed a meta-stable state, which does not necessarily correlate with the biologic function. Thus, in the light of the SB056-lin evident tendency for aggregation, before spending efforts, time and funding on this peptide, which is the less active one among the four analogues, we preferred to examine the other three peptides.

5.2.5.2 SB056-den

SB056-den was investigated in the presence of mixed micelles composed by DPC/SDS at 1/1 molar ratio. Unfortunately, when the (limpid) micelles solution was used to solubilize the peptide, a strongly opalescent solution was obtained, indicating a strong aggregation into larger particles. Spectra acquisition was attempted by the way, and interestingly the ^{1}H spectrum was devoid of almost all the backbone resonances (figure 5.8a), while the signals due to most of the side chains protons were observed. To the best of my knowledge such phenomenon has been never reported in the literature. It might be due to a strong backbone immobilization in the aggregated state, leading to a dramatic relaxation rate increase and, in turn, excessive resonance broadening. On the other hand, side chains resonances were clearly visible, suggesting that immobilization involve only (or mainly) the peptide backbone. However, resonance assignment and structure calculations are mostly based on the backbone resonances, thus, it was not possible to study SB056-den in these conditions through liquid-state NMR.

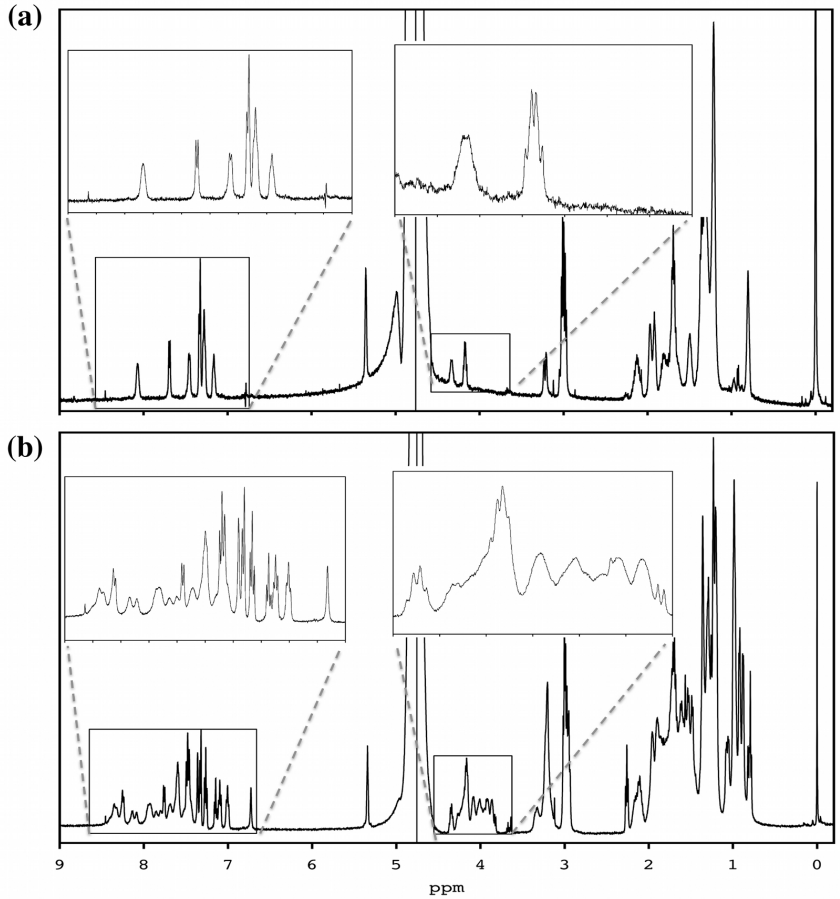

Figure 5.8. ^{1}H NMR spectra acquired on SB056-den. Spectra of SB056-den in the presence of (a) DPC/SDS 1/1 mol/mol ([L]/[P]=25) and (b) DPC/SDS 3/1 mol/mol ([L]/[P]=50). The H^{N} and H^{α} regions are zoomed in the two insets.

In order to decrease the number of peptides per micelle, a new aliquot of SB056-den was solubilized using a solution of mixed micelles formed by DPC/SDS 3/1 mol/mol at a [L]/[P] ratio of 50. In practice, the [L]/[P] ratio was increased by adding only DPC, in order to preserve the system electroneutrality. In these conditions a limpid solution was obtained, indeed, and all the expected resonances were visible in the ^{1}H NMR spectrum (figure 5.8b) allowing to acquire the two-dimensional spectra for structure investigation.

Table A.5 (in the Appendix) reports the chemical shift values and the $H^{N}H^{\alpha}$ J-coupling constants. First, it is interesting to note that, when SB056-den was studied in water/TFE mixtures [7], homologous residues belonging to the two peptide branches were not distinguishable, but those closest to the lysine linker. The peptide was not structured and the high mobility in solution provided homologous residues to be chemically and magnetically equivalent, thus, their resonances to have the same chemical shift. The only inequivalent residues where those closest to the linker due to the intrinsic molecular asymmetry of the dendrimeric scaffold. In the presence of the mixed micelles, on the other hand, both the H^{N} and H^{α} of all the 20 residues were resolved in the 2D spectra (see figure A.6 in the Appendix for an example), meaning that the residues belonging to the different peptide branches were not magnetically equivalent and strongly suggesting SB056-den structuration. Thus, the two peptide branches in the folded structure should have a certain degree of inequivalence. They might be differently folded and/or might differently interact with the micelle.

The NMR results shares some similarities with those collected on the linear monomer. The application of TALOS+ [34], on the basis of the experimental chemical shifts, predicted a helical structure for both the branches ranging from the residue K2/3 to S9. Again, J-couplings around 10 Hz were found from the middle of the amino acid sequence all the way to the linker. Values of ~7 Hz were observed for the first part of the sequence. Such values are typically interpreted as due to dynamic averaging over different conformations, thus, indicative for unstructured protein fragments but, in principle, they might also reflect some specific backbone conformation [33]. The sequential resonances assignment is particularly challenging in the case of dendrimeric peptides. The sequence of the peptide branches is identical, thus it is very difficult to unambiguously attribute the homologous residues. We are really walking on the cutting edge of the peptides/NMR field. There aren't similar cases reported in the literature to the best of my knowledge. Thus, we tried to look at the results without preconceptions, checking all the possibilities, even those unprecedented. Finally, three different hypotheses were put forward, as described hereinafter.

Usually, the so-called "sequential NOEs" are observed in two-dimensional NOESY

spectra arising from the dipolar interaction between the H^{α}_{i} and H^{N}_{i+1}, as well as between the H^{N}_{i} and H^{N}_{i+1}, where the 'i' subscript indicates the i^{th} amino acid residue along the sequence. These cross-peaks are the most important for residues sequential assignment and are observed both for helical and β-type structures. In the case of helical structures, $H^{\alpha}H^{N}_{(i,i+1)}$ have an intensity comparable to, or are slightly less intense than, the $H^{N}H^{N}_{(i,i+1)}$. On the contrary, in the case of β-type conformations, the $H^{\alpha}H^{N}_{(i,i+1)}$ are far more intense than the $H^{N}H^{N}_{(i,i+1)}$ [36]. Helical structure, in addition, usually give rise to a series of "medium-range NOEs", i.e. $H^{\alpha}H^{N}_{(i,i+j)}$, where $2 \leq j \leq 5$. The β-type conformations, on the other hand, can be recognized by the absence of such medium-range NOEs and the presence of $H^{\alpha}H^{N}_{(i,i+j)}$ "long-range NOEs", where $j > 5$.

THE TWO-HELICES HYPOTHESIS

Since sequential NOEs are usually observed despite the specific conformation adopted by the peptide, resonances were firstly assigned by means of these cross-peaks and subsequently checking the resulting attributions for the remaining NOEs. Figure 5.9a schematically shows the NOEs pattern obtained by following this approach (sequential NOEs in blue; medium-range NOEs in green). During the analysis, NOEs were classified as strong, medium and weak on the basis of their relative intensity. Nevertheless, for the sake of clarity, all the lines used in the figure to represent a NOE have the same thickness, but it is important to stress here that the $H^{\alpha}H^{N}_{(i,i+1)}$ and the $H^{N}H^{N}_{(i,i+1)}$ cross-peaks had a comparable intensity. This observation suggested a helical conformation, which appeared to be bolstered by the resulting series of medium-range NOEs. These resonance assignments do agree with TALOS+ [34] predictions but some drawbacks have to be remarked.

One of the branches appear to be more structured than the other. This would provide a plausible explanation for the homologous residues on the two branches being not magnetically equivalent. However, the most probable physical explanation for this difference should be that the more structured branch is interacting with the micelle (that promotes the folding), while the other is unbound and exposed to the solvent. Such a scenario is not fully compatible with a number of other observations and considerations.

The two branches are distinguishable from the NMR point of view and, in the light of the sequential NOEs between the two alanines and the lysine linker we have to conclude that the branch bonded to the alpha-amino group of the linker is the more structured one. What should be the reason why the alpha-branch consistently binds to the micelle while the epsilon-branch doesn't? The two branches, as said, are sequence identical so one should expect to have roughly one half of the peptides in the sample to be micelle-bound with their alpha-

branch and the other half by using the epsilon-branch. Moreover, such a strong difference between the two branches is not compatible with the J-couplings (see above), that resulted to be comparable for homologous residues in the two branches. In particular, if one of the two branches is solvent-exposed and mostly unstructured, one should expect all the J-couplings to be in 6-7 Hz range for that peptide branch, but this was not the case. Finally, the alternate pattern of one hydrophobic / one hydrophilic residue that characterizes the peptide sequence of the SB056 analogues is not suitable to form a helix. The resulting 3D structure for the structured branch would not be amphipathic and, thus, does not provide any possible explanation for a relatively stable binding interaction with the micelle surface.

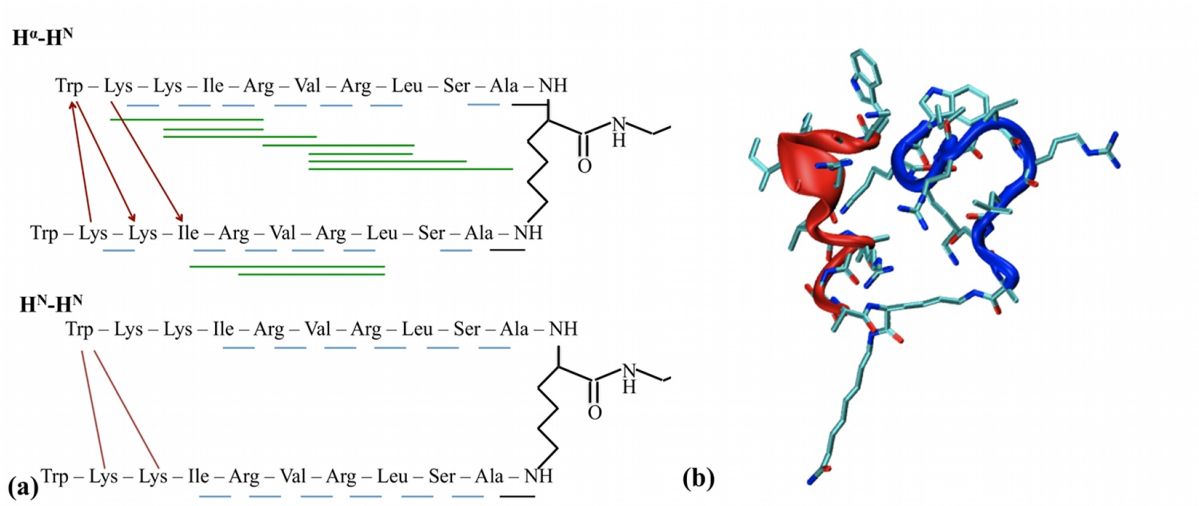

Figure 5.9. The two-helices hypothesis. (a) Schematic representation of the $H^{\alpha}H^{N}$ and $H^{N}H^{N}$ NOEs pattern. Short-range NOEs are shown in blue, medium-range NOEs in green. The resulting inter-branches NOEs are shown in red. For the sake of clarity, all the lines have the same thickness despite the corresponding NOEs relative intensity. (b) The 3D structure obtained from Dynamo calculations. The peptide branch bound to the α-amino group of the lysine linker is shown in red, the one bound to the ε-amino group is in blue.

The most important evidence against this two-helices model is the presence of just few inter-branches NOEs at the N-termini (red in figure 5.9a). First, it has to be mentioned that the resonance due to the protons of the N-terminal NH_3 group are almost never observed in the experimental conditions employed in the present work, since they are in fast exchange with the water hydrogen atoms. This was exactly the case for the tryptophan residue assigned to the epsilon-branch, whereas, quite surprisingly, the alpha-branch N-term protons were observed in our spectra and they resulted to be involved in dipolar interactions with other peptide protons (giving rise to the NOEs represented with the red lines in figure 5.9a). This suggests that the exchange rate between such protons and the solvent is dramatically reduced,

which is typically observed for peptides when intra-molecular hydrogen bonding interactions are established and/or the protons are buried due to the folded structure and are not solvent accessible [33]. Thus, it clearly shows that the two branches are actually close each other, which, again, is not compatible with the picture of one structured branch on the micelle surface, with the other being unstructured and solvent exposed. In addition, why the two branches should come in close contact only with their termini? This is absolutely unlikely, since the two N-termini are the most positively charged regions of the peptide with two lysine residues and the positively charge N-term amino group in each of the two branches.

Nevertheless, a structure calculation was performed on the basis of the aforementioned sequential assignments. A representative structure is shown in figure 5.9b. NOEs violations were never observed.

THE DIMER HYPOTHESIS

Another possible interpretation of the observed NOEs is the formation of a dimer on the micelle surface. Figure 5.10 shows both the sequential assignments and the corresponding 3D model structure. In practice, all the sequential NOEs are preserved (blue in figure 5.10a), while the medium-range interactions are now attributed to residue located on the alpha-branches of two distinct SB056-den peptides (green in figure 5.10a). It has to be mentioned that an antiparallel pairing is absolutely not compatible with the observed NOEs. Only the hypothesized parallel orientation of the two alpha-branches allowed to obtain a consistent assignment of the NOEs. This hypothesis is more compatible with the SRCD data (although in the presence of a different membrane model), that indicated the formation of some β-type conformation, but contradicts TALOS+ [34] predictions. However, almost all the drawbacks of the two-helices hypothesis are not removed. Again, the alpha-branch should be more structured than the epsilon-one, which has not any physical explanation. Why should the homodimer be formed only by alpha-branches pairing? We should expect also epsilon-epsilon and alpha-epsilon homodimers.

Despite such a partial β-type structure provide a straightforward interpretation for the J-couplings of ~10 Hz, at least for half of the peptide sequence, the hypothesized dimer results in the two peptide branches being extremely different, which is not compatible with the comparable J-coupling values observed for homologous residues located in the two branches. In addition, in the light of the [L]/[P] ratio employed (i.e. 50) and taking into account that the DPC/SDS micelles are formed by roughly 50-70 detergent molecules each [37], there is just one peptide per micelle in solution, thus, the probability that two SB056-den molecules bind the same micelle is expected to be rather low.

Another important consideration against the present hypothesis concerns the relative intensity of the sequential $H^{\alpha}H^{N}$ and $H^{N}H^{N}$ NOEs. In the case of β-type structures, usually, the former are significantly more intense than the latter [36], but this was not the case. Even more important, the few inter-branches NOEs (red in figure 5.10a) are preserved when moving from the two-helices to the dimer hypothesis, thus, exactly the same drawbacks pertaining to the two-helices model apply to the dimer hypothesis too. Finally, in the attempt to convert the medium-range NOEs of the two-helices model (the green lines in figure 5.9a) into the corresponding inter-monomers NOEs of the dimer hypothesis (the green lines in figure 5.10a), the two interactions present over the epsilon-branch were not included because they would have imply a close contact between the two epsilon-branches. Where do these two NOEs come from? Should we hypothesize a complex trimer? It is evident that the present hypothesis of a SB056-den dimer is highly questionable at the least.

A structure calculation was performed on the basis of the aforementioned assignments. A representative structure is shown in figure 5.10b. NOEs violations were never observed but two of them were not included as said.

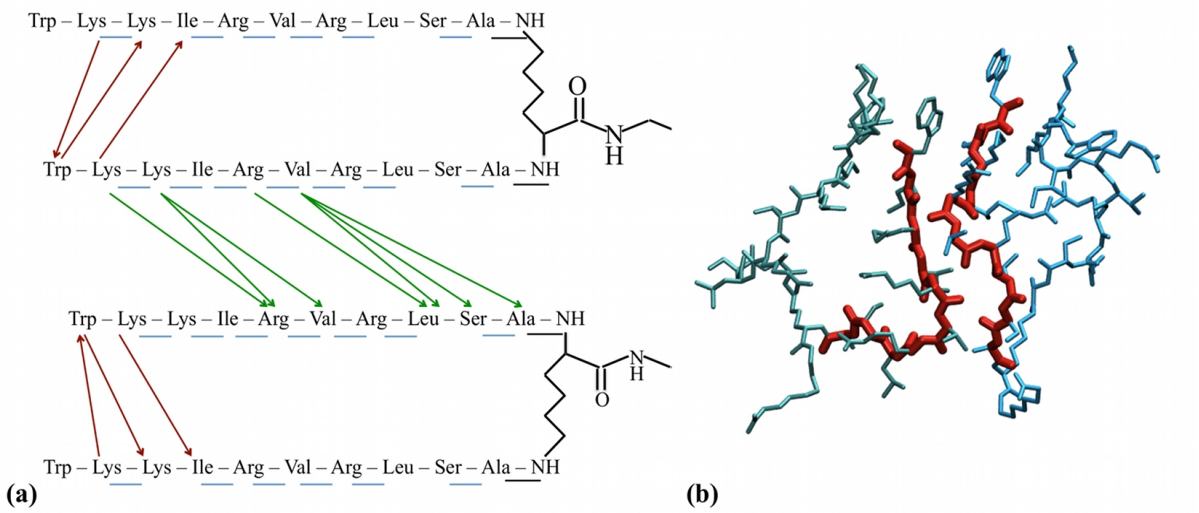

Figure 5.10. The dimer hypothesis. (a) Schematic representation of the $H^{\alpha}H^{N}$ and $H^{N}HN$ NOEs pattern. Short-range NOEs are shown in blue, the inter-monomers NOEs in green. The inter-branches NOEs are still present and shown in red. For the sake of clarity, all the lines have the same thickness despite the corresponding NOEs relative intensity. (b) The 3D structure obtained from Dynamo calculations. The branches bound to the α-amino group of the lysine linker, that are involved in the dimer formation, are shown in red.

THE DOUBLE-HELIX HYPOTHESIS

The assignment of homologous residues to either one or the other peptide branch was driven by the interpretation of a number of NOESY cross-peaks as sequential $H^{\alpha}H^{N}_{(i,\,i+1)}$ and

$H^NH^N_{(i,i+1)}$, as it is usual for standard conformations like α-helices and β-sheets. In the present case, however, this approach led to two distinct hypothesis that suffer from various drawbacks, mainly due to the consequent attribution of the remaining NOESY cross-peaks. In the light of the very special case represented by dendrimeric peptides like the SB056-den, a different assignment approach was attempt, looking for a possible residues assignment combination that justified all the NOEs in a monomeric structure.

In practice, all the NOEs were treated as potential inter-branches "contacts" and homologous residues were iteratively exchanged between the two branches until all the NOEs were assigned (but two ambiguous). A perfectly parallel pairing of the two branches would bring homologous positively charged residues in close contact, thus, a possible one-residue misalignment of the two was taken into consideration. Inter-branches dipolar interaction up to i,i+3 were considered during NOEs assignments. Finally, only one plausible residues combination was found, as shown in figure 5.11a.

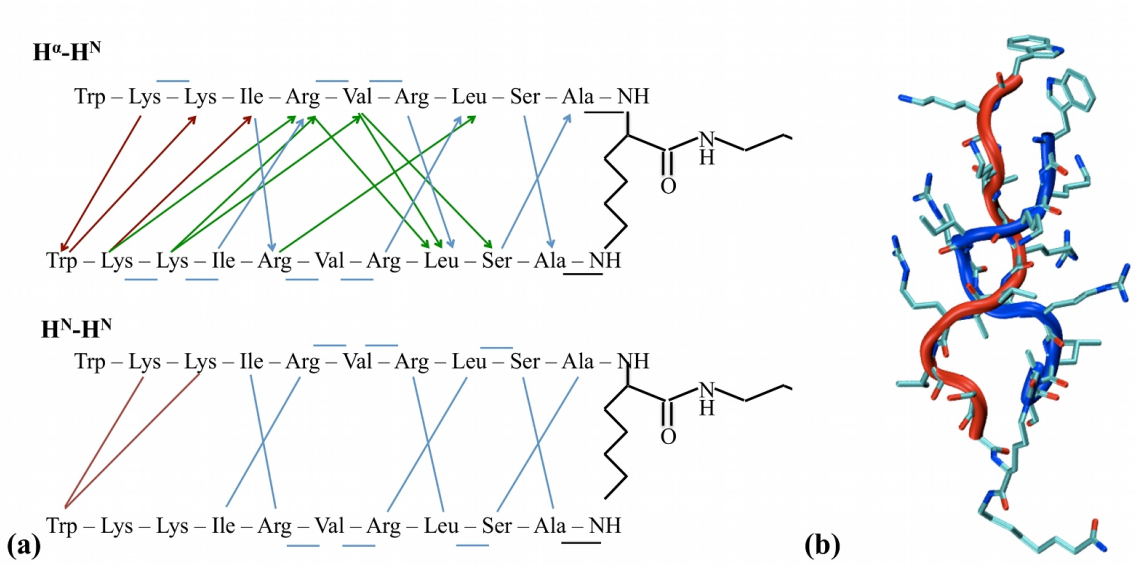

Figure 5.11. The double-helix hypothesis. (a) Schematic representation of the $H^\alpha H^N$ and H^NH^N NOEs pattern. Lines color was preserved from figure 5.9a in order to show the changes in the attributions moving from the original two-helices model to the present hypothesis. For the sake of clarity, all the lines have the same thickness despite the corresponding NOEs relative intensity. (b) The 3D structure obtained from Dynamo calculations. The peptide branch bound to the α-amino group of the lysine linker is shown in red, the one bound to the ε-amino group is in blue.

The corresponding inter-proton distances were restrained during the computational simulated annealing and any one violation was observed in the (10%) conformers with the lowest potential energy. The representative conformation in figure 5.11b shows a peculiar arrangement of the two branches. The two branches are coiled one another forming a right-

handed double-helix. The slight misalignment of the two peptide branches is compatible with the observation of resolved NMR resonances for the homologous residues, providing a valid explanation for their magnetic inequivalence. At the same time, their very similar overall conformation is consistent with the comparable J-couplings observed for the homologous residues. The global helical conformation basically agrees with TALOS+ [34] predictions, and the similarity between the two branches is consistent with the fact that they are sequence identical and it has to be expected that both interact similarly with the micelle.

The only drawback of the 3D structure we obtained is represented by the fact that it is not amphipathic. The positively charged residues are not segregated together on a side of the folded structure but, rather, they seem to point towards multiple directions since they repel each other. However, it is important to stress here that Dynamo (http://spin.niddk.nih.gov/NMRPipe/dynamo/) calculations are performed "*in vacuo*", thus, neither the solvent molecules nor the micelle were explicitly present during the simulated annealing and, in turn, there were no other potential energy terms to "drive" the relative orientation of the peptide side chains but their electrostatic repulsion. Further details were obtained through explicit all-atom molecular dynamics simulations (see below).

5.2.5.3 β-SB056-den

β-SB056-den was investigated in the same conditions as for the SB056-den analogue. Similarly, when a [L]/[P] ratios of 25 was used to reproduce the conditions of the SRCD experiments, peptide solubility resulted to be low. The solution was slightly opalescent and a particulate was visible with the naked eye in the test tube. In order to reduce the number of peptides per micelle, a new sample was prepared with a [L]/[P] ratio of 50, obtained by using a higher amount of DPC but keeping that of the SDS. Finally, DPC/SDS molar ratio was 3/1 but system electroneutrality was preserved. The solution was limpid and transparent but, differently from the case of the SB056-den analogue discussed above, it showed an increased viscosity. The presence of the peptides clearly altered the aggregation state of the detergents dispersion, such that the solution might not be considered as a micelles dispersion but different kind of molecular assemblies could be formed.

When a TOCSY experiment was performed with the usual mixing time of 80 ms, the resulting spectrum was devoid of most of the expected cross-peaks. A possible explanation is that molecular motions decreased with increasing the viscosity of the solution, causing protons relaxation to become faster. As a result, nuclear ^{1}H magnetization probably relaxed within a time shorter than the TOCSY mixing time applied. A trail spectrum was acquired

with a shorter mixing time (40 ms), but this resulted to be too short for an efficient magnetization transfer, leading to a TOCSY spectrum characterized by the presence of cross-peaks only for those ^{1}H nuclei separated by a maximum of three consecutive bonds, i.e. a COSY-like spectrum. The increased relaxation rate is also supported by β-SB056-den showing a ^{1}H spectrum characterized by broader signals than observed in the case of SB056-den (figure 5.12). Thus, the interaction with the detergents appeared to be stronger for the optimized dendrimeric peptide than for its non-optimized analogue, in agreement with the fluorescence spectroscopy data (although a different membrane model was employed).

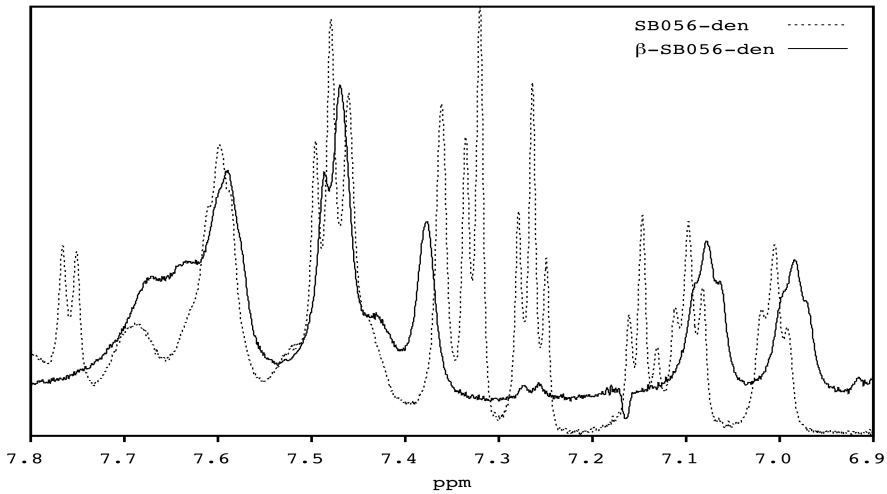

Figure 5.12. β-SB056-den suffered of signal broadening. Tryptophan's side chain signals are shown for instance from both SB056-den and β-SB056-den. It is clearly evident how the latter suffered from a significant signal broadening.

However, NMR data shared numerous similarities with those collected for the original non-optimized dendrimeric peptide. Resonance assignments revealed that the homologous residues belonging to the two peptide branches were not magnetically equivalent. Chemical shifts values are reported in Table A.6 (in the Appendix) and are comparable to those obtained for SB056-den. The J-coupling constants are not reported in the table since their values were abnormally higher than 10 Hz. Due to signal broadening, the measure of J-couplings were possibly affected by a systematic overestimation but it is plausible that they were higher than the dynamic range (6-8 Hz). TALOS+ [34] predicted a helical conformation. Similarly to the case of SB056-den, the NOEs can be interpreted in different ways. In the light of the discussion above, the dimer hypothesis can be rule out. Figure 5.13 shows the two possible interpretations corresponding to either the two-helices or the double-helix hypothesis. It is interesting to note, in the present case, the absence of the inter-branches NOEs at the N-termini.

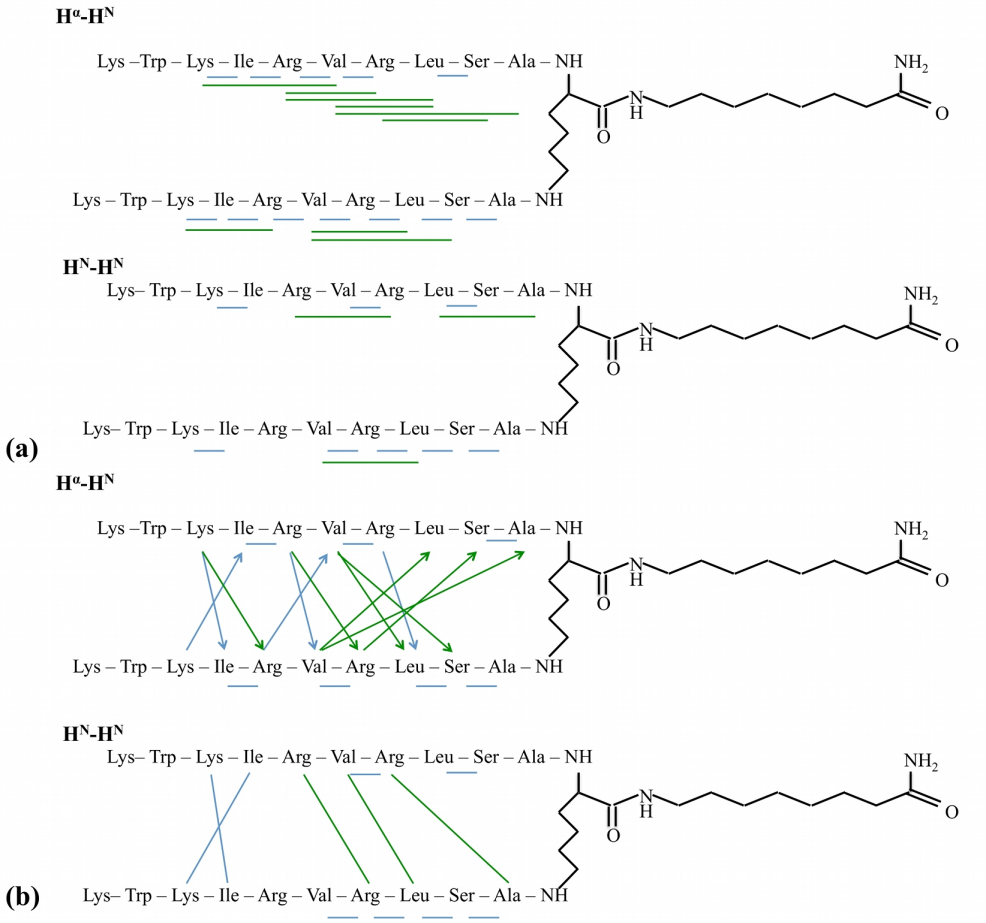

Figure 5.13. NOEs assignments of the two structures hypothesized for β-SB056-den. The sequential and medium-range NOEs pertaining to the two-helices (a) and the double-helix (b) model for β-SB056-den. Sequential NOEs are coloured in blue, medium-range NOEs are coloured in green. For the sake of clarity, all the lines have the same thickness despite the corresponding NOEs relative intensity.

5.2.5.4 β-SB056-lin

The last analogue was investigated in the presence of mixed micelles constituted by DPC/SDS at 3/1 molar ratio, at a [L]/[P] of 25, as done for the non-optimized original SB056-lin. As soon as the micelle solution was used to solubilize the peptide, an extremely viscous, although perfectly limpid and transparent, solution was obtained, resembling a sort of liquid-crystalline phase. It is clear that this last analogue is involved in some striking interactions with the detergents employed. The physical state of the sample dramatically changed, investing the entire volume of the solution in test tube. This phenomenon has never been reported in the literature for peptides, and, even comparing the four SB056 analogues, appears to be peculiar to the optimized β-SB056-lin. It is thus interesting to recall that this analogue exhibited the strongest binding interaction with the lipid vesicle used for fluorescence

spectroscopy investigations (see above). Unfortunately, the extreme viscosity of the solution did not allow the study through liquid-state NMR.

5.2.6 Investigating the insertion of the SB056-den into the micelle through paramagnetic relaxation enhancement

The Mn^{2+} ion is paramagnetic and can be used as a valuable probe to investigate peptides insertion into a membrane model through liquid-state NMR [38, 39]. In the chapters 3 and 4 of the present Ph.D. thesis, this method was already applied in the case of two natural peptides.

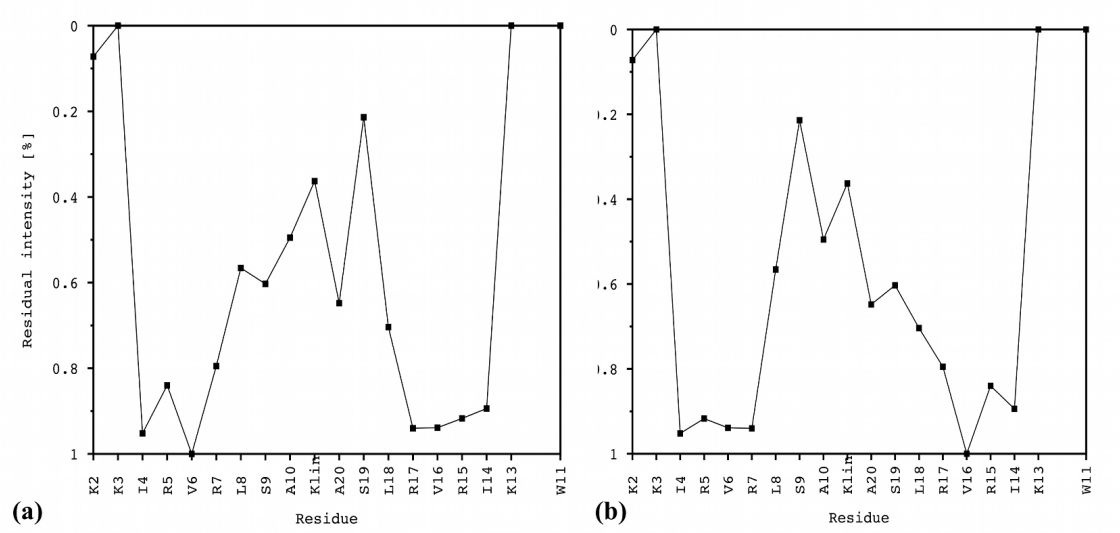

Figure 5.14. Paramagnetic relaxation enhancement experiments on SB056-den. Residual intensity of the TOCSY cross-peaks in the H^N–H^α region, calculated as the ratio between data acquired in the presence and absence of Mn^{2+} 0.1 mM. The data reported in the two panels are exactly the same but residues are placed in a different order, on the basis of the structural hypothesis taken into account. In (a) the order corresponding to either the two-helices and the dimer models was used. In (b) the double-helix order is represented. On the left, residue numbers form 1 to 10 were used for the alpha-branch; residues belonging to the epsilon-bracnh are numbered from 11 to 20; the linker was placed in the middle of the plot. The y-axis was reversed in order to have buried residues at the bottom.

A series of TOCSY spectra were collected in the presence of different concentration of Mn^{2+} and the intensity variation of the H^N-H^α cross-peaks was monitored by calculating the ratio between the TOCSY spectrum acquired in the presence and in the absence of the paramagnetic ions. Figure 5.14 shows the resulting residual intensity as a function of the amino acid residue. The less residual intensity, the more solvent exposed the residue, and vice-versa. Despite the specific hypothesis, i.e. the two-helices, the dimer or double-helix, an

almost symmetric profile was obtained, clearly indicating that the two peptide branches similarly interact with the membrane model. This further supports the double-helix model when compared to the other two hypothesis. Indeed, the former is the only one justifying a similar environment for both the branches, while the latter lead to assume a marked difference for the two peptide units of the dendrimeric SB056-den.

An interesting and quite surprising feature emerging from these paramagnetic relaxation enhancement experiments is represented by the linker resulting to be more solvent-exposed than the peptide branches, except for the N-termini. Indeed, the lipophilic tail, which is directly bound to the lysine linker, was completely exposed to the solvent, as revealed by its signals disappearing in the presence of Mn^{2+} right at the lowest concentration (data not shown). This evidence clearly poses some concern against the role of the supposed lipophilic tail, which was added to the dendrimeric scaffold during the very first stage of its design. The idea was to improve the membrane affinity but probably the amide group at the end of the tail is too polar and causes, in turn, the tail to prefer the solvent instead of the micelle interior.

5.2.7 Insights from molecular dynamic simulations

In order to improve the structural models obtained from "*in vacuo*" simulated annealing procedure, using experimental NMR geometrical restraints, all-atom MD simulations were performed. At this stage, we focused only on the SB056-den, whose NMR structural investigation led to three different hypotheses. We believe it is fundamental, first, to elucidate which is the most reliable structural model before concluding anything about these novel AMPs. MD can be extremely useful in such a case, since it is possible to simulate a system with both the water molecules and one micelle (composed by DPC/SDS 3/1 mol/mol) explicitly present, thus providing additional potential energy terms to drive the peptide towards a more realistic conformation. Thus, three different systems were set up, one for each of the above presented hypotheses, including the correspondent NMR restraints.

In all the cases, few nanoseconds were sufficient for the peptide to approach the micelle from the solvent. The peptide started interacting with the micelle surface through the N-termini. This was not surprising since these are the more positively charged regions of the peptide and the micelle has a net negative charge due to the presence of the SDS. The micelle remained fairly stable for the entire simulations when compared to a simulation performed in the absence of any peptides. In particular, the radial distribution functions computed for different chemical groups of the detergents resulted to be comparable. The radius of gyration (~ 1.6 nm) was comparable to that obtained for pure DPC micelles [39]. This is in agreement

with one of our studies in which the hydrodynamic diameter of mixed DPC/SDS micelles has been measured with dynamic light scattering and no significant variations have been observed by varying their composition [37].

Figures 5.15, 5.16 and 5.17 show the most relevant results for the two-helices, the dimer and the double-helix model, respectively. The distance between the center of mass of each residue and that of the micelle (time averaged) were calculated to show the different degree of interaction/insertion of the peptide in the three cases. A representative 3D picture is also provided.

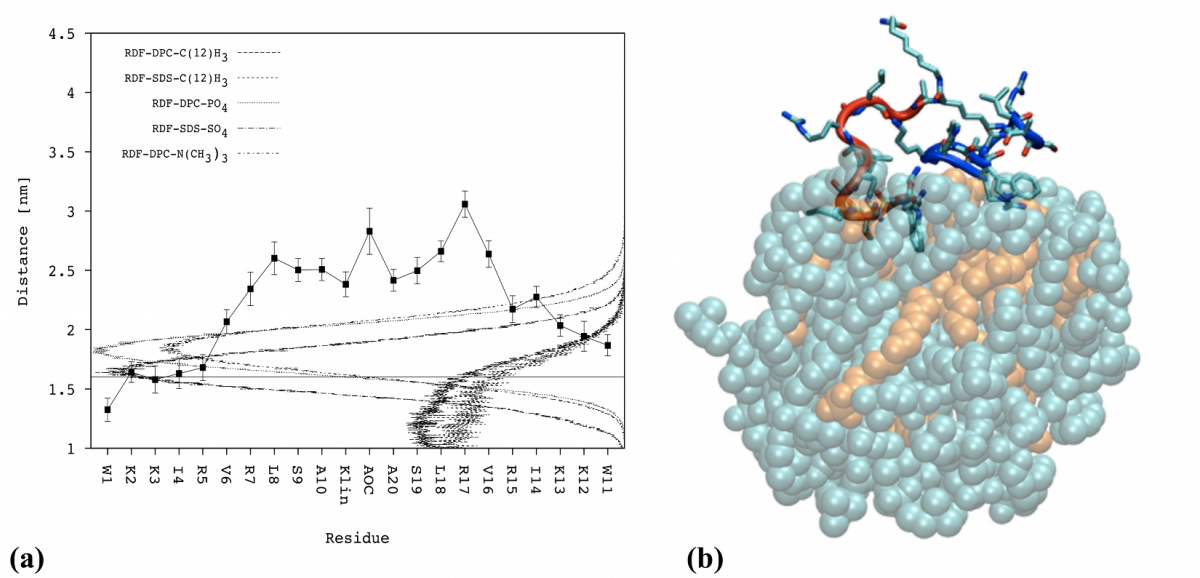

Figure 5.15. Results of the MD simulations: the two-helices hypothesis. (a) The residues center of mass distance (time averaged) from the center of mass of the micelle is shown (filled squares). The solid horizontal line is reported as a reference for the radius of gyration of the micelle. The differently dashed curves are the radial distribution functions obtained for different chemical groups of DPC and SDS. (b) A 3D picture of the equilibrium structure adopted by the peptide interacting with the micelle is shown. The peptide branch bound to the α-amino group of the lysine linker is shown in red, the one bound to the ε-amino group is in blue.

Both the two-helices and the dimer models have never shown a strong interaction with the micelle involving the entire peptide. After the first adhesion through the N-termini the majority of the residues remained unbound and solvent-exposed. The two-helices overall structure was more stable than that of the homodimer, due to the NMR restraints applied still leaving a higher number of degrees of freedom for the latter. Definitely, MD simulations showed that these two models are not prone to interact with the mixed micelle employed. The distance profile obtained for the amino acid residues is absolutely not compatible with the

paramagnetic relaxation enhancement results (figure 5.14). Thus, all the drawbacks that emerged from the NMR data discussion seem to be confirmed.

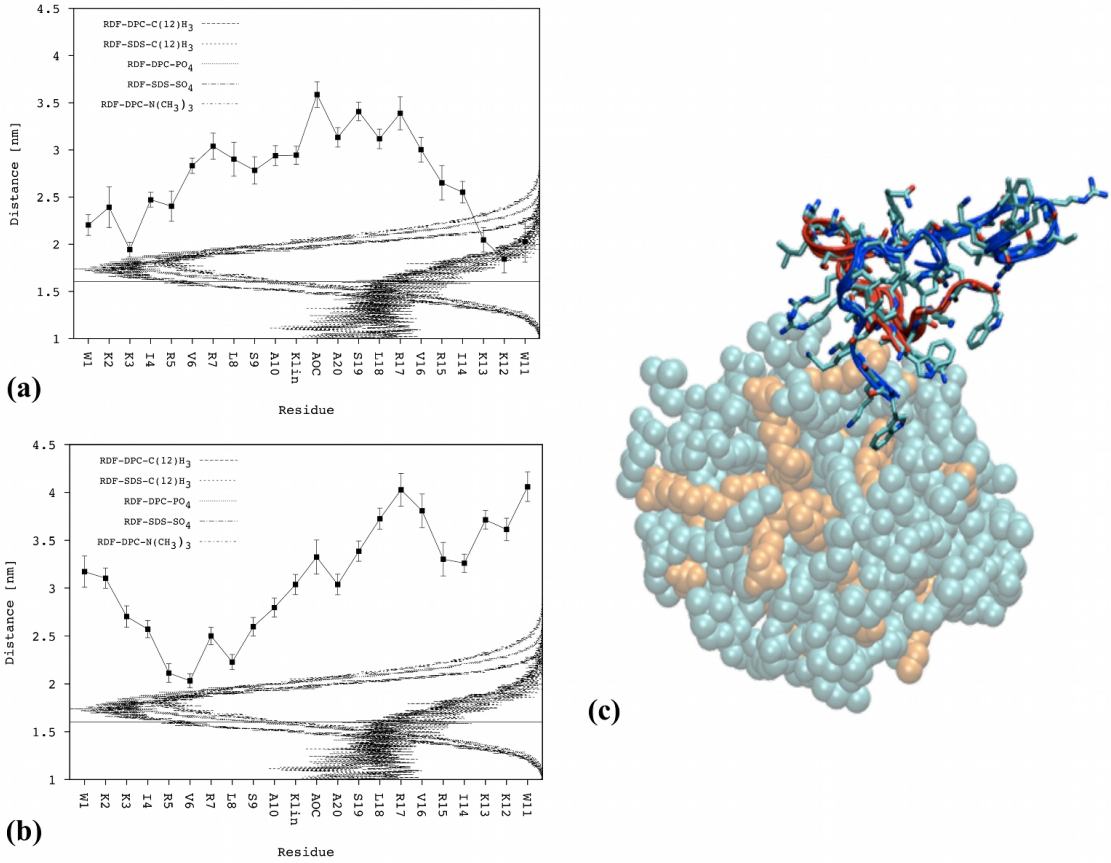

Figure 5.16. Results of the MD simulations: the dimer hypothesis. The residues center of mass distance (time averaged) from the center of mass of the micelle is shown (filled squares) for each of the two SB056-den molecules involved in the homodimer, (a) and (b), respectively. The solid horizontal line is reported as a reference for the radius of gyration of the micelle. The differently dashed curves are the radial distribution functions obtained for different chemical groups of DPC and SDS. (c) A 3D picture of the equilibrium structure adopted by the peptide interacting with the micelle is shown. The peptide branch bound to the α-amino group of the lysine linker is shown in red, the one bound to the ε-amino group is in blue.

On the other hand, the double-helix conformer rapidly bound on the micelle surface and started to immerse between the detergents head groups, until the whole peptide was embedded. This situation was reached within the first 10 ns and remained stable for the entire simulation. These results strongly support the double-helix model as a plausible conformation particularly suitable to interact with a membrane model such as the mixed micelles employed. The distance profile obtained for the amino acid residues (figure 5.17a) is absolutely compatible with the paramagnetic relaxation enhancement results (figure 5.14). Indeed, it is almost symmetric with both the peptide branches located at the membrane/water interface. In

particular, the two profiles are comparable to a high extent confirming, in addition, that the lysine linker and the amino-octanoic tail prefer to interact with the solvent.

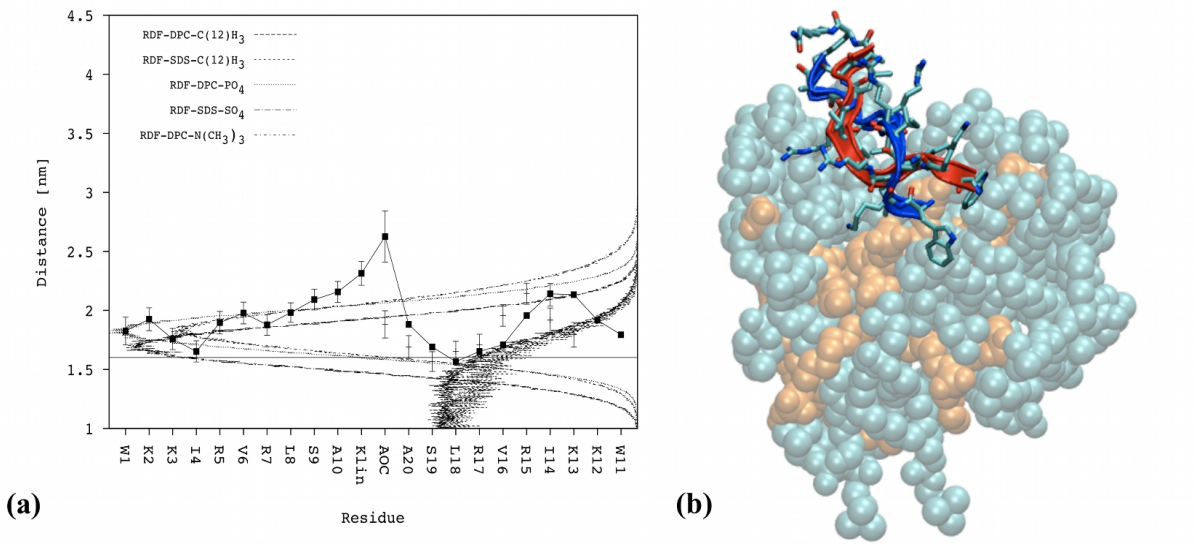

Figure 5.17. Results of the MD simulations: the double-helix hypothesis. (a) The residues center of mass distance (time averaged) from the center of mass of the micelle is shown (filled squares). The solid horizontal line is reported as a reference for the radius of gyration of the micelle. The differently dashed curves are the radial distribution functions obtained for different chemical groups of DPC and SDS. (b) A 3D picture of the equilibrium structure adopted by the peptide interacting with the micelle is shown. The peptide branch bound to the α-amino group of the lysine linker is shown in red, the one bound to the ε-amino group is in blue.

Although the overall structure is not amphipathic it appears to be stabilized by the electrostatic interactions between the numerous positively charged residues and the detergent head groups. These charged residues are spread all around the double-helix axis and, being longer than the hydrophobic residues, shield the latter from the solvent contacts. Interestingly, when the time averaged values of Φ and Ψ backbone angles were plotted on the Ramachandran space a strikingly valid explanation for the experimental J-couplings have been found. Indeed, all the residues from R5 to A10 on both branches are located in the β-region (figure 5.18), in very good agreement with the J-coupling values of ~10 Hz. Thus, in the light of these analysis, the double-helix conformation can actually seen as a β-twisted structure, which does agree with the SRCD data too.

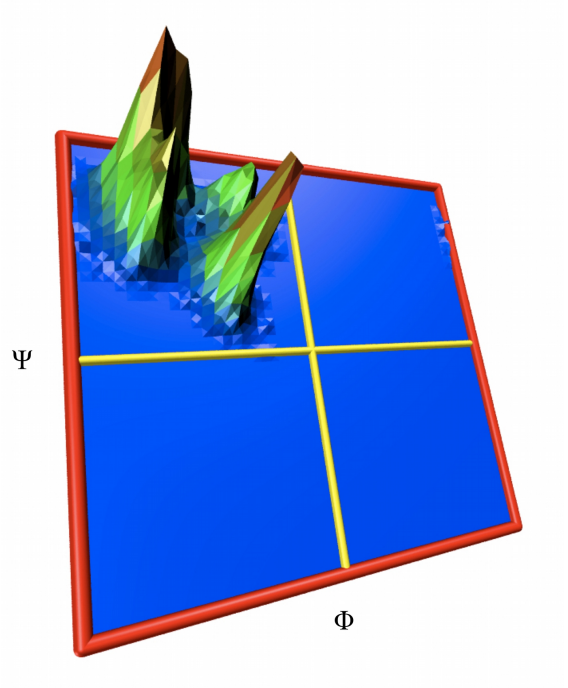

Figure 5.18. Ramachandran plot of time averaged values of Φ and Ψ backbone angles. All the residues from R5 to A10 on both branches are located in the β-region of Ramachandran plot, justifying the J-coupling values of ~10 Hz.

5.3 Summary and conclusions

Starting from the antimicrobial peptide SB056, which was previously obtained by semi-empirical optimization after high-throughput screening of a phage library [40], its amino acid sequence has been optimized in order to improve its amphipathic profile, aiming at improving the antimicrobial activity. Inspection of the original sequence [WKKIRVRLSA] revealed that, with the only exception of the first two residues, it is characterized by an alternating pattern of one hydrophobic and one cationic/polar amino acid. In this respect, it resembles other peptides that are known to form β-sheets [8, 10, 11]. A rational optimization was performed by inverting the position of the first two residues, obtaining the β-SB056 analogue [KWKIRVRLSA]. This modification was predicted to improve peptide amphipathicity but preserving the overall positive charge (+5 for linear and +10 for dendrimeric peptides).

MIC assays showed that sequence optimization succeeded in providing a better antimicrobial potency. In the absence of added electrolytes, thus far from the concentration encountered *in vivo*, it was quite surprising to find that β-SB056-lin had a higher activity than β-SB056-den. A possible explanation, might be that the perfect amphipathic profile obtained

with sequence optimization in β-SB056-lin can be worsen in the dendrimeric form. Anyway, the advantages offered by the dendrimeric scaffold appeared to be fundamental as soon as the environment approaches the *in vivo* conditions. Indeed, with the addition of electrolytes to the medium, the biological activity of both the linear peptides significantly decreased, while it was preserved by the dendrimeric peptides. In other words, dendrimeric peptides seem to be resistant to relatively high salt concentration, which is one of the main issue when linear neutral AMPs are applied *in vivo* [1, 12].

Binding investigation confirmed that electrostatics plays the major role either in the determination of selectivity towards prokaryotic membranes and as the first stage of antimicrobial action. Indeed, the activity order found with the MIC assays was consistent with binding affinity order. Dendrimeric peptides preserved a marked binding even in the presence of relatively high salt concentration.

Through surface pressure analysis, the ability of the four analogues to perturb lipid monolayers was investigated. The results were in agreement with either the MIC assays and binding investigations. The more the binding, the more the monolayer perturbation. However, the data as a function of the content of negatively charged lipids in the monolayer revealed that perturbation might be hindered when the electrostatic interaction between the peptide and the lipid head groups become excessive. This might be particularly severe for certain Gram-positive bacteria whose plasma membrane is particularly rich in negatively charged lipids [18, 19]. In the literature, indeed, there are many works where a decreased antimicrobial activity for peptides intentionally enriched with cationic residues has been reported [41–43].

SRCD spectroscopy showed that, in the presence of negatively charged vesicles, all the SB056 analogues have a clear tendency for β-type structuration. The extent of the folding depended on the content of negatively charged lipids in the membrane model. Each of the peptides reached a maximum of structural order at a different value of %PG, then showing a reduction in the spectra ellipticity. Indeed, deviations from the canonical β-strand spectral shape were observed with further increasing the vesicles' negative charge. Intensity loss and band broadening was observed for both the positive and the negative bands, that can be attributed to the absorption flattening and differential scattering phenomena. These are usually interpreted in terms of aggregation [44, 45]. The more the binding, the more the aggregated peptides on the bilayer, the more the absorption flattening and differential scattering affecting the CD spectrum.

A detailed structural investigation was attempted using mixed DPC/SDS micelles as membrane model through liquid-state NMR. The aim was particularly challenging due to the

extreme novelty of these peptides. The data collected for SB056-lin surprisingly suggested a helical folding but, the strong aggregation and precipitation tendency forced us to postpone an in-depth analysis, since the samples appeared to be not sufficiently stable over time.

Moving to the SB056-den the data obtained were promising although really complicated to be unambiguously interpreted. Three different hypotheses have been put forward: a two-helices structure, a homodimer or an unexpected double-helix. However, the first two models were not consistent with a number of experimental observation and considerations. Finally, the double-helix, although really unusual, was the only hypotheses that fit with the data. Molecular dynamics simulations have bolstered such model, providing new insights and justification of the NMR data.

The β-SB056-den could be investigated with NMR. Data were comparable to those collected on the SB056-den. Due to the extreme complexity of the aforementioned case, we postpone the in-depth analysis of this sequence optimized peptide to a second stage. Finally, the β-SB056-lin showed a very strong interaction with the detergents molecules, such that, probably, their aggregation state was completely changed and it was not sure that we could still consider the micelles as the molecular assemblies actually present in our solution.

We are aware that the 3D structure of the SB056 peptides has not been fully solved, but, given the complexity and the novelty of the present case, we believe that our results are very interesting and put the basis to continue the investigations. The NMR data for both the SB056-lin and the β-SB056-den were basically comparable to those of SB056-den. Thus, we think that we are on the right direction in defining the common features of this novel class of AMPs. However, it has to be mentioned that there is a gap between the biophysical characterization and the structural study presented in this work, since the former was performed using lipid bilayers, while micelles were employed for the latter. We cannot state whether the double-helix conformation was induced by the high curvature of the micelle or it is the active conformation adopted on large lipid bilayers. In the future, other membrane models need to be employed, such as bicelles, and concentration dependent investigations have to be undertaken in order to elucidate the possible structure variation with aggregation.

Finally, it is very interesting to note that both NMR and MD simulations agreed in localizing the linker and the tail outside the micelle. The tail was originally designed as a lipophilic anchor to improve membrane affinity. From the present study, however, a different picture emerged and open new possibilities for further improvements.

5.4 References

1. Rotem, S., and A. Mor. 2009. Antimicrobial peptide mimics for improved therapeutic properties. Biochim. Biophys. Acta. 1788: 1582–92.

2. Diamond, G., and N. Beckloff. 2009. The roles of antimicrobial peptides in innate host defense. Curr. Pharm. Des. 15: 2377–92.

3. Peschel, A., and H.G. Sahl. 2006. The co-evolution of host cationic antimicrobial peptides and microbial resistance. Nat. Rev. Microbiol. 4: 529–36.

4. Sadler, K., and J.P. Tam. 2002. Peptide dendrimers: applications and synthesis. Rev. Mol. Biotechnol. 90: 195–229.

5. Giuliani, A., and A.C. Rinaldi. 2011. Beyond natural antimicrobial peptides: multimeric peptides and other peptidomimetic approaches. Cell. Mol. Life Sci. 68: 2255–66.

6. Bruschi, M., G. Pirri, A. Giuliani, S.F. Nicoletto, I. Baster, et al. 2010. Synthesis, characterization, antimicrobial activity and LPS-interaction properties of SB041, a novel dendrimeric peptide with antimicrobial properties. Peptides. 31: 1459–67.

7. Scorciapino, M.A., G. Pirri, A. V Vargiu, P. Ruggerone, A. Giuliani, et al. 2012. A novel dendrimeric peptide with antimicrobial properties: structure-function analysis of SB056. Biophys. J. 102: 1039–48.

8. Blazyk, J., R. Wiegand, J. Klein, J. Hammer, R.M. Epand, et al. 2001. A novel linear amphipathic beta-sheet cationic antimicrobial peptide with enhanced selectivity for bacterial lipids. J. Biol. Chem. 276: 27899–906.

9. Wadhwani, P., J. Reichert, E. Strandberg, J. Burck, J. Misiewicz, et al. 2013. Stereochemical effects on the aggregation and biological properties of the fibril-forming peptide $[KIGAKI]_3$ in membranes. Phys. Chem. Chem. Phys. 15: 8962–71.

10. Wadhwani, P., E. Strandberg, N. Heidenreich, J. Bürck, S. Fanghänel, et al. 2012. Self-assembly of flexible β-strands into immobile amyloid-like β-sheets in membranes as revealed by solid-state ^{19}F NMR. J. Am. Chem. Soc. 134: 6512–5.

11. Meier, M., and J. Seelig. 2008. Length dependence of the coil <--> beta-sheet transition in a membrane environment. J. Am. Chem. Soc. 130: 1017–24.

12. Bowdish, D.M.E., D.J. Davidson, and R.E.W. Hancock. 2005. A re-evaluation of the role of host defence peptides in mammalian immunity. Curr. Protein Pept. Sci. 6: 35–51.

13. Minahk, C.J., and R.D. Morero. 2003. Inhibition of enterocin CRL35 antibiotic activity by mono- and divalent ions. Lett. Appl. Microbiol. 37: 374–9.

14. Bals, R., X. Wang, Z. Wu, T. Freeman, V. Bafna, et al. 1998. Human beta-defensin 2 is a salt-sensitive peptide antibiotic expressed in human lung. J. Clin. Invest. 102: 874–80.

15. Lee, I., Y. Cho, and R. Lehrer. 1997. Effects of pH and salinity on the antimicrobial properties of clavanins. Infect. Immun. 65: 2898–2903.

16. Silverthorn, D.U. 2005. Human Physiology: An Integrated Approach. 3rd ed. Pearson Education Inc., San Francisco, CA, USA.

17. Tam, J.P., Y.A. Lu, and J.L. Yang. 2002. Antimicrobial dendrimeric peptides. Eur. J. Biochem. 269: 923–32.

18. Epand, R.M., and R.F. Epand. 2009. Domains in bacterial membranes and the action of antimicrobial agents. Mol. Biosyst. 5: 580–7.

19. Shaw, N. 1974. Lipid Composition as a Guide to the Classification of Bacteria. Adv. Appl. Microbiol. 17: 63–108.

20. Zhao, H., and P. Kinnunen. 2002. Binding of the antimicrobial peptide temporin L to liposomes assessed by Trp fluorescence. J. Biol. Chem. 277: 25170–7.

21. Christiaens, B., S. Symoens, S. Vanderheyden, Y. Engelborghs, A. Joliot, et al. 2002. Tryptophan fluorescence study of the interaction of penetratin peptides with model membranes. Eur. J. Biochem. 269: 2918–26.

22. Breukink, E., C. van Kraaij, R. A. Demel, R.J. Siezen, O.P. Kuipers, et al. 1997. The C-terminal region of nisin is responsible for the initial interaction of nisin with the target membrane. Biochemistry. 36: 6968–76.

23. Epand, R. 2006. Membrane lipid composition and the interaction of pardaxin: the role of cholesterol. Protein Pept. Lett. 13: 1–5.

24. Zasloff, M. 2002. Antimicrobial peptides of multicellular organisms. Nature. 415: 389–95.

25. Tolokh, I.S., V. Vivcharuk, B. Tomberli, and C.G. Gray. 2009. Binding free energy and counterion release for adsorption of the antimicrobial peptide lactoferricin B on a POPG membrane. Phys. Rev. E. Stat. Nonlin. Soft Matter Phys. 80: 031911.

26. Scorciapino, M.A., G. Pirri, A.V. Vargiu, P. Ruggerone, A. Giuliani, et al. 2012. A novel dendrimeric peptide with antimicrobial properties: structure-function analysis of SB056. Biophys. J. 102: 1039–48.

27. Zhao, H., A.C. Rinaldi, A. Di Giulio, M. Simmaco, and P.K.J. Kinnunen. 2002. Interactions of the antimicrobial peptides temporins with model biomembranes. Comparison of temporins B and L. Biochemistry. 41: 4425–36.

28. Maget-Dana, R. 1999. The monolayer technique: a potent tool for studying the interfacial properties of antimicrobial and membrane-lytic peptides and their interactions with lipid membranes. Biochim. Biophys. Acta. 1462: 109–40.

29. Brockman, H. 1999. Lipid monolayers: why use half a membrane to characterize protein-membrane interactions? Curr. Opin. Struct. Biol. 9: 438–43.

30. Janmey, P., and P. Kinnunen. 2006. Biophysical properties of lipids and dynamic membranes. Trends Cell Biol. 16: 538–46.

31. Marsh, D. 1996. Lateral pressure in membranes. Biochim. Biophys. Acta. 1286: 183–223.

32. Miles, A.J., and B. a Wallace. 2006. Synchrotron radiation circular dichroism spectroscopy of proteins and applications in structural and functional genomics. Chem. Soc. Rev. 35: 39–51.

33. Cavanagh, J., W. Fairbrother, A.G. Palmer III, M. Rance, and N.J. Skelton. 2007. Protein NMR Spectroscopy–Principles and Practice. Elsevier Academic Press, Oxford.

34. Shen, Y., F. Delaglio, G. Cornilescu, and A. Bax. 2009. TALOS+: a hybrid method for predicting protein backbone torsion angles from NMR chemical shifts. J. Biomol. NMR. 44: 213–23.

35. Lovell, S., I. Davis, W.B. Arendal III, P.I.W. de Bakker, J.M. Word et al. 2003. Structure validation by Cα geometry: ϕ, ψ and Cβ deviation. Proteins Struct. Funct. Genet. 450: 437–50.

36. Bruch, M.D. 1996. NMR Spectroscopy Techniques, 2nd ed. Marcel Dekker Inc., New York, NY, USA.

37. Manzo, G., M. Carboni, A.C. Rinaldi, M. Casu, and M.A. Scorciapino. 2013. Characterization of sodium dodecylsulphate and dodecylphosphocholine mixed micelles through NMR and dynamic light scattering. Magn. Reson. Chem. 51: 176–83.

38. Abbassi, F., C. Galanth, M. Amiche, K. Saito, C. Piesse, et al. 2008. Solution structure and model membrane interactions of temporins-SH, antimicrobial peptides from amphibian skin. A NMR spectroscopy and differential scanning calorimetry study. Biochemistry. 47: 10513–25.

39. Scorciapino, M.A., G. Manzo, A.C. Rinaldi, R. Sanna, M. Casu, et al. 2013. Conformational Analysis of the Frog Skin Peptide, Plasticin-L1, and Its Effects on Production of Proinflammatory Cytokines by Macrophages. Biochemistry. 52: 7231–41.

40. Pini, A., A. Giuliani, C. Falciani, Y. Runci, C. Ricci et al. 2005. Antimicrobial activity of novel dendrimeric peptides obtained by phage display selection and rational modification. Antimicrob. Agents Chemother. 49: 2665–72.

41. Teixeira, V., M.J. Feio, and M. Bastos. 2012. Role of lipids in the interaction of antimicrobial peptides with membranes. Prog. Lipid Res. 51: 149–77.

42. Tossi, A., L. Sandri, and A. Giangaspero. 2000. Amphipathic, alpha-helical antimicrobial peptides. Biopolymers. 55: 4–30.

43. Dathe, M., and T. Wieprecht. 1999. Structural features of helical antimicrobial peptides: their potential to modulate activity on model membranes and biological cells. Biochim. Biophys. Acta. 1462: 71–87.

44. Bustamante, C., I.J. Tinoco, and M.F. Maestre. 1983. Circular differential scattering can be an important part of the circular dichroism of macromolecules. Proc. Natl. Acad. Sci. U. S. A. 80: 3568–72.

45. Wallace, B.A., and C.L. Teeters. 1987. Differential absorption flattening optical effects are significant in the circular dichroism spectra of large membrane fragments. Biochemistry. 26: 65–70.

HDPs represent a class of biological active peptides and were shown to exert a fundamental role in the innate immunity response of almost all the forms of life [1, 2]. Some of them, called AMPs, are the most extensively studied and directly kill the microorganisms through several mechanisms, which involve the perturbation of plasma membranes and/or the interaction with molecules or mechanisms necessaries for bacterial cell survival [3–5]. Recently, many HDPs revealed to act differently, i.e. as immunoregulatory molecules, helping the host organism to solve the infection. The modes of action behind these immunoregulatory activities most likely involve several targets of action but currently remain largely unknown [2, 6]. There is a wide consensus in the literature about the fact that most of the HDPs studied so far fold in a regular secondary structure (e.g., α-helix, β-sheet, extended structure). The quest for the clarification of structure- to-function relationships is one of the most intriguing and challenging aspect in the field of HDPs, as identified activity-related structural features might help to design new sequences with improved activity and pharmacokinetic [1, 2, 4, 6]. Despite many sequences have been reported and the knowledge on the modes of action of these molecules has improved significantly in the last decade, many drawbacks still prevent HDP insertion into clinical trials. The most important is the inhibition of their activity when moving to *in vivo* experimentation. Proteases easily hydrolyse linear peptides, that is almost all naturally occurring AMPs, causing an absolutely insufficient bioavailability at the infection site [1–3, 6]. Moreover, the antimicrobial activity of most cationic peptides is severely lowered by the presence of mono- and divalent cations at physiological concentrations, since they compete with peptides for the binding on the surface of cells [7]. Many strategies have been developed to overcome these and other problems linked to the possible clinical use of HDPs. One of the most promising, is the use of the MAP approach to synthetize multimeric-branched peptides [8, 9].

During the present Ph.D. program, the structure-to-function relationship was investigated for three different peptides, specifically chosen to span different categories of typical HDPs, from directly antimicrobial to immunomodulatory, from helical to β-structured, from natural to synthetic. The three peptides of choice have a different origin, different structural features and a remarkably different behaviour. The results reported herein confirmed as differences in the primary structure might translate into large variations of the biological behaviour.

When comparing Esc(1-18) and Plasticin-L1 (Chapter 3 and 4, respectively), the primary role of the electrostatics in directing and selecting the activity of HDPs is evident. The former behaves as a classical cationic AMP with a helical folding and a mechanism of action mainly driven by the electrostatic interactions with the negative components of the membrane model, whereas, in the presence of a purely zwitterionic (thus, neutral) model it showed neither structuration nor insertion. On the other hand, Plasticin-L1, which has no net electric charge, is devoid of direct antimicrobial activity. However, the stability demonstrated by its structure when in contact with micelles suggests a mechanism involving the interaction with plasma membranes behind its immunoregulatory effect. Nevertheless, the study performed on the SB056 peptide analogues, which is actually the core and the most innovative part of the present thesis, demonstrated that the peptide net positive charge is only a part of the story.

Electrostatic attraction is certainly fundamental for the biologic activity, especially during the first stages, but the specific charges distribution along the amino acid sequence is also extremely important and may deeply affect peptide's activity. Indeed, despite β-optimized SB056 peptides bear the same net charge of original analogues, the improvement of the sequence amphipathicity provided a far stronger interaction with the membrane models employed, even with the zwitterionic ones. This may be seen as detrimental since may deserve selectivity reduction, but the advantages of the dendrimeric scaffold became evident when moving to conditions similar to those encountered *in vivo*. The investigation on the SB056 peptides confirmed their outstanding potentiality: the dendrimeric forms of both the sequences (the original and the β-optimized) demonstrated to preserve their activities in conditions near to those encountered in physiological fluids. In particular, the presence of relatively high salt concentration inhibited almost completely the binding for the two linear analogues, while only a slight reduction was observed for the two dendrimers. Importantly, the affinity for the purely zwitterionic models was removed, probably indicating restoring of peptide selectivity, which is particularly encouraging. The strong interaction with detergents and lipids demonstrated by the SB056 analogues, and the strong dependence of their biophysical behavior on the negative surface charge of the membrane model suggest anionic lipid clustering as the key feature underlying the mechanism of action [10–13].

However, the comparable MIC values obtained for Gram-positive and Gram–negative bacteria that are known to have a remarkably different average content of anionic lipids in the plasma membrane, clearly show that overall activity of the SB056 peptides can be regarded as almost membrane composition independent. It might be that they are able to 'tune' the killing mechanism to the membrane composition, or their mechanism is fairly general and is effective

even with a relatively low amount of negatively charged lipids. The most interesting result obtained in this work is perhaps the unusual structure proposed for the SB056-den, which, by analogy, seems to be relevant also to the other analogues. Among the different structural models put forward, the double-helix is the only one really consistent with both the experimental and computational data in our hands, revealing to be comparable to a β-twisted structure. However, we cannot conclude whether the double-helix conformation is induced by the high curvature of the micelle and/or by the specific experimental conditions employed for which a unique peptide per micelle is expected. Whether it is the active conformation adopted on larger lipid bilayers still needs to be confirmed. The double-helix might also be a sort of pre-aggregation state, prone to evolved towards an extended oligomeric state with increasing the peptide local concentration. Nevertheless, these interesting findings open new insights on the structural studies of HDPs and peptides in general, suggesting that canonical structures such as the α-helix and β-sheet are only some possible conformations and that, sometime, we need to look beyond the schemes.. Another interesting result concern the tail added to the dendrimeric scaffold in order to improve membrane affinity. Despite the specific folded structure, the present study revealed that such a tail, together with the lysine linker, is not a membrane anchor but has a stronger affinity for the solvent than for the micelle core. In other words, it did not appear hydrophobic as it was intended for. The problem might be the polar amide group at the end of the tail and/or its relatively restricted length.

Definitely, the present work has put the basis for further investigations and improvements of the investigated peptides. The SB056 analogues, in particular, are really promising for a possible development towards *in vivo* applications. The first step should be an in-depth characterization of the local concentration dependent structure adopted. To this aim, the present Ph.D. work had revealed severe limitations to the use of detergents micelles. Their size is not sufficient to allow peptides oligomerization, which is particularly important for β-structured molecules. This might lead to the observation of monomeric structures that are difficult to be related to the mode of action. In addition, when aggregation/oligomerization is particularly promoted by the inherent characteristics of the peptide under investigation, detergent micelles appear to be not sufficiently stable and their chemo-physical state might change easily. Thus, in the next future it will be mandatory to move to another membrane model. Bicelles are thought to be particularly suitable since they are larger in size and represent an almost flat assembly of lipid molecules [14]. While larger liposomes cannot be used in liquid-state NMR investigations, bicelles are characterized by a sufficient mobility in aqueous solutions allowing for in-depth structural investigations. Peptide isotope-labeling has to be also

taken into consideration, since it gives the possibility to perform more sophisticated and sensitive two- and three-dimensional NMR data acquisition.

Then, the peptide sequence and dendrimeric scaffold can be certainly improved in order to maximize antimicrobial efficacy. As said, the tail has to be modified either by removing the polar end group and/or tuning the length depending on the bilayer thickness, for instance. As far as the peptide sequence is concerned, lysine residues are reported in the literature to be less suitable than arginines to favor peptides insertion and promote perturbation mechanisms [15, 16]. Thus, the substitution of lysines with arginines in SB056 sequence might improve the antimicrobial activity. In parallel, further studies are needed to ascertain the actual mode of action of the three peptides investigated. Liposomes calcein-leakage experiments could provide insights about the pore-forming activity [17, 18]. Properly prepared liposomes can be employed in fluorescence spectroscopy investigations to assess fusogenic properties [19, 20] and anionic lipid clustering [21].

6.1 References

1. Hancock, R.E.W., and H.G. Sahl. 2006. Antimicrobial and host-defense peptides as new anti-infective therapeutic strategies. Nat. Biotechnol. 24: 1551–7.
2. Haney, E.F., and R.E.W. Hancock. 2013. Peptide design for antimicrobial and immunomodulatory applications. Biopolymers. 100: 572–83.
3. Jenssen, H., P. Hamill, and R.E.W. Hancock. 2006. Peptide antimicrobial agents. Clin. Microbiol. Rev. 19: 491–511.
4. Diamond, G., N. Beckloff, A. Weinberg, and K.O. Kisich. 2009. The roles of antimicrobial peptides in innate host defense. Curr. Pharm. Des. 15: 2377–2392.
5. Jenssen, H., and R.E.W. Hancock. 2010. Therapeutic potential of HDPs as immunomodulatory agents. In: Antimicrobial peptides. Methods and protocols. A. Giuliani and A.C. Rinaldi (eds.), Humana Press-Springer, New York, NY, USA, 329-47.
6. Choi, K.-Y., L.N.Y. Chow, and N. Mookherjee. 2012. Cationic host defence peptides: multifaceted role in immune modulation and inflammation. J. Innate Immun. 4: 361–70.
7. Bowdish, D.M.E., D.J. Davidson, and R.E.W. Hancock. 2005. A re-evaluation of the role of host defence peptides in mammalian immunity. Curr. Protein Pept. Sci. 6: 35–51.

8. Falciani, C., L. Lozzi, A. Pini, F. Corti, M. Fabbrini, et al. 2007. Molecular basis of branched peptides resistance to enzyme proteolysis. Chem. Biol. Drug Des. 69: 216–21.

9. Giuliani, A., and A.C. Rinaldi. 2011. Beyond natural antimicrobial peptides: multimeric peptides and other peptidomimetic approaches. Cell. Mol. Life Sci. 68: 2255–66.

10. Epand, R.M., and R.F. Epand. 2010. Biophysical analysis of membrane-targeting antimicrobial peptides: membrane properties and the design of peptides specifically targeting Gram-negative bacteria. In: Antimicrobial Peptides: discovery, design and novel therapeutic strategies. G. Wang (ed.), CABI, Wallingford, UK, 116 –27.

11. Epand, R.M., and R.F. Epand. 2011. Bacterial membrane lipids in the action of antimicrobial agents. J. Pept. Sci. 17: 298–305.

12. Nguyen, L.T., E.F. Haney, and H.J. Vogel. 2011. The expanding scope of antimicrobial peptide structures and their modes of action. Trends Biotechnol. 29: 464–72.

13. Wadhwani, P., R.F. Epand, N. Heidenreich, J. Bürck, A.S. Ulrich, et al. 2012. Membrane-active peptides and the clustering of anionic lipids. Biophys. J. 103: 265–74.

14. Marcotte, I., and M. Auger. 2005. Bicelles as model membranes for solid- and solution-state NMR studies of membrane peptides and proteins. Concepts Magn. Reson. Part A. 24A: 17–37.

15. Mishra, A., G.H. Lai, N.W. Schmidt, V.Z. Sun, A.R. Rodriguez, et al. 2011. Translocation of HIV TAT peptide and analogues induced by multiplexed membrane and cytoskeletal interactions. Proc. Natl. Acad. Sci. U. S. A. 108: 16883–8.

16. Schmidt, N.W., A. Mishra, G.H. Lai, M. Davis, L.K. Sanders, et al. 2011. Criterion for amino acid composition of defensins and antimicrobial peptides based on geometry of membrane destabilization. J. Am. Chem. Soc. 133: 6720–7.

17. Schibli, D.J., L.T. Nguyen, S.D. Kernaghan, Ø. Rekdal, and H.J. Vogel. 2006. Structure-function analysis of tritrpticin analogs: potential relationships between antimicrobial activities, model membrane interactions, and their micelle-bound NMR structures. Biophys. J. 91: 4413–26.

18. Coccia, C., A.C. Rinaldi, V. Luca, D. Barra, A. Bozzi, et al. 2011. Membrane interaction and antibacterial properties of two mildly cationic peptide diastereomers, bombinins H2 and H4, isolated from Bombina skin. Eur. Biophys. J. 40: 577–88.

19. Pan, J., C.B. Lai, W.R.P. Scott, and S.K. Straus. 2010. Synthetic fusion peptides of tick-borne encephalitis virus as models for membrane fusion. Biochemistry. 49: 287–96.

20. Yang, R., J. Yang, and D. Weliky. 2003. Synthesis, enhanced fusogenicity, and solid state NMR measurements of cross-linked HIV-1 fusion peptides. Biochemistry. 42: 3527–35.

21. Kakio, A., S. Nishimoto, Y. Kozutsumi, and K. Matsuzaki. 2003. Formation of a membrane-active form of amyloid β-protein in raft-like model membranes. Biochem. Biophys. Res. Commun. 303: 514–18.

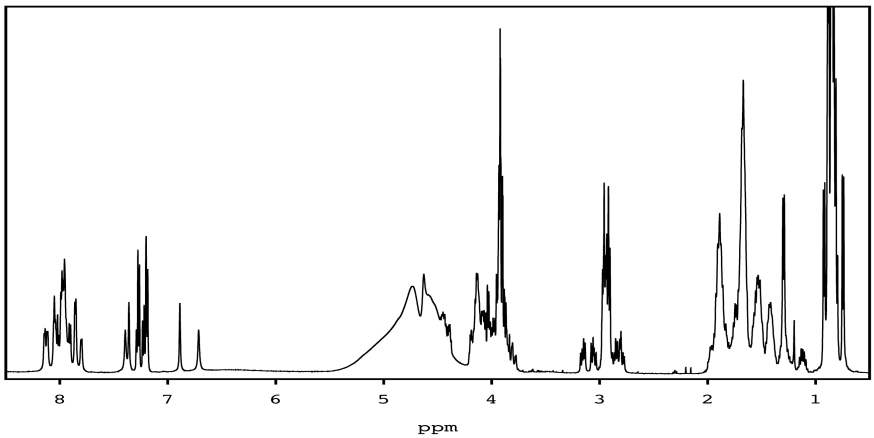

Figure A.1. Esc(1-18) in TFE/water solutions. ^{1}H spectrum of Esc(1-18) in the 30% v/v TFE/water solutions.

Table A.1. ^{1}H and ^{13}C resonance assignments for Esc(1-18) in the 30% and the 50% v/v TFE/water solutions.

Residue	TFE 30%							TFE 50%						
	^{1}H (ppm)				^{13}C (ppm)		$^{3}J_{H^{N}H^{\alpha}}(Hz)$	^{1}H (ppm)				^{13}C (ppm)		$^{3}J_{H^{N}H^{\alpha}}(Hz)$
	HN	Hα	Hβ	Others	Cα	Cβ		HN	Hα	Hβ	Others	Cα	Cβ	
G1	---	3.926			44.086		---	7.969	3.891 3.832			45.735		7.53
I2	8.051	4.028	1.741	γ 1.314 1.122 γ1 0.743 δ 0.805	61.828	37.661	4.88	8.076	4.064	1.779	γ 1.364 1.164 γ1 0.783 δ 0.857	61.950	37.681	4.62
F3	8.042	4.427	3.136 3.032	δ/δ' 7.192 ε/ε' 7.277 ζ 7.219	---	37.569	4.88	7.967	4.464	3.212 3.093	δ/δ' 7.230 ε/ε' 7.317 ζ 7.259	59.095	37.557	4.88
S4	7.904	4.338	3.991 3.936		58.507	63.082	6.41	7.936	4.237	4.021 3.962		59.632	62.925	7.65
K5	8.014	3.923	1.880	γ 1.530 1.420 δ 1.671 ε 2.920	---	31.244	6.18	7.798	4.138	1.971	γ 1.590 1.498 δ 1.723 ε 3.006	57.558	31.193	4.88

				ζ	---							ζ	---		
L6	8.138	4.122	1.836	γ	1.770	56.394	41.028	4.04	7.851	4.190	1.762	γ	1.740	56.363	41.320	6.26
				δ	0.823						1.614	δ	0.938			
					0.799								0.889			
A7	8.051	4.009	1.294			53.375	16.837	4.88	8.076	4.060	1.357			53.533	16.473	5.05
G8	7.965	3.808				45.683		4.88	7.969	3.925				42.321		4.95
		3.775								3.865						
K9	7.951	3.930	1.878	γ	1.530	58.553	31.244	4.88	7.987	4.135	1.942	γ	1.570	57.558	31.193	5.52
					1.420								1.465			
				δ	1.671							δ	1.723			
				ε	2.920							ε	2.961			
				ζ	---							ζ	---			
K10	7.927	4.155	1.890	γ	1.530	57.346	31.244	4.88	7.899	4.214	1.933	γ	1.590	57.363	31.193	9.40
					1.420								1.498			
				δ	1.671							δ	1.731			
				ε	2.920							ε	3.006			
				ζ	---							ζ	---			
L11	8.112	4.127	2.655	γ	1.638	56.394	40.655	5.19	8.111	4.187	1.731	γ	1.670	56.363	40.790	5.14
				δ	0.856							δ	0.957			
					0.834								0.909			
K12	7.798	4.085	1.892	γ	1.530	57.671	31.244	4.96	7.952	3.999	1.931	γ	1.552	58.314	31.193	5.05
					1.420								1.490			
				δ	1.671							δ	1.718			
				ε	2.920							ε	2.972			
				ζ	---							ζ	---			
N13	7.853	4.451	2.848	δ ‘	---	---	37.420	5.19	7.886	4.492	2.907	δ ‘	---	---	37.594	4.88
			2.765	δ’’	---						2.853	δ’’	---			

L14	7.852	4.139	1.698	γ	1.679	56.394	41.256	6.1	8.141	4.176	1.902	γ	1.730	56.363	40.908	4.20
			1.551	δ	0.866						1.571	δ	0.937			
					0.818								0.909			
L15	7.982	4.100	1.806	γ	1.584	56.394	41.028	4.65	8.018	4.167	1.863	γ	1.830	56.363	41.025	5.04
			1.704	δ	0.860						1.776	δ	0.933			
					0.831								0.899			
I16	7.960	4.049	1.964	γ	1.584	61.758	37.296	4.88	7.955	4.095	2.006	γ	1.632	61.730	37.316	6.10
					1.271								1.315			
				γ1	0.919							γ1	0.968			
				δ	0.840							δ	0.894			
S17	7.943	4.188	3.973			59.506	61.828	4.88	7.892	4.427	4.041			58.363	61.681	9.77
			3.910								3.975					
G18	7.965	3.884				42.451		4.88	8.006	3.971				43.854		7.53
		3.851														

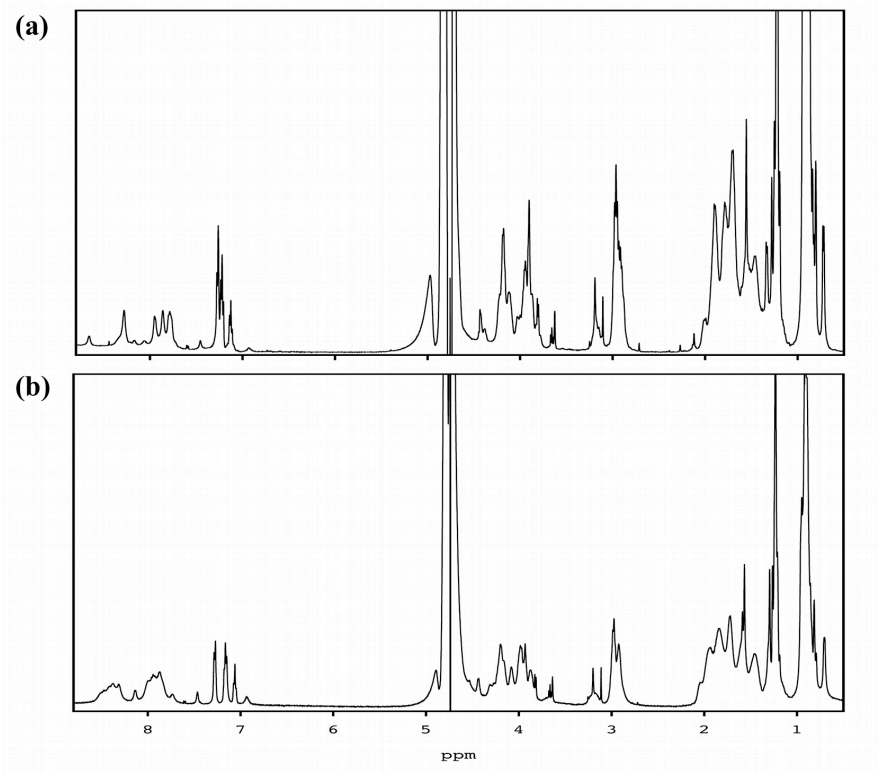

Figure A.2. Esc(1-18) in micelle solutions. ^{1}H spectrum of Esc(1-18) (a) in DPC and (b) in DPC/SDS 3/1 mol/mol buffered solution (pH 7.4).

Table A.2. ^{1}H and ^{13}C resonance assignments for Esc(1-18) in DPC and DPC/SDS 3/1 molar ratio buffered solution (pH 7.4). J coupling constants were not used for structure calculations and are not reported

Residue	DPC						DPC/SDS 3/1 mol/mol					
	^{1}H (ppm)				^{13}C (ppm)		^{1}H (ppm)				^{13}C (ppm)	
	HN	Hα	Hβ	Others	Cα	Cβ	HN	Hα	Hβ	Others	Cα	Cβ
G1	---	3.966 3.924			45.010		---	3.930			45.405	
I2	8.347	3.910	1.780	γ 1.388 1.162 γ1 0.725 δ 0.836	63.405	37.972	8.315	3.878	1.765	γ 1.417 1.165 γ1 0.705 δ 0.854	64.077	38.251
F3	8.659	4.384	3.202 3.145	δ/δ' 7.262 ε/ε' 7.220 ζ 7.126	60.090	38.049	8.382	4.311	3.232 3.152	δ/δ' 7.279 ε/ε' 7.162 ζ 7.060	---	---
S4	8.361	4.194	4.029 3.964		56.176	62.685	8.522	3.999	---		---	---
K5	7.795	4.179	1.904	γ 1.569 δ 1.702 ε 2.947 HNζ ---	59.099	32.131	7.920	4.086	1.966	γ 1.452 δ 1.666 ε 2.972 ζ ---	---	32.339
L6	7.862	4.188	1.790 1.586	γ --- δ 0.946 0.881	56.889	42.151	8.016	4.157	1.979	γ 1.875 δ 0.892	57.413	---
A7	7.952	4.121	1.335		53.565	18.570	8.369	3.998	1.307		---	18.476
G8	a	a			a		b	b			b	
K9	8.061	4.134	1.898	γ 1.498 δ 1.697	59.099	32.131	7.944	4.147	1.883	γ 1.594 δ 1.719	57.413	32.339

				ε 2.982						ε 2.991			
				ζ ---						ζ ---			
K10	8.064	4.241	1.923	γ 1.505	59.099	32.131	7.838	4.208	1.853	γ 1.561	56.851	32.339
				δ 1.736						δ 1.821		
				ε 2.948						ε 2.916		
				ζ ---						ζ ---		
L11	8.286	4.102	1.780	γ 1.750	57.357	41.469	7.962	4.261	1.952	γ 1.801	61.520	---
			1.659	δ 0.937						δ 0.900		
				0.895								
K12	8.278	3.876	1.897	γ 1.454	59.664	32.131	8.313	3.855	1.944	γ 1.497	64.077	32.339
				δ 1.707						1.460		
				ε 2.917						δ 1.732		
				ζ ---						ε 2.925		
										ζ ---		
N13	7.935	4.543	2.887	δ ‘ ---			---	4.530	2.920	δ ‘ 7.738	53.139	---
				δ’’ ---						δ’’ 6.932		
L14	7.862	4.184	1.886	γ 1.804	60.686	42.200	8.424	4.073	1.842	γ 1.820	---	---
			1.685	δ 0.946						δ 0.953		
				0.880								
L15	7.770	4.224	1.819	γ 1.802	61.134	42.151	7.995	4.189	1.932	γ 1.875	61.520	---
			1.614	δ 0.914						δ 0.915		
				0.875								
I16	7.794	4.179	2.013	γ 1.554	61.557	38.256	7.877	4.197	2.052	γ 1.572	61.841	38.441
				1.280						1.320		
				γ1 0.942						γ1 0.957		
				δ 0.881						δ 0.887		
S17	8.172	4.430	3.967		58.967	63.609	8.136	4.435	3.974		59.437	63.958
G18	a	a			a		8.314	3.928			45.405	

Footnotes:

a, resonances deriving from the two glycines were not unambiguously identified, no one inter-residue NOEs was observed for these glycines, and no torsional restraints were included for them during structure calculations.

b, HN chemical shift value for this glycine was identified equal to 8.482, through inter-residue NOEs involving this residue.

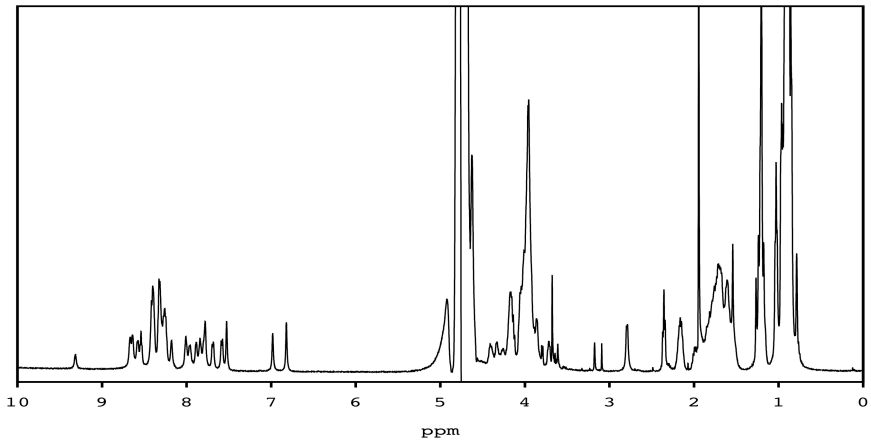

Figure A.3. Plasticin-L1 in micelle solutions. ^{1}H spectrum of Plasticin-L1 in DPC buffered solutions (pH 7.4).

Table A.3. ^{1}H and ^{13}C resonance assignments for Plasticin-L1 in the DPC and the DPC/SDS 1:1 mol/mol buffered solutions (pH 7.4). $^{3}J_{HNH\alpha}$ coupling constants are also reported

Residue	DPC							DPC/SDS 1/1 mol/mol						
	^{1}H (ppm)				^{13}C (ppm)		$^{3}J_{H^{N}H^{\alpha}}(Hz)$	^{1}H (ppm)				^{13}C (ppm)		$^{3}J_{H^{N}H^{\alpha}}(Hz)$
	HN	Hα	Hβ	Others	Cα	Cβ		HN	Hα	Hβ	Others	Cα	Cβ	
G1	---	4.053 3.934			42.838		---	---	4.061 3.906			43.335		---
L2	9.351	4.211	1.786 1.662	γ 1.749 δ1 1.005 δ2 0.975	57.391	---	9.285	8.711	4.187	1.746 1.625	γ --- δ 0.933	61.115	41.049	6.841
V3	8.704	3.749	2.189	γ1 1.054 γ2 0.954	71.668	30.865	7.127	8.183	3.818	2.214	γ1 0.990 γ2 0.929	64.727	31.144	7.168
N4	8.347	4.450	2.827	δ' 7.780 δ'' 6.982	---	37.770	7.330	8.128	4.447	2.793	δ' 7.947 δ'' 7.590	---	---	9.541
G5	8.362	3.993			44.834		---	8.222	4.039 3.942			45.248		7.085

L6	8.292	4.204	1.898 1.851	γ 1.698 δ1 0.950 δ2 0.926	57.391	---	7.068	8.059	4.174	1.855	γ --- δ ---	56.838	---	6.938
L7	8.456	4.086	1.885 1.653	γ 1.847 δ1 0.933 δ2 0.909	57.049	41.735	9.948	8.323	4.080	1.822 1.631	γ --- δ ---	57.273	---	6.981
S8	8.212	4.194	3.995 3.963		60.993	62.378	7.068	8.077	4.142	3.973 3.921		61.115	62.693	6.938
S9	7.920	4.369	4.058 3.968		70.786	62.860	7.156	7.873	4.340	4.023 3.964		55.858	63.116	6.908
V10	7.820	4.091	2.214	γ1 1.069 γ2 0.994	63.741	31.969	7.036	7.806	4.068	2.184	γ1 1.039 γ2 0.969	63.962	---	7.002
L11	7.993	4.423	1.824	γ 1.650 δ1 0.934 δ2 0.910	---	42.278	7.991	7.953	4.362	1.722	γ --- δ ---	---	---	6.908
G12	7.875	4.049			44.572		10.257	a	a			a		---
G13	8.277	4.019			44.834		6.923	7.922	4.040 3.968			45.248		---
G14	8.430	3.961			44.834		10.335	a	a			a		---
Q15	8.442	4.371	2.188 2.020	γ 2.385 ε’ 7.528 ε’’ 6.820	55.529	28.644	7.592	8.325	4.339	2.172 1.987	γ 2.356 ε’ 7.477 ε’’ 6.767	55.858	28.896	7.092
G16	8.391	3.993			44.834		---	8.458	4.006 3.940			45.248		---

G17	8.572	4.035 3.976			44.834		10.384	8.158	3.993			45.248		---
G18	8.421	3.992			44.834		6.923	a	a			a		---
G19	8.358	4.083 4.049			44.834		10.472	8.255	3.969			45.248		---
L20	8.669	4.222	1.750 1.586	γ --- δ1 0.974 δ2 0.926	56.398	42.418	7.330	8.240	4.173	1.718 1.545	γ --- δ ---	57.551	42.530	6.795
L21	8.614	4.291	1.797 1.724	γ 1.709 δ1 0.947 δ2 0.882	60.827	40.779	10.181	8.178	4.264	1.769	γ 1.659 δ1 0.927 δ2 0.856	55.048	42.638	10.021
G22	8.043	3.893			45.970		10.137	7.930	3.873			46.138		10.291
G23	8.312	4.002			44.834		10.332	8.155	4.040 3.925			45.248		10.140
I24	7.726	4.169	1.941	γ1' 1.557 γ1'' 1.247 γ2 0.951 δ 0.902	61.723	30.692	7.904	7.624	4.150	1.908	γ1' 1.509 γ1'' 1.213 γ2 0.913 δ 0.865	61.994	38.992	10.344
L25	7.613	4.331	1.676 1.640	γ 1.634 δ1 0.937 δ2 0.911	54.567	---	7.370	7.604	4.266	---	γ --- δ ---	55.048	---	10.018

Footnotes:

a, these three glycines were not unambiguously identified; two of them were characterized by the following chemical shift values: HN 8.255, Hα 3.969, Cα 45.248. The other glycines: HN 8.307, Hα 3.961, Cα 45.248. However no one inter-residue NOEs was observed for these three glycines, and no torsional restraints were included for them during structure calculations.

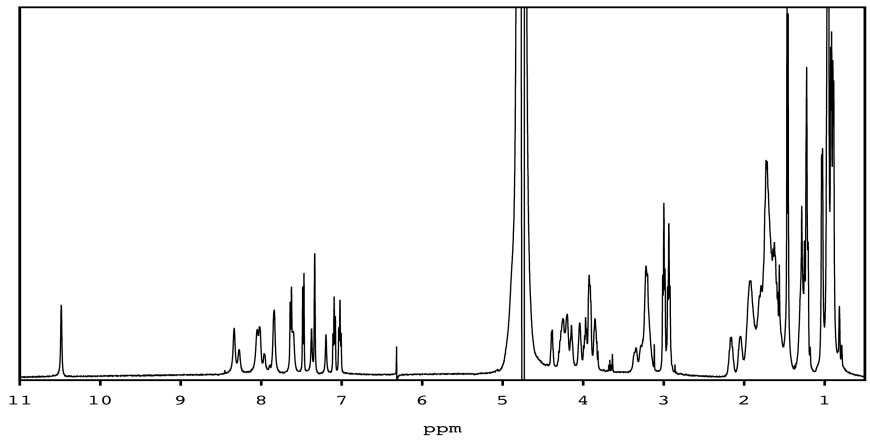

Figure A.4. SB056-lin in micelle solution. ^{1}H spectrum of SB056-lin in DPC/SDS 3/1 mol/mol buffered solutions (pH 7.4).

Table A.4. ^{1}H and ^{13}C resonance assignments for SB056-lin in the DPC/SDS 3:1 mol/mol buffered solutions (pH 7.4) and [L]/[P]=25. $^{3}J_{HNH\alpha}$ coupling constants are also reported

Residue	**SB056-lin**							
	^{1}H (ppm)					**^{13}C (ppm)**		$^{3}J_{H^{N}H^{\alpha}}(Hz)$
	HN	**Hα**	**Hβ**	**Others**		**Cα**	**Cβ**	
W1	---	4.311	3.377	HN1	10.485	56.542	30.082	---
				2H	7.341			
				4H	7.633			
				5H	7.022			
				6H	7.095			
				7H	7.477			
K2	7.895	4.258	1.892	γ	1.521	57.155	30.192	9.38
				δ	1.730			
				ε	3.002			
				HNζ	---			
K3	8.227	4.236	1.754	γ	1.311	57.155	30.192	6.53
				δ	1.607			
				ε	2.935			

				HNζ	---			
I4	8.166	3.871	2.029	γ’	1.683	53.206	37.838	9.65
				γ’’	1.300			
				γ1	0.948			
				δ	0.955			
R5	8.377	4.088	1.886	γ	1.678	58.204	30.192	9.349
				δ	3.223			
				HNε	7.429			
				HNη	---			
V6	7.535	3.952	2.164	γ’	1.033	---	31.914	6.73
				γ’’	0.961			
R7	7.765	4.190	1.881	γ	1.668	57.155	32.945	9.08
			1.735	δ	3.170			
				HNε	7.370			
				HNη	---			
L8	8.026	4.276	1.730	γ	1.805	55.865	42.106	9.319
			1.632	δ’	0.922			
				δ’’	0.892			
S9	7.854	4.396	3.972			58.925	63.820	9.513
			3.901					
A10	8.002	4.292	1.461			52.432	19.324	9.384

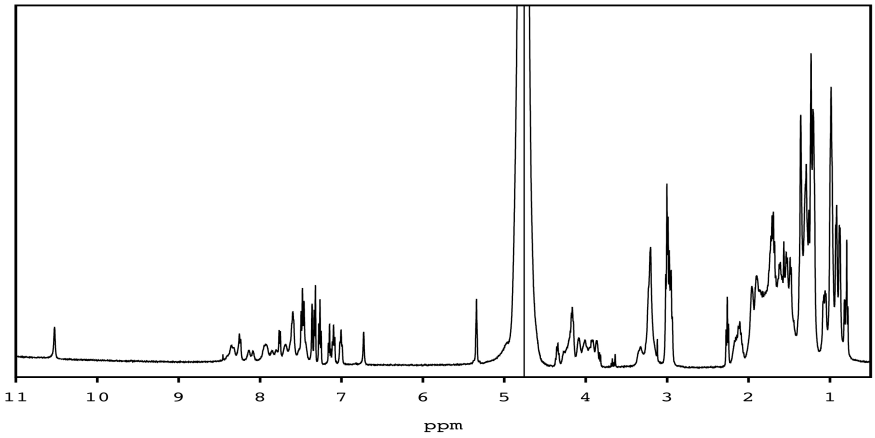

Figure A.5. SB056-den in micelle solution. ^{1}H spectrum of SB056-den in DPC/SDS 3/1 mol/mol buffered solutions (pH 7.4).

Table A.5. ^{1}H and ^{13}C resonance assignments for SB056-den in the DPC/SDS 3:1 mol/mol buffered solutions (pH 7.4) and [L]/[P]=25. $^{3}J_{HNH\alpha}$ coupling constants are also reported.

Residue[a]	SB056-den																	
	^{1}H (ppm)												^{13}C (ppm)				$^{3}J_{H^{N}H^{\alpha}}$ (Hz)	
	HN		Hα		Hβ		Others						Cα		Cβ			
W1	8.246	---	4.603	4.098	3.215	3.343	HN1	10.525	10.525				57.517	57.251	39.451	---	7.06	---
					2.999	3.201	2H	7.362	7.362									
							4H	7.322	7.598									
							5H	7.141	7.004									
							6H	7.255	7.098									
							7H	7.327	7.488									
K2	---	7.468	4.079	4.348	1.776	1.781	γ	1.275	1.363				57.760	55.322	32.612	32.869	---	7.17
						1.634	δ	1.626	1.691									
							ε	2.948	2.969									
							HNζ	---	---									
K3	8.392	7.760	4.216	4.169	1.904	1.837	γ’	1.551	1.359				57.760	57.271	32.008	33.711	---	6.824
					1.833	1.734	γ’’	1.460										
							δ	1.626	1.722									
							ε	2.948	2.990									
							HNζ	---	---									
I4	7.951	7.931	3.865	3.918	2.113	2.095	γ’	1.497	1.682				64.474	65.082	37.620	37.620	7.51	6.82

							γ''	---	1.304							
							γ1	1.270	0.994							
							δ	---	0.975							
R5	8.350	8.321	3.957	4.024	1.988	1.983	γ	1.687	1.696	59.465	---	29.884	29.884	6.90	10.51	
					1.898	1.882	δ	3.220	3.220							
							HNε	---	---							
							HNη	---	---							
V6	7.699	7.681	3.866	3.910	2.173	2.163	γ'	1.079	1.053	63.623	63.128	---	31.862	10.24	9.89	
							γ''	1.010	0.978							
R7	7.811	7.854	4.243	4.257	1.951	1.951	γ	1.756	1.756	61.301	---	35.413	35.011	---	---	
							δ	3.214	3.214							
							HNε	---	---							
							HNη	---	---							
L8	8.261	8.136	4.160	4.175	1.590	1.590	γ	1.879	1.879	57.271	57.251	27.727	27.727	10.39	10.27	
							δ'	0.921	0.921							
							δ''	0.880	0.880							
S9	8.085	7.911	4.151	4.204	4.033	4.021				61.123	60.259	63.006	63.006	10.10	10.24	
					3.994	3.992										
A10	7.597	7.524	4.271	4.342	1.531	1.482				53.490	52.393	18.692	19.418	---	10.24	
K linker	7.628		4.170		1.849		γ'	---		57.251		---		---		
							δ	---								
							ε'	3.308								
							ε''	3.160								
							HNζ	7.584								
Lipidic tail							HN8	7.437								
							HC8	3.204								
							HC7	1.548								
							HC6	1.350								
							HC5	1.350								

				HC4	1.350		
				HC3	1.607		
				HC2	2.260		
				HN1’	7.462		
				HN1’’	6.724		

Footnotes:

a, the residues belonging to different branches of the peptide were distinguishable on the basis of the chemical shift values; for each residue, table reports the resonance attributions in the left or right column for the ones belonging to one or the other branch. The unique positioning of the residues depends on the different structural hypothesis taken into account as explained in the text.

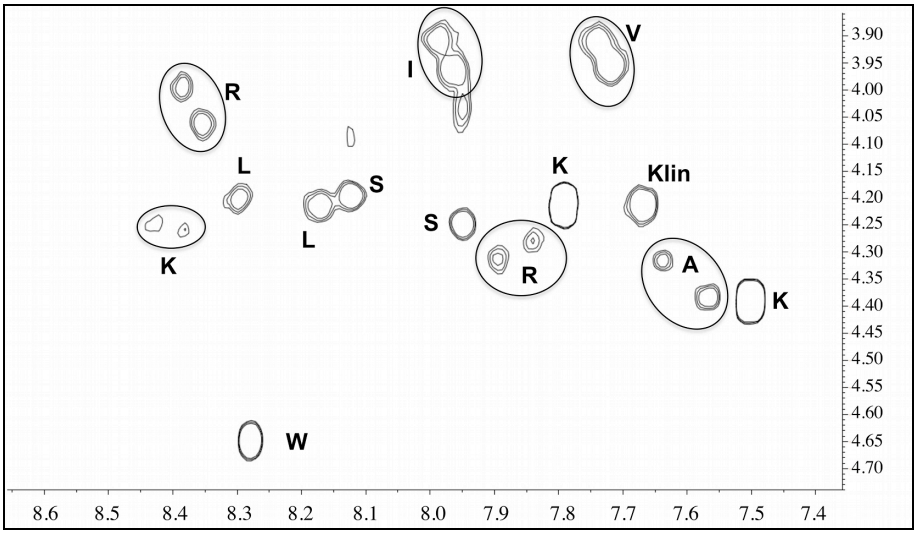

Figure A.6. SB056-den assignments. Residue assignments of H^N-H^α region of ^1H TOCSY spectrum of SB056-den in DPC/SDS 3/1 mol/mol buffered solutions (pH 7.4).

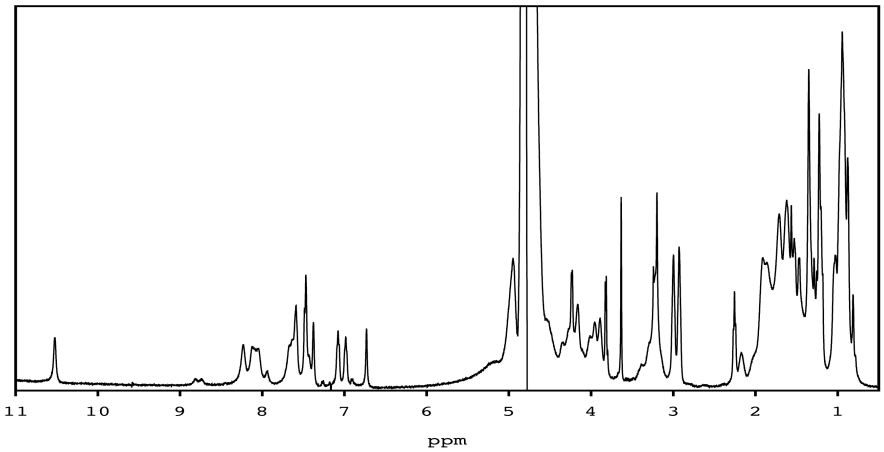

Figure A.7. β-SB056-den in micelle solution. ^1H spectrum of β-SB056-den in DPC/SDS 3/1 mol/mol buffered solutions (pH 7.4).

Table A.6. ^{1}H and ^{13}C resonance assignments for β-SB056-den in the DPC/SDS 3:1 mol/mol buffered solutions (pH 7.4) and [L]/[P]=25. $^{3}J_{HNH\alpha}$ coupling constants are not reported.

Residue[a]	β-SB056-den													
	^{1}H (ppm)										^{13}C (ppm)			
	HN		Hα		Hβ		Others				Cα		Cβ	
K1	---	b	3.898	b	1.740	b	γ	1.335	b		56.091	b	34.048	b
							δ	1.629						
							ε	2.926						
							HNζ	---						
W2	---	b	4.622	b	3.386	b	HN1	10.519	b		---	b	---	b
					3.297		2H	7.373						
							4H	7.589						
							5H	6.982						
							6H	7.076						
							7H	7.476						
K3	8.806	8.740	4.355	4.356	1.854	1.918	γ’	1.429	1.431		57.002	57.002	32.095	32.095
							δ	1.703	1.715					
							ε	2.999	2.999					
							HNζ	---	---					
I4	8.125	8.037	3.894	3.954	1.926	1.907	γ’	1.627	1.627		---	---	37.934	37.934
							γ’’	1.262	1.262					
							γ1	0.945	0.945					
							δ	0.936	0.936					
R5	8.246	8.245	4.027	4.120	1.918	1.894	γ	1.715	1.687		---	---	30.261	30.261
							δ	3.223	3.226					
							HNε	---	---					
							HNη	---	---					
V6	7.678	7.670	3.877	3.945	2.177	2.156	γ’	1.047	1.023		64.913	64.099	32.112	32.212
							γ’’	0.987	0.973					
R7	8.047	8.069	4.252	4.297	1.930	1.914	γ	1.794	1.687		60.198	---	30.261	30.261

					δ	3.212	3.226			
					HNε	---	---			
					HNη	---	---			
L8	8.095	8.125	4.163	4.178	1.606	1.607	γ	1.859	1.859	57.391 57.391	28.565	27.811
							δ’	0.913				
							δ’’	0.843	0.913			
									0.874			
S9	8.217	7.938	4.164	4.211	4.040	3.981				61.148 61.451	63.178	63.351
A10	7.637	7.589	4.270	4.336	1.520	1.468				53.677 52.554	19.013	19.713
K linker	7.632		4.167		1.819		γ’	---		56.700	33.774	
							δ	---				
							ε’	3.301				
							ε’’	---				
							HNζ	7.596				
Lipidic tail							HN8	7.427				
							HC8	3.198				
							HC7	---				
							HC6	1.361				
							HC5	1.361				
							HC4	1.361				
							HC3	1.599				
							HC2	2.258				
							HN1’	7.462				
							HN1’’	6.734				

Footnotes:

a, the residues belonging to different branches of the peptide were distinguishable on the basis of the chemical shift values; for each residue, table reports the resonance attributions in the left or right column for the ones belonging to one or the other branch. The unique positioning of the residues depends on the different structural hypothesis taken into account as explained in the text.

b, these residues were not distinguishable.